NASA/CR-2009-215757

Orion Landing Simulation
Eight Soil Model Comparison

Stephen D. Mark
ATK Space Division, Hampton, Virginia

June 2009

NASA STI Program . . . in Profile

Since its founding, NASA has been dedicated to the advancement of aeronautics and space science. The NASA scientific and technical information (STI) program plays a key part in helping NASA maintain this important role.

The NASA STI program operates under the auspices of the Agency Chief Information Officer. It collects, organizes, provides for archiving, and disseminates NASA's STI. The NASA STI program provides access to the NASA Aeronautics and Space Database and its public interface, the NASA Technical Report Server, thus providing one of the largest collections of aeronautical and space science STI in the world. Results are published in both non-NASA channels and by NASA in the NASA STI Report Series, which includes the following report types:

- TECHNICAL PUBLICATION. Reports of completed research or a major significant phase of research that present the results of NASA programs and include extensive data or theoretical analysis. Includes compilations of significant scientific and technical data and information deemed to be of continuing reference value. NASA counterpart of peer-reviewed formal professional papers, but having less stringent limitations on manuscript length and extent of graphic presentations.

- TECHNICAL MEMORANDUM. Scientific and technical findings that are preliminary or of specialized interest, e.g., quick release reports, working papers, and bibliographies that contain minimal annotation. Does not contain extensive analysis.

- CONTRACTOR REPORT. Scientific and technical findings by NASA-sponsored contractors and grantees.

- CONFERENCE PUBLICATION. Collected papers from scientific and technical conferences, symposia, seminars, or other meetings sponsored or co-sponsored by NASA.

- SPECIAL PUBLICATION. Scientific, technical, or historical information from NASA programs, projects, and missions, often concerned with subjects having substantial public interest.

- TECHNICAL TRANSLATION. English-language translations of foreign scientific and technical material pertinent to NASA's mission.

Specialized services also include creating custom thesauri, building customized databases, and organizing and publishing research results.

For more information about the NASA STI program, see the following:

- Access the NASA STI program home page at *http://www.sti.nasa.gov*

- E-mail your question via the Internet to help@sti.nasa.gov

- Fax your question to the NASA STI Help Desk at 443-757-5803

- Phone the NASA STI Help Desk at 443-757-5802

- Write to:
  NASA STI Help Desk
  NASA Center for AeroSpace Information
  7115 Standard Drive
  Hanover, MD 21076-1320

NASA/CR-2009-215757

Orion Landing Simulation
Eight Soil Model Comparison

Stephen D. Mark
ATK Space Division, Hampton, Virginia

National Aeronautics and
Space Administration

Langley Research Center
Hampton, Virginia 23681-2199

Prepared for Langley Research Center
under Contract NNL07AA00B

June 2009

Acknowledgments

The author would like to acknowledge Edwin Fasanella and Karen Lyle of the NASA Langley Research Center for their technical support and guidance throughout this analysis effort. The author would also like to thank James Corliss for his guidance and for providing pictures of the soils.

Available from:

NASA Center for AeroSpace Information
7115 Standard Drive
Hanover, MD 21076-1320
443-757-5802

Abstract

LS-DYNA® finite element simulations of a rigid Orion Crew Module (CM) were used to investigate the CM impact behavior on eight different soil models. Ten different landing conditions, characterized by the combination of CM vertical and horizontal velocity, hang angle, and roll angle were simulated on the eight different soils. The CM center of gravity accelerations, pitch angle, kinetic energy, and soil contact forces were the outputs of interest. The simulation results are presented, with comparisons of the CM behavior on the different soils. The soils analyzed in this study can be roughly categorized as soft, medium, or hard, according to the CM accelerations that occur when landing on them. The soft group is comprised of the Carson Sink Wet soil and the Kennedy Space Center (KSC) Low Density Dry Sand. The medium group includes Carson Sink Dry, the KSC High Density In-Situ Moisture Sand and High Density Flooded Sand, and Cuddeback B. The hard soils are Cuddeback A and the Gantry Unwashed Sand. The softer soils were found to produce lower peak accelerations, have more stable pitch behavior, and to be less sensitive to the landing conditions. This investigation found that the Cuddeback A soil produced the highest peak accelerations and worst stability conditions, and that the best landing performance was achieved on the KSC Low Density Dry Sand.

Table of Contents

List of Figures

List of Tables

Nomenclature

CBA	Cuddeback A
CBB	Cuddeback B
CEV	Crew Exploration Vehicle
CG	Center of Gravity
CLL	Contingency Land Landing
CM	Crew Module
CPU	Central Process Unit
CSD	Carson Sink Dry
CSW	Carson Sink Wet
ft/s	Feet per Second
GUS	Gantry Unwashed Sand
HDFS	High Density Flooded Sand
HDISMS	High Density In-Situ Moisture Sand
KSC	Kennedy Space Center
LaRC	Langley Research Center
LDDS	Low Density Dry Sand
NASA	National Aeronautics and Space Administration
TSSFAC	Time Step Scale Factor

1.0 Introduction

The National Aeronautics and Space Administration (NASA) is developing the Constellation architecture including the Ares launch vehicle and Orion Crew Module (CM) to achieve the Vision for Space Exploration. The Orion CM, also known as the Crew Exploration Vehicle (CEV), will return to Earth using parachutes to slow the vehicle down after an atmospheric reentry. While a water landing is planned, the design will also include preparations for a Contingency Land Landing (CLL) situation that could occur due to either 1) a launch abort during which the CM is blown back onshore or 2) a landing from orbit in which the CM returns to Earth over land rather than water [ref. 1]. In a land landing without auxiliary attenuation, the soil properties have a large effect on the severity of the impact experienced by the CM, and there are a variety of possible landing zone soil types. The goal of this research was to evaluate the effect of different soils on the CM landing dynamics via finite element simulations.

LS-DYNA®† soil and foam material models (*MAT_SOIL_AND_FOAM) for eight (8) different soils were obtained from previous work performed by Applied Research Associates, Inc. [ref. 2, 3]. These 8 soil models were utilized in rigid CM LS-DYNA landing simulations for ten (10) different combinations of the following initial conditions: hang angle, roll angle, vertical velocity, and horizontal velocity.

2.0 Background on Human Tolerance to Impact

To understand the risks associated with a contingency land landing, the limits on tolerable occupant accelerations must be understood [ref. 1]. The accelerations on the seat and occupant in an impact are measured along local X-, Y-, and Z-axes, where for a non-inclined (0^o pitch) capsule impact, the X-axis is in the vertical direction and the Z-axis is horizontal. The astronauts will be lying on their backs in a supine position [ref. 4], and the vertical impact force for a flat capsule impact is along the X-axis perpendicular to the spine and is distributed over a large area. Human tolerance for accelerations in this direction is almost twice that for accelerations along the spine [ref. 5]. Accelerations along the Y-direction (laterally on the astronaut) have similar human tolerance limits to the Z-axis accelerations if the occupants are effectively restrained against lateral movement, and the Y-axis accelerations can be minimized via Orion's roll-control system. Consequently, it is more important to minimize the Z-axis accelerations than the X-axis accelerations for passive contingency land landing scenarios.

3.0 LS-DYNA Simulation Modeling Methods & Assumptions

LS-DYNA [ref. 6] is a general-purpose non-linear explicit commercial finite element code that is especially effective at modeling the dynamic response of structures experiencing impacts, and also includes a capability for modeling soils. Structures can be represented using both solid and shell elements, and a variety of contact definitions are available, allowing contact between objects with dissimilar stiffness to be represented accurately.

3.1 Soil Models

A Lagrangian soil definition was used, modeling the soil as a block of 146,250 single integration point solid elements. Figure 1 shows the landing simulation model, including the 324 x 324 x 115.4-inch soil block. The soil mesh size is uniformly 4.3 x 4.3 x 4.4 inches, with the 4.4-inch dimension in the vertical (x-axis) direction. Earlier work had determined that a soil block of this depth would be sufficient to avoid problems of stress reflections from the bottom of the block back to the top that could affect the CM accelerations. It was found that a soil block of this depth would match the results of a smaller block utilizing a non-reflecting boundary definition, but at a lower cost in computing power. This mesh size

†Trade names and trademarks are used in this report for identification only. Their usage does not constitute an official endorsement, either expressed or implied, by the National Aeronautics and Space Administration.

was chosen for compatibility reasons, as a similar mesh size has been and is being used in other Orion simulation studies.

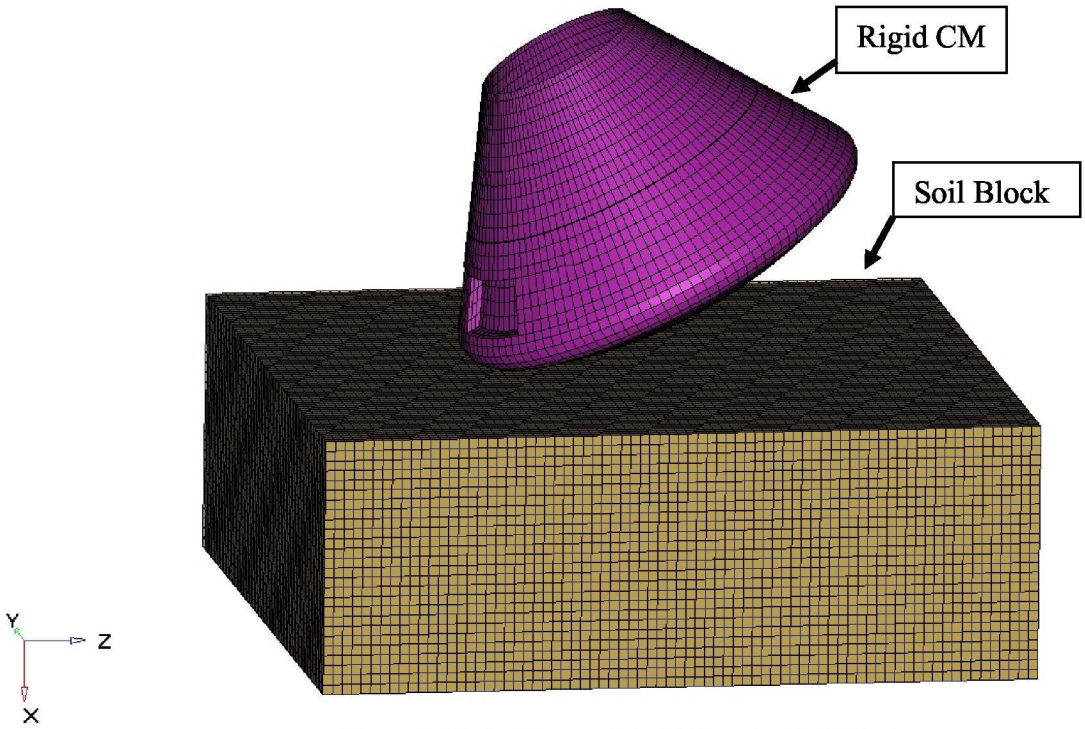

Figure 1. Finite Element Model Showing Soil Block

The Cuddeback soils represent conditions at Cuddeback Lake near Edwards Air Force Base in California, as illustrated in Figure 2. The Carson Sink soils represent conditions at the Carson Sink area of Nevada, and are shown in Figure 3. Figure 4 shows pictures of the Kennedy Space Center (KSC) Low Density Dry Sand and the High Density In-Situ Moisture Sand.
Figure 5 shows pictures of the KSC High Density Flooded Sand and the Gantry Unwashed Sand. More detail about the material testing and development of these soil models can be found in reports from Applied Research Associates, Inc. [ref. 2, 3].

Cuddeback Lakebed "A" (Harder Areas)

Cuddeback Lakebed "B" (Softer Areas)

Figure 2. Photos of Cuddeback A and Cuddeback B Soils

Carson Sink, NV (Dry Areas)

Carson Sink, NV (Wet Areas)

Figure 3. Photos of Carson Sink Dry and Wet Soils

KSC Low Density Dry Sand (Dry Beach Areas)

KSC High Density In-Situ Moisture Sand

Figure 4. Photos of KSC High Density In-Situ Moisture Sand and KSC Low Density Dry Sand

KSC High Density Flooded Sand (Surf-line Areas)

Gantry Unwashed Sand (Purchased Sand-Clay Mix)

Figure 5. Photos of KSC High Density Flooded Sand and Gantry Unwashed Sand

The eight soil models evaluated are designated in this report as:

1) Cuddeback A (CBA) - The hard dry clay found at the center area of Cuddeback Lake.
2) Cuddeback B (CBB) - A softer soil located at the outer region of Cuddeback Lake.
3) Carson Sink Dry (CSD) - The soil at Carson Sink above the waterline.
4) Carson Sink Wet (CSW) - The sand/soil at Carson Sink just below the waterline.
5) Kennedy Space Center Low Density Dry Sand (KSC-LDDS) - The soft shoreline sand near the beach dunes, above the waterline.
6) Kennedy Space Center High Density In-Situ Moisture Sand (KSC-HDISMS) - The light vegetation covered sand around the launch pad.
7) Kennedy Space Center High Density Flooded Sand (KSC-HDFS), the wet beach sand near the waterline.
8) Gantry Unwashed Sand (GUS) - A sand-clay mix of soil found at the Gantry test area of the NASA Langley Research Center (LaRC). (This soil mixture was purchased.)

Figure 6 shows the compressive stress versus strain curves for the material models, as obtained from testing [ref. 2, 3]. The curve for the KSC Low Density Dry Sand Option 1 model has a substantial slope change at 0.03 strain. The Carson Sink Wet and Dry soils have much shallower curves than the other soils. The soils operate on different parts of these curves at different times, and in different locations in the soil contact area. Figure 7 shows the same plot, but only out to a strain of 0.1, allowing it to be more easily visible that the KSC Low Density Dry Sand curve is indeed the lowest curve, except for the region between 0.010 and 0.013, where it coincides with the Carson Sink Wet curve. It is also easier to see in Figure 7 that the Gantry Unwashed Sand model always has a higher slope than the Cuddeback A model. The KSC High Density Flooded Sand slope exceeds that of Cuddeback A above 0.01 strain. The range of pressures tested was limited to 100 psi because the initial use of these soil models was in conjunction with airbag-equipped Orion capsules in landing simulations where no higher contact pressure would be seen. There is some uncertainty in the simulation results, because some elements experience pressures in excess of the tested values, and it is unknown if the soil material properties will extrapolate, which is how LS-DYNA models them.

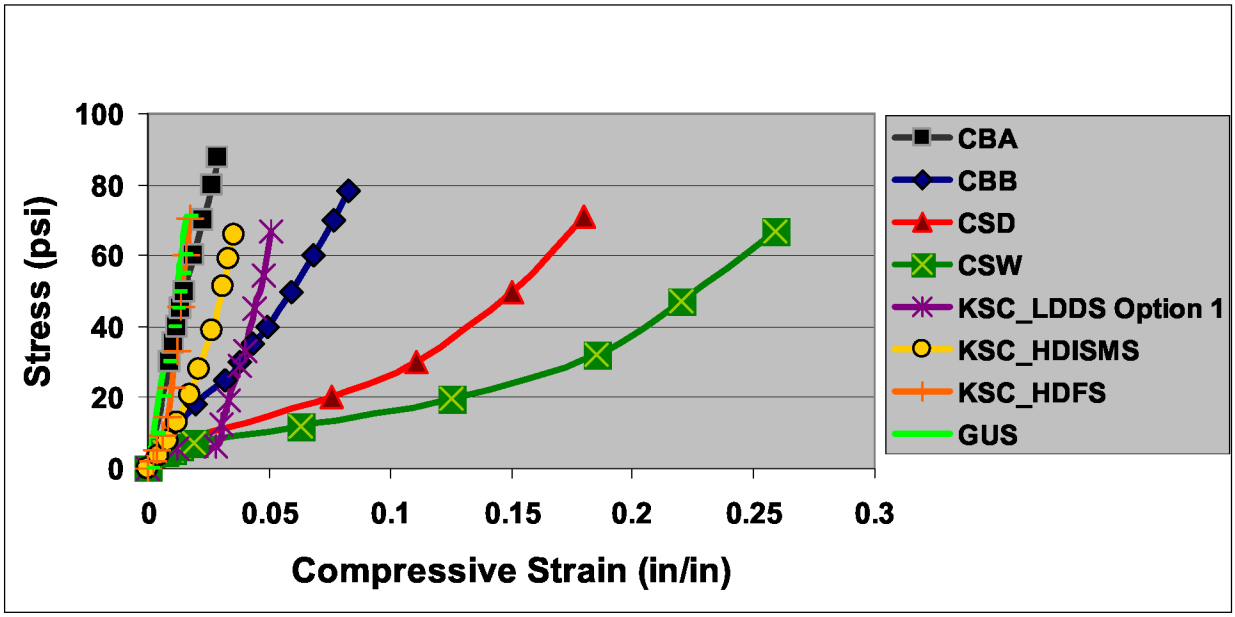

Figure 6. Soil Stress versus Strain Curves

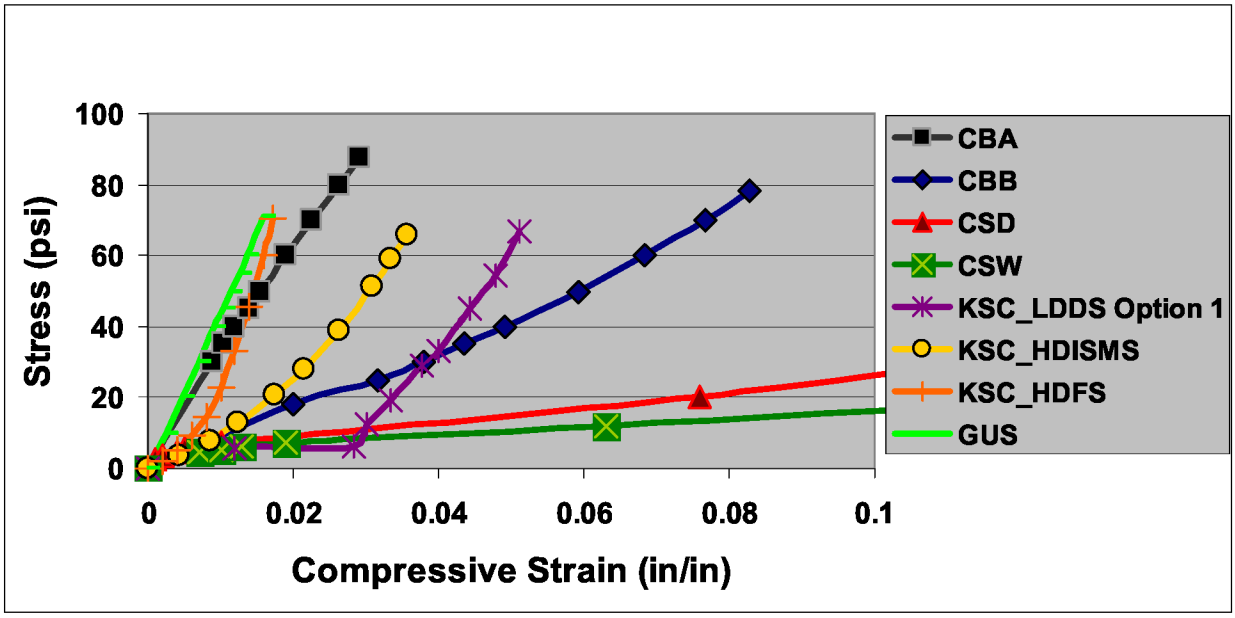

Figure 7. Soil Stress versus Strain Curves, zoom plot

When computing the soil stiffness, the confining pressure ensured that the soil would not fail in shear. However, typically a soil will fail in shear in an impact event. The shear failure of the soil is also dependent on the pressure on the soil. The corresponding shear strength envelope is referred to as the yield surface in LS-DYNA [ref. 6], and is defined in the (MAT_SOIL_AND_FOAM) material model by the coefficients of the curve defining the second invariant of the stress deviator tensor, designated J2, which at yield can be defined by the equation:

$$J2 = A0 + A1*P + A2*P^2$$

A0, A1, and A2 are the coefficients defined in the soil model and determined from testing, and P is the mean pressure (stress) on the soil. The mean stress P is defined as

$$P = (\sigma_a + 2*\sigma_c)/3$$

where: σ_a = the axial pressure on the cylindrical test specimen of soil
σ_c = the confining pressure around the sides of the test soil column

The stress difference $\sigma_a - \sigma_c$ is the yield strength of the soil in shear.

The shear strength of a soil is highly dependent on the mean stress level, or pressure, of the soil. Applied Research Associates performed triaxial compression testing, and created a best fit to the test data for each soil's strength envelope [ref. 2, 3]. The strength envelope is illustrated in Figure 8 by a plot of the shear yield stress versus the mean stress. The Cuddeback A soil has the highest shear strength at pressure loadings under 50 psi. Above 50 psi, the Cuddeback B soil has the highest shear strength. This higher shear strength for Cuddeback A means that the edges of the contact with the soil will not fail in shear as easily as the other soils. The Carson Sink Dry soil shear strength approaches the Cuddeback A value as the pressure increases. Cuddeback A also has the largest y-intercept on this graph, corresponding to the tensile strength of the soil arising from its cohesiveness.

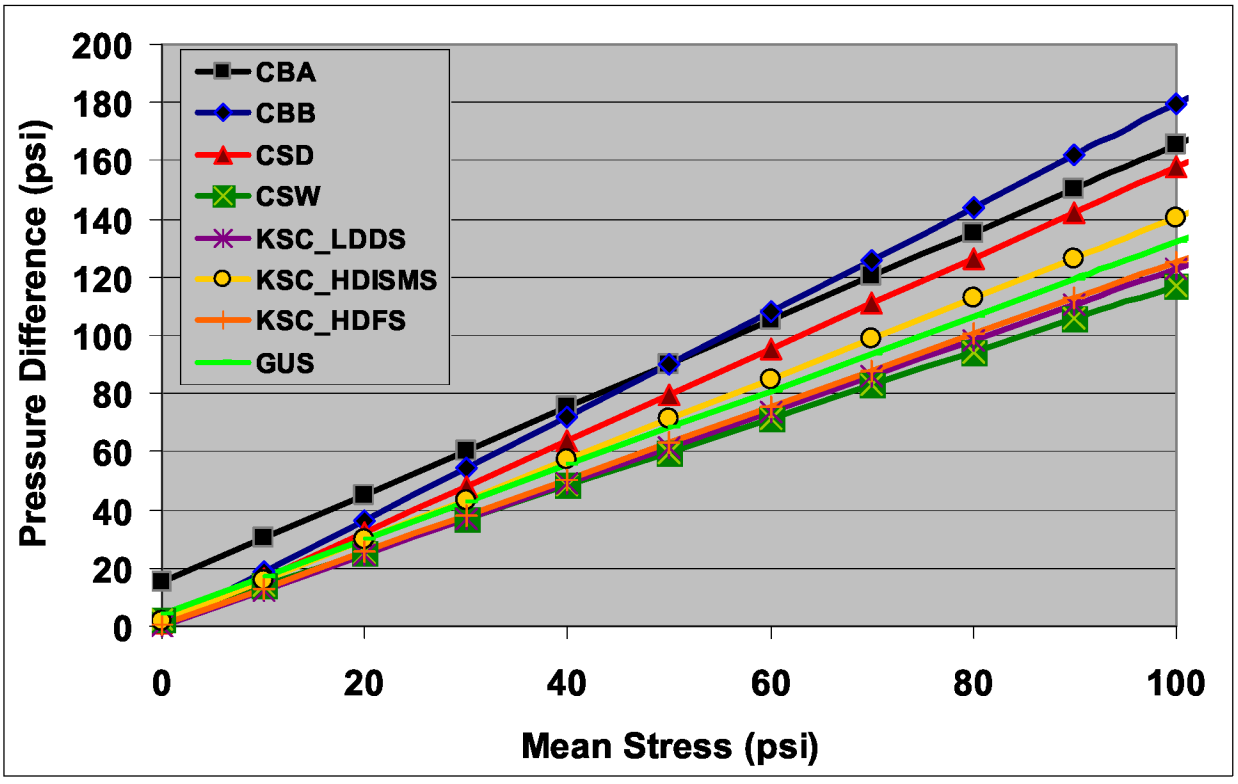

Figure 8. Soil Strength Curves (Standard)

The soil pressure is not constant throughout the area of contact. The net reaction force from the soil may be driven by low pressure loaded soil elements in the outer area of the contact and not the peak loaded pressure elements at the center of the contact patch. Further analysis is required to determine whether operating outside the tested range of pressures on the soil will result in significant errors in calculations of the accelerations.

3.2 Orion Crew Module Modeling

Figure 9 illustrates the finite element model, shown after impact for a KSC High Density Flooded Sand case. The CM is modeled as a rigid body in LS-DYNA, with mass and inertia properties specified as follows:

Weight = 18,940 pounds
Mass Moments of Inertia:
Ixx = 216,252 in-lb-s^2
Iyy = 136,104 in-lb-s^2
Izz = 177,684 in-lb-s^2

The CM is represented by 5864 shell elements, with a mesh size that varies from 1.3- to 5-inches square. The mesh size is 4-5 inches in the shoulder and bottom (heat shield) edge region that contacts the soil on initial impact. The CM is made rigid by assigning it a rigid material.

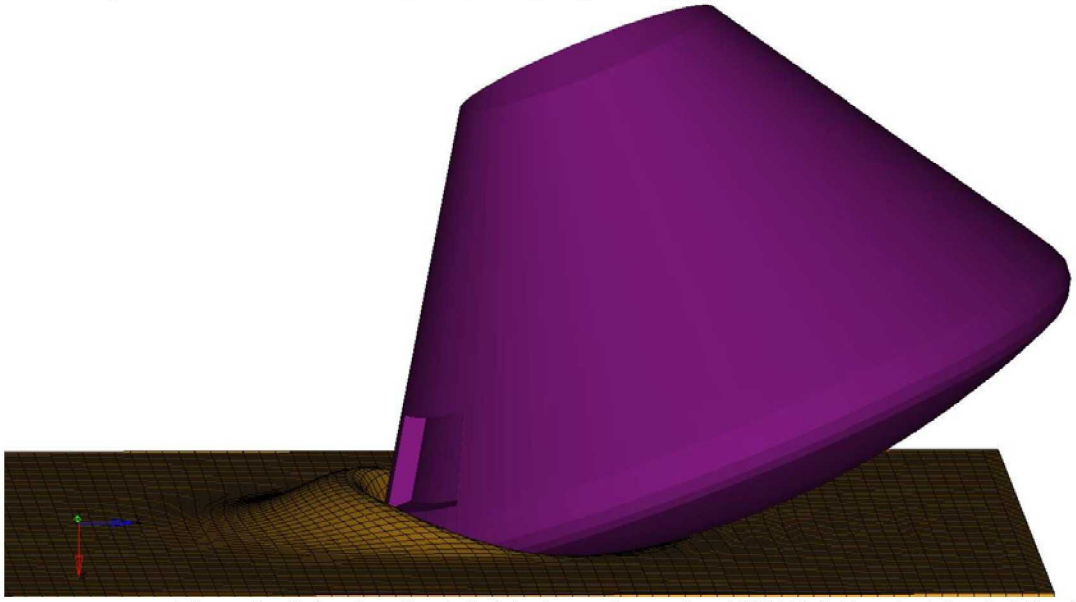

Figure 9. Orion Landing Model, shown impacting KSC High Density Flooded Sand

3.3 Coordinate System and Angle Definitions

The X-axis of the global coordinate system is defined positive in the downward direction. Gravity is applied in the model along the positive X-axis. The Y- and Z-axes are horizontal, with the negative Z-axis in the direction of the CM horizontal velocity. The CM CG accelerations are output in a local coordinate system that rotates and translates along with the CM. The CM local coordinate system is oriented with the X-axis aligned with the CM main axis and positive from the top of the CM downward. The Z-axis is negative towards the side of the CM on which initial soil contact will occur. The CG is offset 5.7 inches in the negative direction along the local CM Z-axis, and is 52.6 inches along the local CM X-axis above the bottom center point of the heat shield.

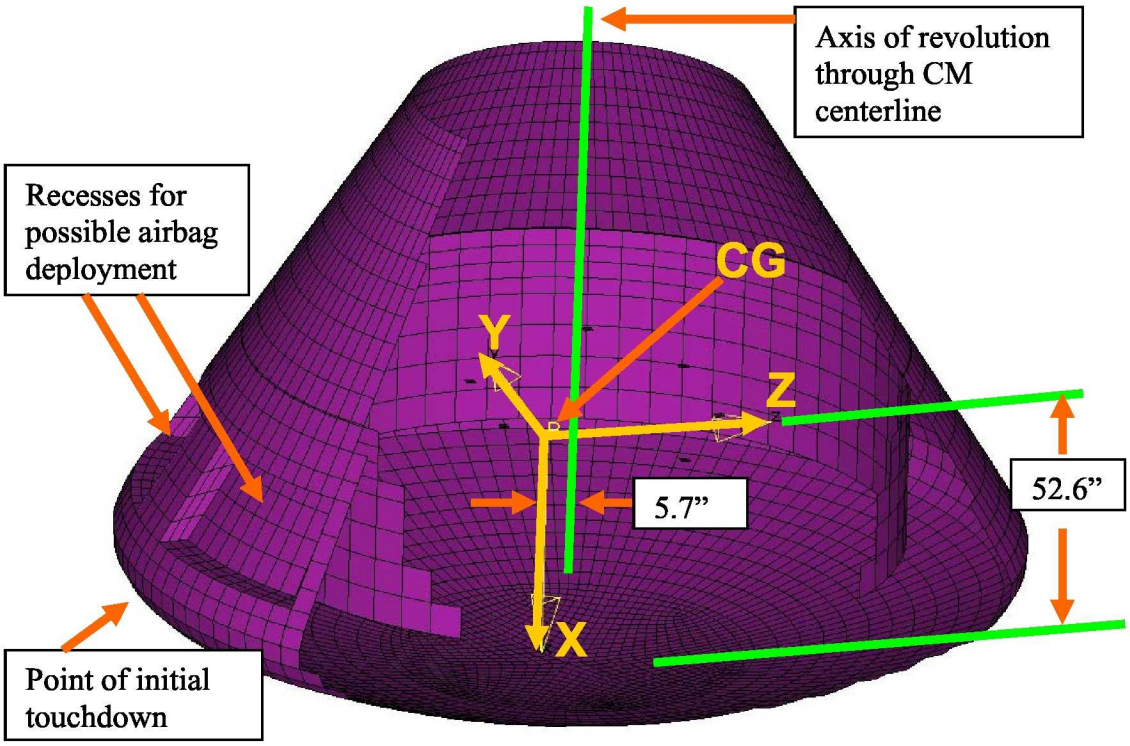

Figure 10. CM cut-away view showing Local Coordinate System

The hang angle is defined as the fore/aft pitch rotation about the local Y-axis. The nominal 28° hang angle represents a -28° rotation about the Y-axis. The roll angle is defined as the rotation about the global X-axis.

3.4 Contact Definition

An automatic surface-to-surface contact with the option SOFT = 1 was used between the CM and the soil in LS-DYNA. SOFT = 1 is used to provide effective contact between materials with very different elastic moduli, or stiffnesses, which is the case for the rigid CM and the different soils. An elastic modulus corresponding to steel was specified for the rigid CM for contact purposes ($E = 2.9 \times 10^7$ psi). Both static and dynamic friction coefficients were set to 0.5. Other options specified in the contact were SBOPT = 5 and DEPTH = 5, which invoke additional logic to ensure smooth sliding and to check for edge-to-edge penetrations between elements [ref. 6].

3.5 Simulation General Parameters

A time step scale factor (TSSFAC) between 0.1 and 0.3 was specified to improve the contact stability. The value of TSSFAC was adjusted for each case until spikes in the contact forces were minimized, with different values resulting for different soil models. All simulations were executed in double precision using an SMP version of LS-DYNA on four CPUs. Each simulation was executed for 2 seconds. A 10,000 Hz sampling rate was used for the outputs.

4.0 Summary of Simulation Results

LS-DYNA simulations were performed for ten landing conditions on the eight different soil models, resulting in a matrix of eighty cases. Table 1 summarizes the ten different combinations of landing

conditions evaluated, with the parameter changed from the baseline conditions highlighted in red bold face print for cases 2-10. All acceleration time-history curves were filtered with a 60-Hz Butterworth filter, and peak values were extracted from the filtered data. The contact force data presented was not filtered. The acceleration and contact force time-history plots are shown for 0.5 seconds, since the peak values occur within this time. The pitch angle was plotted for the full 2.0 seconds of simulation time, allowing evaluation of the potential for rollover. Appendices B and C contain graphs of the contact force and CM kinetic energy time-histories for all simulation cases.

Table 1. Simulation Cases

Case	Hang Angle	Roll Angle	Vertical Velocity	Horizontal Velocity
1	28°	0°	25 ft/s	20 ft/s
2	**18°**	0°	25 ft/s	20 ft/s
3	**38°**	0°	25 ft/s	20 ft/s
4	28°	**45°**	25 ft/s	20 ft/s
5	28°	**90°**	25 ft/s	20 ft/s
6	28°	**180°**	25 ft/s	20 ft/s
7	28°	0°	**15 ft/s**	20 ft/s
8	28°	0°	**35 ft/s**	20 ft/s
9	28°	0°	25 ft/s	**0 ft/s**
10	28°	0°	25 ft/s	**40 ft/s**

Figure 11 illustrates the 10 landing condition cases, showing the orientations and the vector direction of the initial velocity. Note the orientation change for the capsule for the roll cases (cases 4-6).

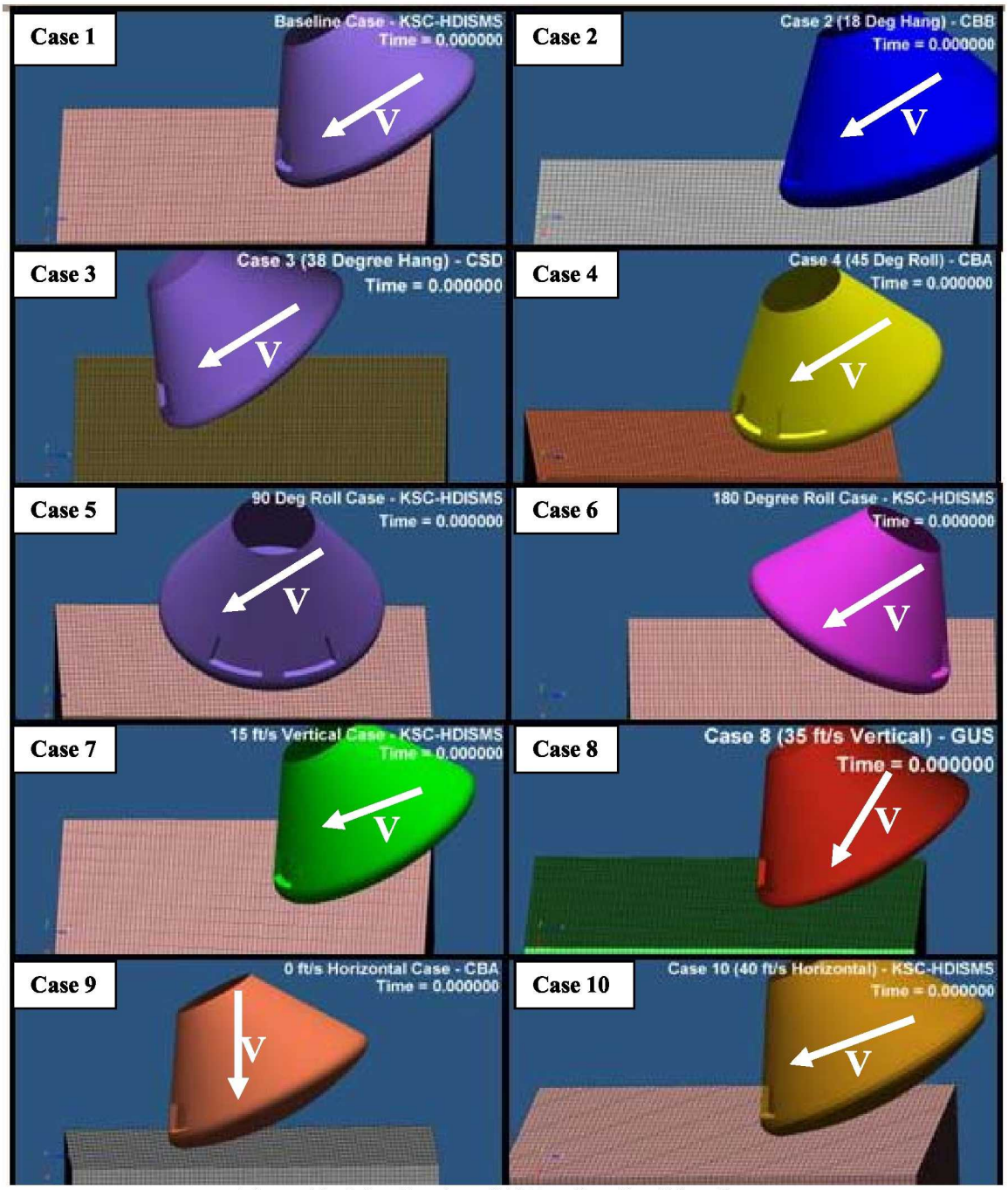

Figure 11. Visualization of 10 Landing Condition Cases

4.1 Summary of X-axis Acceleration Results

Table 2 shows the peak X-axis accelerations for each of the ten cases, on all eight soils, and these results are plotted in Figure 12. The Cuddeback A soil and Gantry Unwashed Sand produce the highest peak X-axis accelerations, while the Carson Sink Wet and KSC Low Density Dry Sand produce the lowest. Although the Cuddeback A soil has the highest X-axis acceleration peak for the baseline landing conditions, the Gantry Unwashed Sand X-axis acceleration peak is the highest at a hang angle of 18°. The CM X-axis acceleration peaks are primarily driven by the landing conditions, but the soil also has a

significant effect. The lowest X-axis acceleration peak on the Cuddeback A soil is higher than the highest X-axis acceleration on the Carson Sink Wet soil.

The general trends on all the soils can be summarized as follows:

- The CM X-axis accelerations increase as the vertical velocity increases.
- As the hang angle decreases, the X-axis acceleration peak increases.
- The peak X-axis acceleration is reduced as the horizontal velocity is increased.
- The peak X-axis acceleration increases as the roll angle increases.
- The hang angle has a comparatively large effect on the peak X-axis acceleration.

Table 2. CM X-axis Peak Accelerations for 80 Cases (units are g's)

soil										
	case 1	case 2	case 3	case 4	case 5	case 6	case 7	case 8	case 9	Case 10
	Base-line	18° hang	38° hang	45° roll	90° roll	180° roll	15 ft/s V	35 ft/s V	0 ft/s H	40 ft/s H
CBA	12.2	19.5	9.7	12.1	12.2	14.8	9.0	16.8	12.5	9.1
CBB	5.6	12.3	5.5	6.1	6.9	8.4	3.1	11.0	7.4	4.5
CSD	5.6	9.8	3.6	5.9	6.5	7.4	2.7	9.4	6.5	4.6
CSW	4.5	8.1	3.0	4.6	5.2	6.1	2.1	8.0	5.3	3.5
KSC_LDDS	3.9	9.3	2.6	4.2	5.0	6.0	1.8	8.4	5.4	3.0
KSC_HDISMS	5.8	13.2	4.5	6.1	7.1	8.6	2.7	11.6	7.6	4.6
KSC_HDFS	6.3	12.7	4.9	6.1	6.7	8.1	2.9	11.3	7.1	4.6
GUS	8.9	19.7	6.1	9.2	10.2	12.5	4.3	16.5	11.1	7.2

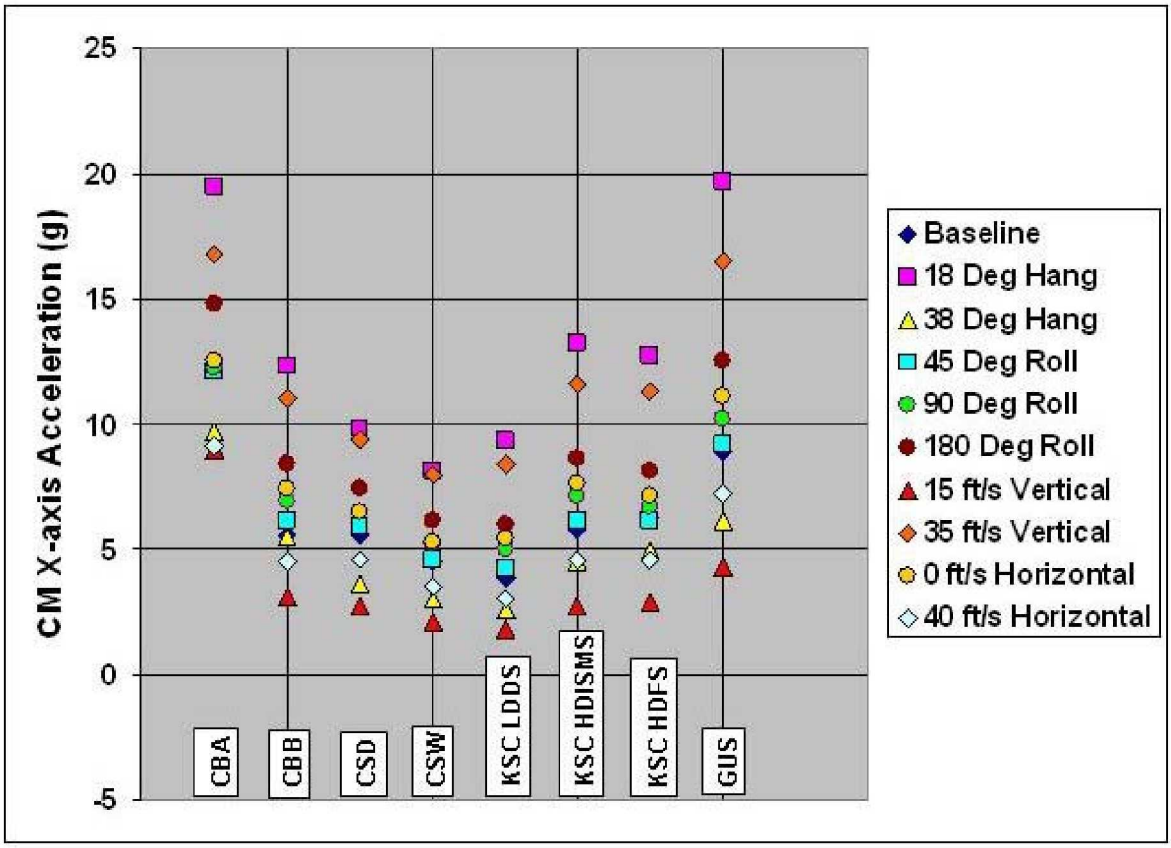

Figure 12. Plot of CM X-axis Peak Accelerations for 80 Cases

4.2 Summary of Z-axis Acceleration Results

Table 3 shows the peak Z-axis accelerations for each of the ten cases, on all eight soils, and these results are plotted in Figure 13. The CM Z-axis acceleration ranking of the landing cases across the different soils is similar, with some exceptions. The Z-axis accelerations are the lowest for the 180° roll angle case; however, this landing condition has inherent reduced stability that results in rollover of the CM for all the soils in this study except the KSC Low Density Dry Sand and High Density Flooded Sand.

The general trends on all the soils can be summarized as follows:

- The CM Z-axis accelerations increase as the vertical velocity increases.
- The CM Z-axis accelerations increase as the horizontal velocity increases.
- The CM Z-axis accelerations decrease as the roll angle increases.
- The Z-axis accelerations are higher for both the 18° and 38° hang angles, compared to the 28° baseline, except on the Cuddeback A soil, where the 38° hang angle case is lower than the baseline.

The following soil effects can be noted:

- Z-axis accelerations on the Carson Sink Dry soil are not affected by the hang angle.
- The harder soils generally exhibit a larger sensitivity to the input parameters.

Table 3. CM Z-axis Peak Accelerations for 80 Cases (units are g's)

soil	case 1	case 2	case 3	case 4	case 5	case 6	case 7	case 8	case 9	case 10
	Base-line	18° hang	38° hang	45° roll	90° roll	180° roll	15 ft/s V	35 ft/s V	0 ft/s H	40 ft/s H
CBA	21.4	19.8	27.2	18.2	14.3	5.7	13.0	26.7	15.5	25.9
CBB	11.5	12.5	16.9	10.1	7.4	4.4	8.7	15.7	7.2	15.8
CSD	10.0	10.1	10.3	8.9	6.2	3.0	6.5	13.8	7.3	12.0
CSW	7.6	8.4	7.9	6.7	4.7	1.8	5.3	10.7	5.4	9.0
KSC_LDDS	5.8	8.5	7.1	5.2	3.5	1.7	4.3	9.8	4.0	7.9
KSC_HDISMS	10.1	12.6	13.1	8.8	6.6	3.9	7.2	14.5	7.4	12.8
KSC_HDFS	10.1	11.5	11.3	8.4	6.6	3.9	6.0	12.9	7.8	11.6
GUS	13.1	19.3	15.6	11.6	8.6	5.2	9.2	21.1	10.4	16.0

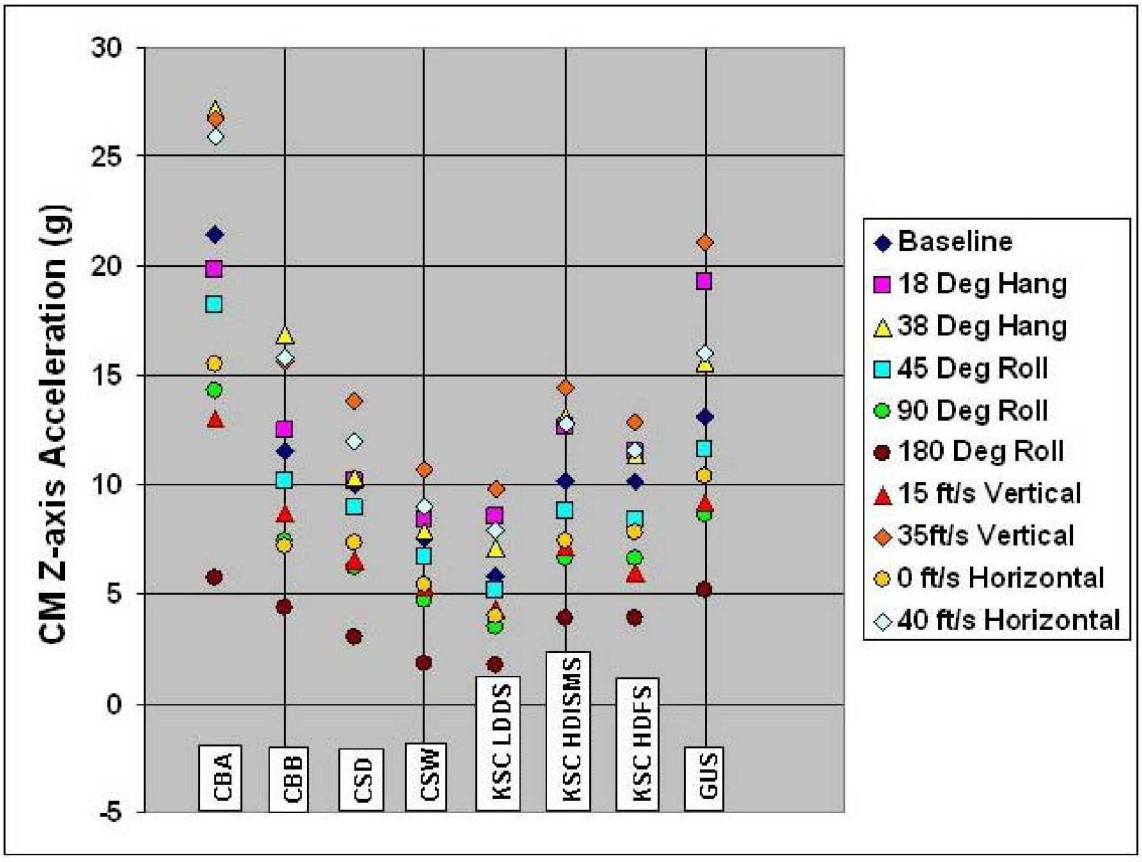

Figure 13. Plot of CM Z-axis Peak Accelerations for 80 Cases

4.3 Summary of Soil Crater Depth

Table 4 lists the depth of vertical penetration into the soil by the CM for all the simulations, and these results are plotted in Figure 14. These depths were determined from contour plots of the soil deformation. Analysis of the soil penetration depth is relevant because it is desired to correctly model the physical behavior of the soil; when tests are performed, soil depth and/or berm height are additional variables available for correlation between simulation and test data. The largest penetration occurs for the larger hang angle case and the larger horizontal and vertical velocity cases. The soil penetration is lowest for the 180° roll case, as this CM landing orientation induces the CM to pitch forward onto the bottom of the

heat shield, rather than digging in at the edge of the heat shield as the baseline case does. The penetration depths on the Cuddeback A soil and the Gantry Unwashed Sand are lower than all the other soils for each set of landing conditions, and generally have comparable values across the different landing conditions simulated. However, the Gantry Unwashed Sand has a lower sensitivity to the vertical velocity. For the KSC High Density In-Situ Moisture Sand, approximately the same soil penetration occurred for the 18° hang angle, 90° roll angle, and 0 ft/s horizontal velocity cases. The Carson Sink Wet soil and KSC Low Density Dry Sand cases have the largest penetration depth for the baseline, 38° hang angle, 35 ft/s vertical velocity, and 40 ft/s horizontal velocity cases.

The general trends on all the soils can be summarized as follows:

- The soil penetration increases as the hang angle increases.
- The soil penetration increases as the horizontal velocity increases.
- The soil penetration increases as the vertical velocity increases.
- Soil penetration is reduced as the roll angle is increased.
- Except for the Cuddeback A soil, the higher horizontal velocity has a larger effect on the penetration depth than the higher vertical velocity.

The following soil effect can be noted:

- The softer the soil, the more sensitive the resulting hole depth is to either the hang angle or the horizontal velocity.

Table 4. Depth of Soil Penetration (global X-axis – units are inches)

soil	case 1	case 2	case 3	case 4	case 5	case 6	case 7	case 8	case 9	case 10
	Base-line	18° hang	38° hang	45° roll	90° roll	180° roll	15 ft/s V	35 ft/s V	0 ft/s H	40 ft/s H
CBA	6.5	4.6	8.2	6.3	5.3	4.1	4.3	8.2	5.3	7.7
CBB	11.4	8.5	15.0	11.0	9.2	8.7	9.2	13.0	8.8	14.5
CSD	13.7	10.1	17.3	12.8	11.2	8.5	10.6	16.5	10.9	17.6
CSW	16.8	12.4	22	15.7	13.6	10.3	13.3	20.0	13.4	23.1
KSC_LDDS	16.9	13.9	23.7	15.6	13	10.2	15.9	18.3	12.8	24.6
KSC_HDISMS	11.5	8.9	15.3	10.7	9.0	7.0	10.1	12.8	8.9	15.7
KSC_HDFS	12.2	9.6	18.1	11.0	8.9	7.0	12.5	13.1	8.9	17.5
GUS	7.9	5.2	11.1	7.0	6.0	4.8	7.2	8.8	6.0	10.5

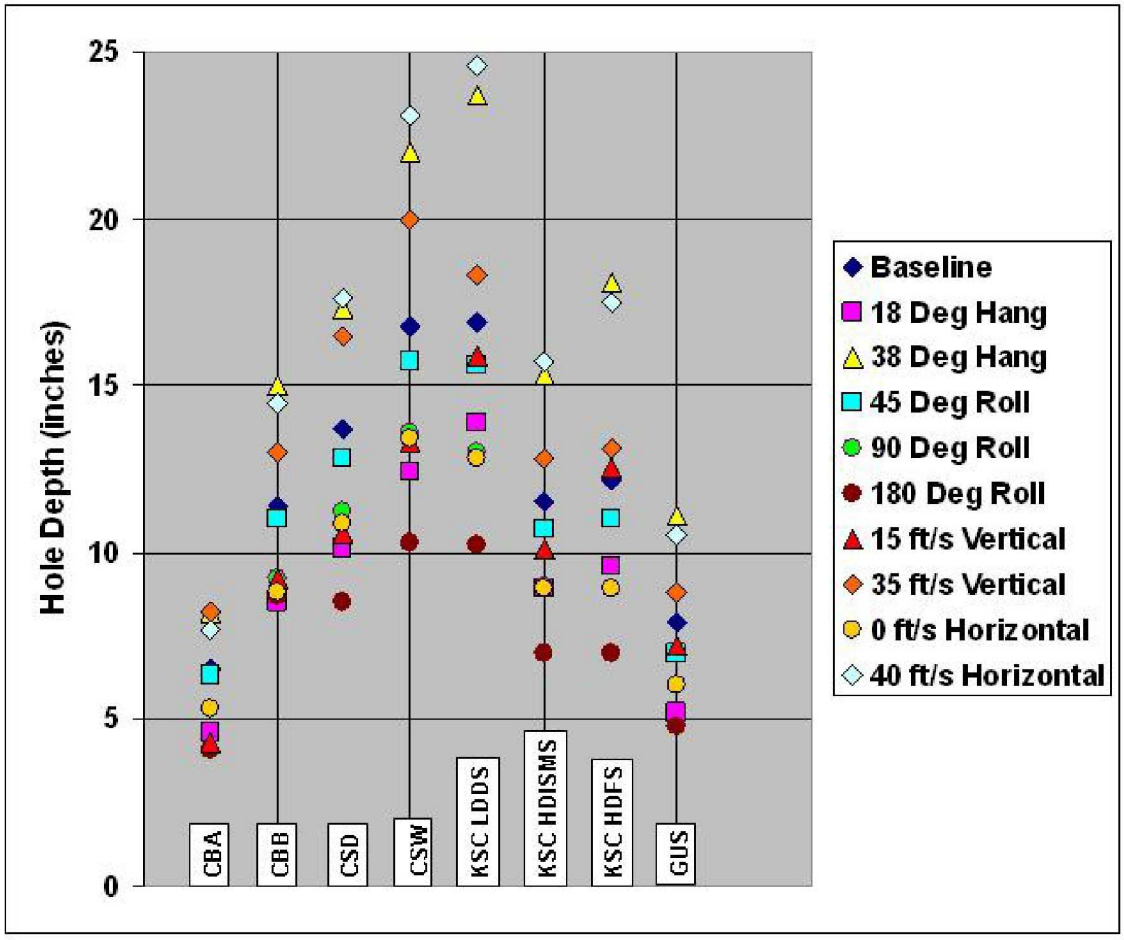

Figure 14. Plot of Depth of Soil Penetration (global X-axis)

The berm heights are presented and discussed in Appendix D.

5.0 Detailed Simulation Results

5.1 Baseline Landing Conditions Case Results

The baseline landing conditions were 25 ft/s vertical velocity, 20 ft/s horizontal velocity, 28° pitch angle, 0° roll angle, with a (static and dynamic) friction coefficient between the CM and soil of 0.5. The friction coefficient was not changed in any of the simulations performed for this report. Figure 15 shows the model with the baseline input conditions impacting the KSC High Density In-Situ Moisture Sand. Figure 16 presents a sequence of simulation animation snapshots illustrating the behavior of the baseline case on the KSC High Density In-Situ Moisture Sand. Upon initial impact, the CM pitches down as it digs into the soil, bounces back out of the hole in the soil that is dug, and then rocks forward slightly into the depression in the soil. Throughout this report, where similar sequences of simulation snapshots are shown to illustrate the landing behavior, different soil models were chosen, with the intention of illustrating the range of soil types throughout the report, or illustrating distinctive behavior of a particular soil for a specific landing scenario.

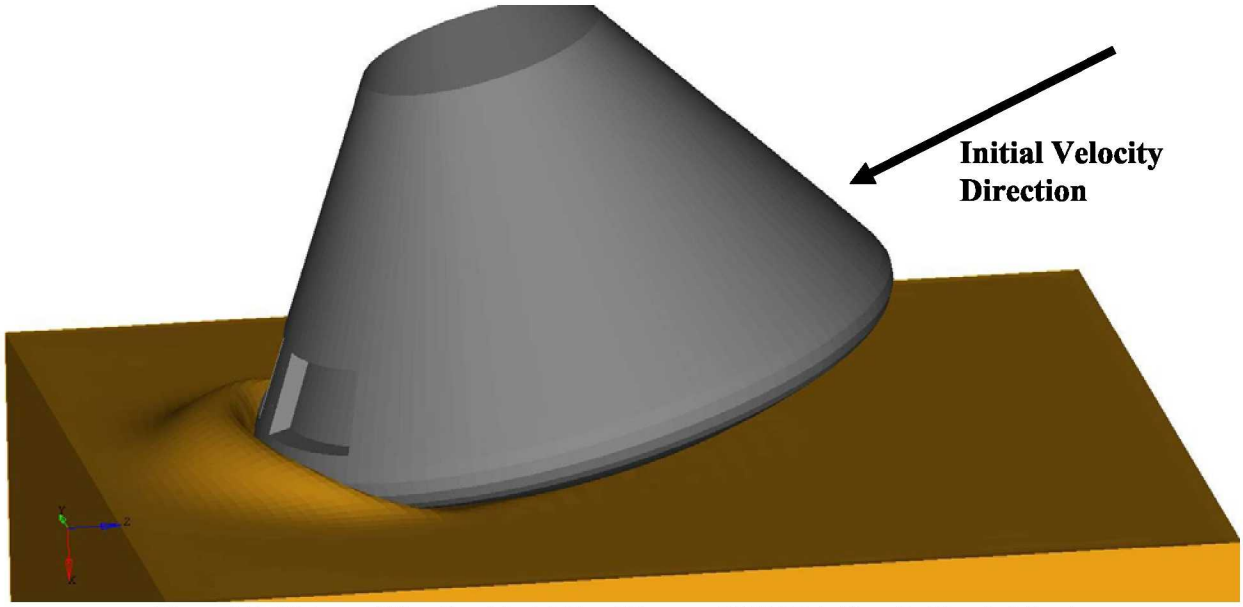

Figure 15. Picture of Baseline Model Conditions on KSC High Density Flooded Sand

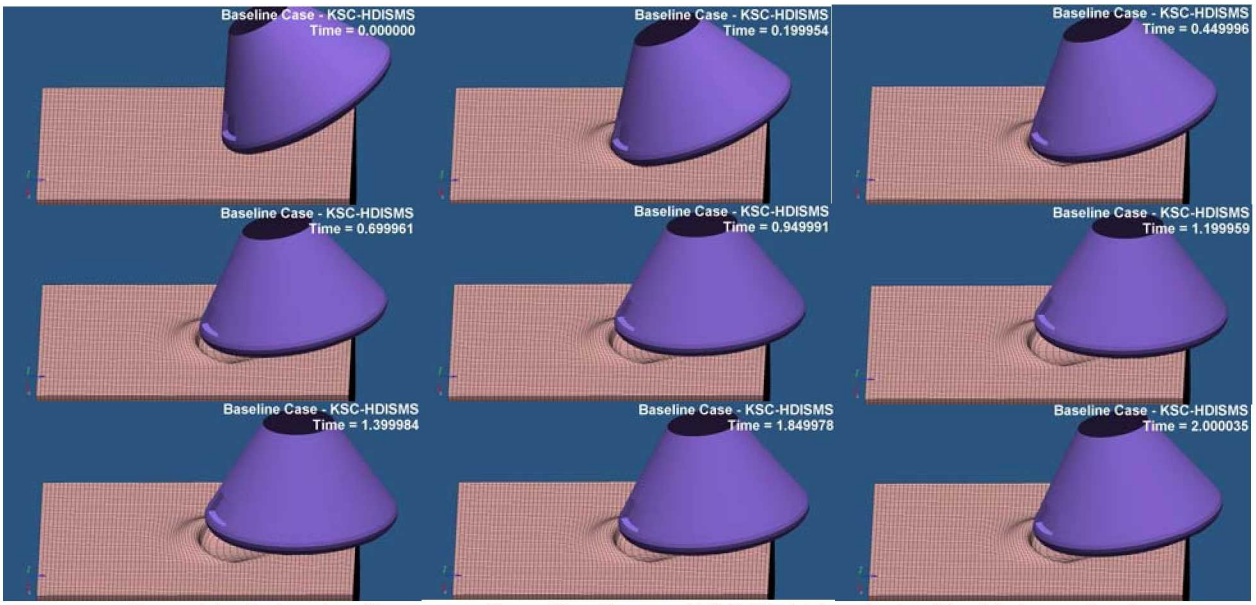

Figure 16. Animation Sequence of Baseline Case on KSC High Density In-Situ Moisture Sand

The CM X-, Y-, and Z-axis accelerations are shown in Figure 17, Figure 18, and Figure 19, respectively. The highest peak accelerations occur when impacting the Cuddeback A soil, followed by the Gantry Unwashed Sand. The acceleration time-histories for the Cuddeback A and Gantry Unwashed Sand cases share the same initial slope, but the accelerations in the Gantry Unwashed Sand model drop off earlier, resulting in a lower peak. Only the Cuddeback A soil model simulation has a second acceleration spike occurring at 0.35 seconds that results when the CM bounces back and impacts the soil on the bottom of the heat shield. On the other soils, instead of bouncing back, the soil deforms sufficiently upon the initial impact that the CM rolls back along the bottom of the heat shield, as illustrated in Figure 16. The lowest peak X- and Z-axis accelerations occur when impacting the KSC Low Density Dry Sand. The other 5 soils have roughly comparable X-axis acceleration peaks, but Cuddeback B has a slightly higher Z-axis acceleration peak. The shape of the Cuddeback B and KSC High Density In-Situ Moisture Sand X- and Z-axis acceleration curves are very similar, but of different magnitudes.

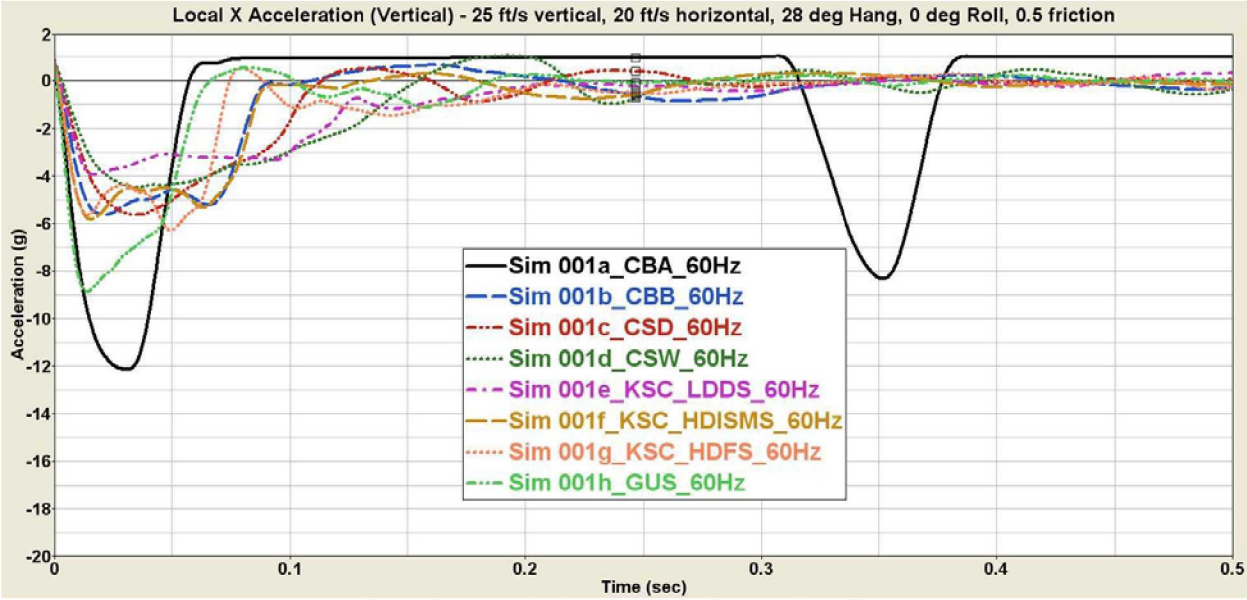

Figure 17. X-axis Accelerations for Baseline Case

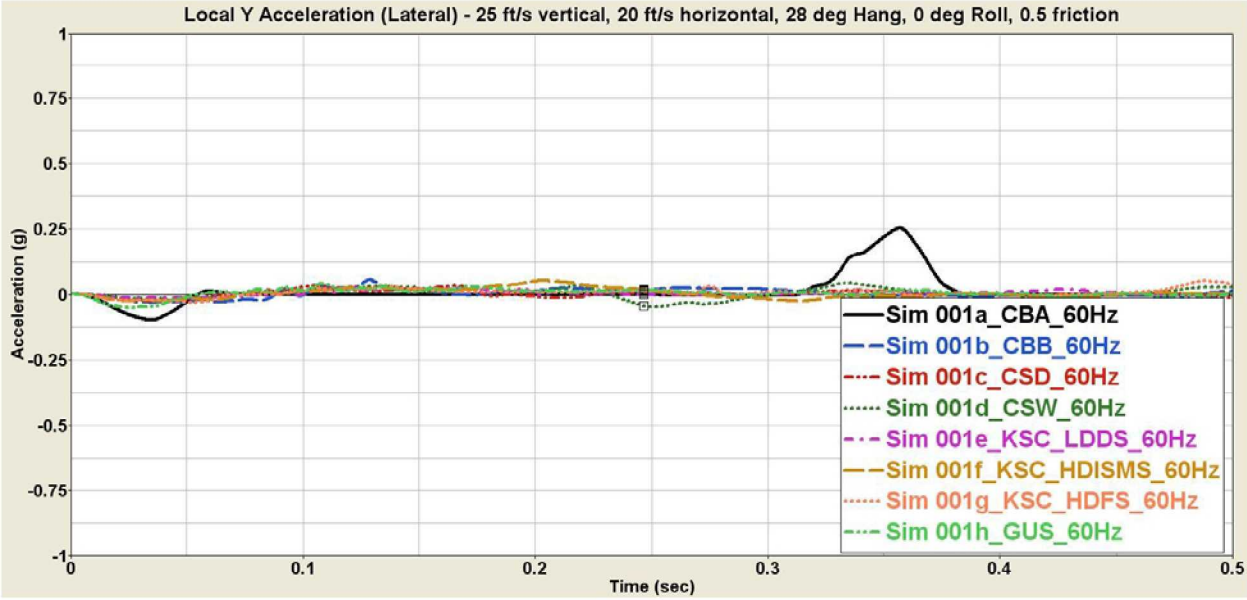

Figure 18. Y-axis Accelerations for Baseline Case

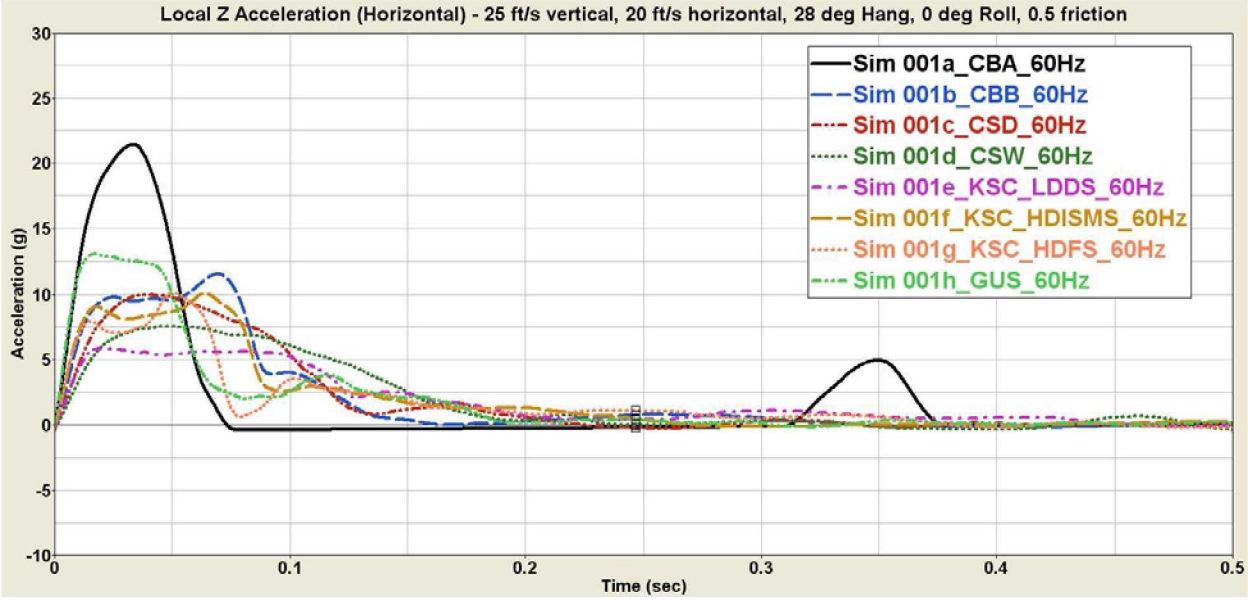

Figure 19. Z-axis Accelerations for Baseline Case

The vertical, lateral, and longitudinal contact forces between the CM and the soil are shown in Figure 20, Figure 21, and Figure 22, respectively. The contact forces mostly parallel the trends of the accelerations, since the soil stiffness plays a large part in these forces, together with the initial conditions of the CM just prior to impact. However, the forces plotted here are measured in the global coordinate system so there is not a direct correlation with the CM accelerations reported in the CM local coordinate system. The horizontal contact forces are greater than half the vertical contact forces, despite the specified coefficient of friction of 0.5 because deformation of the soil also contributes to the directionality of the contact forces when the CM digs into the soil.

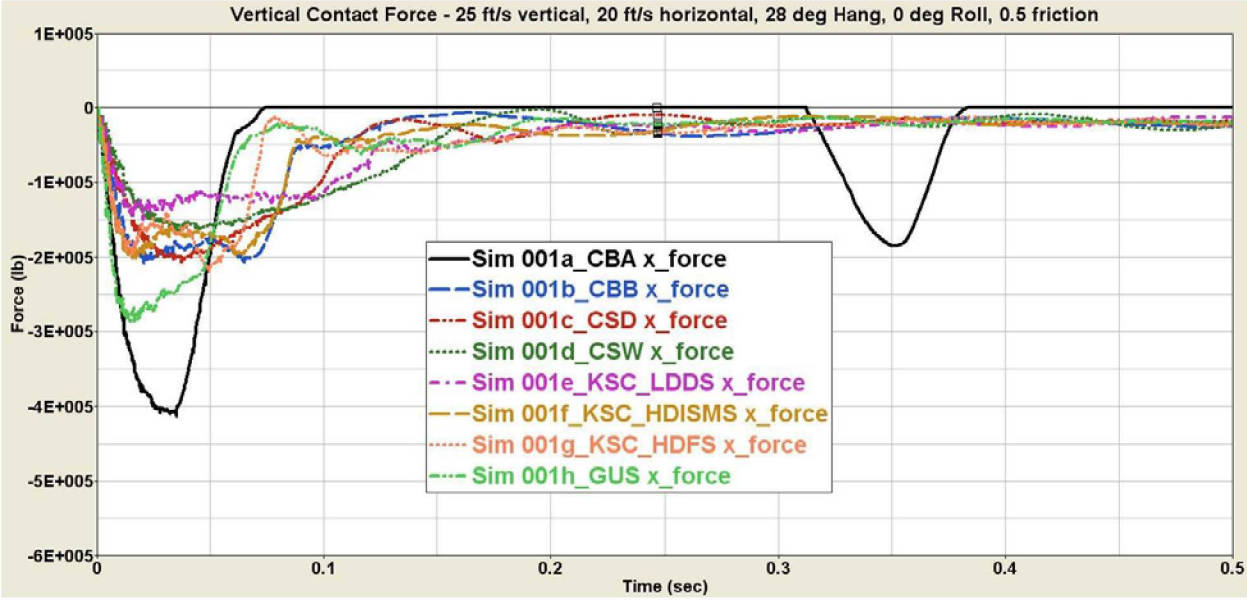

Figure 20. X (Vertical) Contact Force for Baseline Case

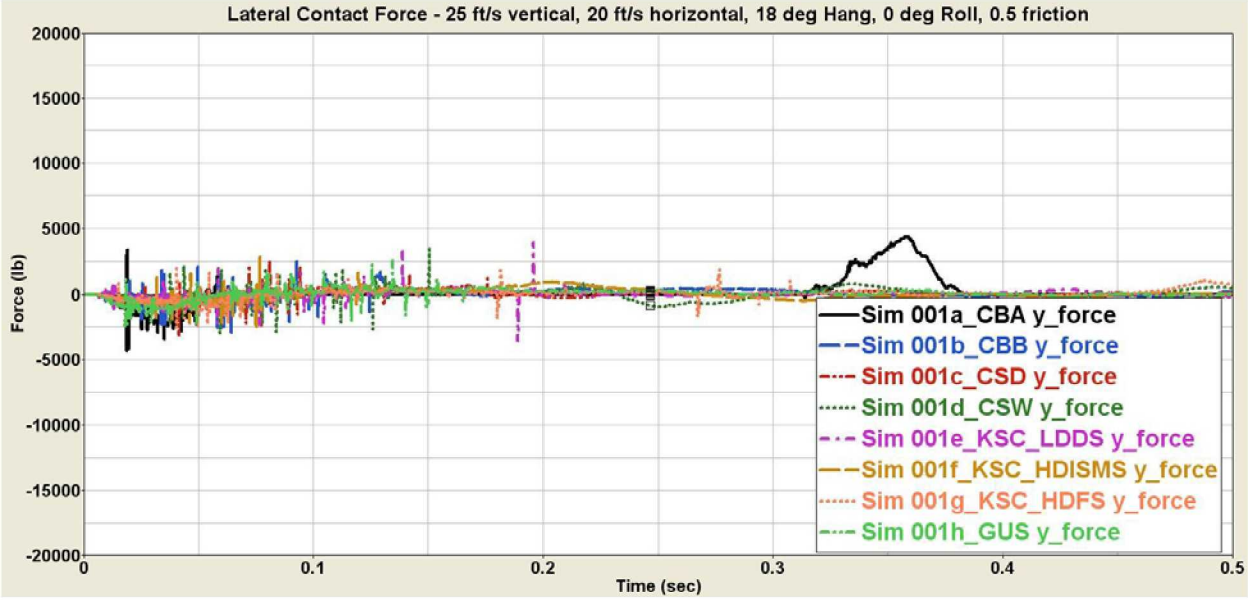

Figure 21. Y (Lateral) Contact Force for Baseline Case

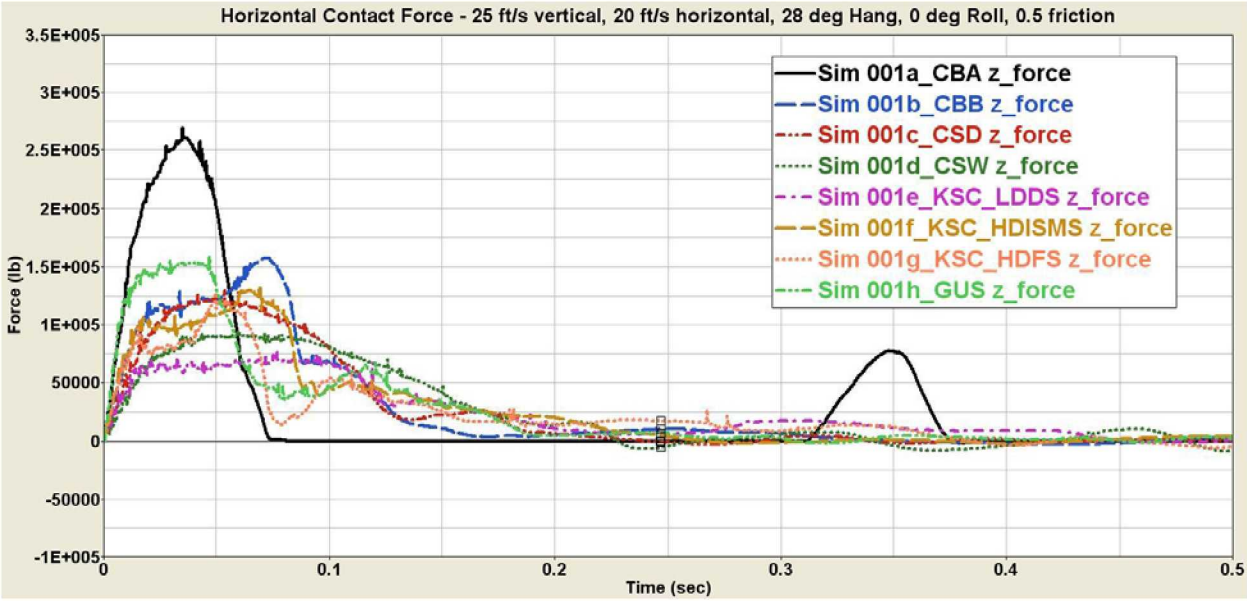

Figure 22. Z (Longitudinal) Contact Force for Baseline Case

Figure 23 shows the effect of the eight soil models on the pitch angle time-histories for the baseline case. The largest and earliest pitch angle change occurs when impacting the Cuddeback A soil. The KSC Low Density Dry Sand and High Density Flooded Sand, and the Carson Sink Wet and Dry soils reach a fixed pitch attitude within the two seconds duration of the simulation, indicating that they have come to rest. A pitch angle of 45° or higher was considered indicative of an unstable response, and thus likely to rollover. The CM does not become unstable for the baseline case on any of the soil models.

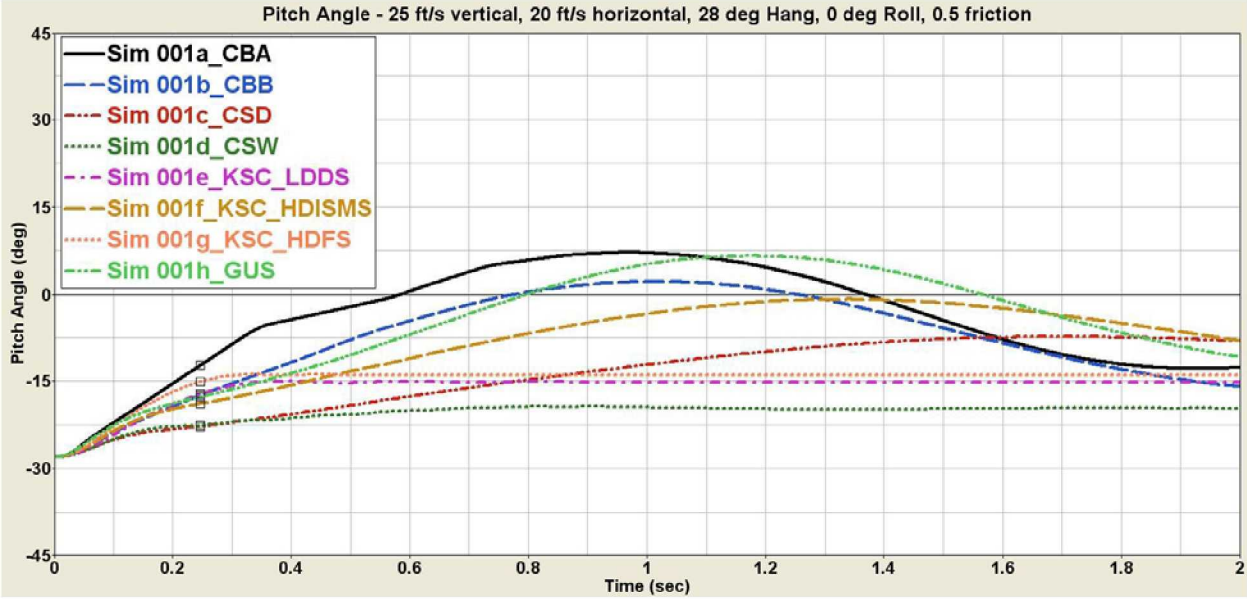

Figure 23. CM Pitch for Baseline Case

Figure 24 shows the CM kinetic energy versus time curves for the eight soil model cases. The higher acceleration cases have more abrupt velocity changes, and thus exhibit the sharpest decrease in the kinetic energy. The Cuddeback A soil is very stiff and has the highest shear strength envelope of all the soils, a combination that produces a more elastic soil impact. As a result, after the initial impact on the Cuddeback A soil, which is complete by approximately 0.06 seconds, the leading edge of the CM rebounds upward from the soil. The CM rotates backward until a secondary impact on the bottom of the heat shield occurs at approximately 0.35 seconds. During the rebound, the CG falls further downward, converting gravitational energy into kinetic energy, which explains why the Cuddeback A kinetic energy curve shown in Figure 24 increases from 0.1 to 0.3 seconds. The KSC Low Density Dry Sand and Carson Sink Wet soils exhibit the slowest reduction in the kinetic energy over time, due to the low stiffness and low shear strength of these two soils.

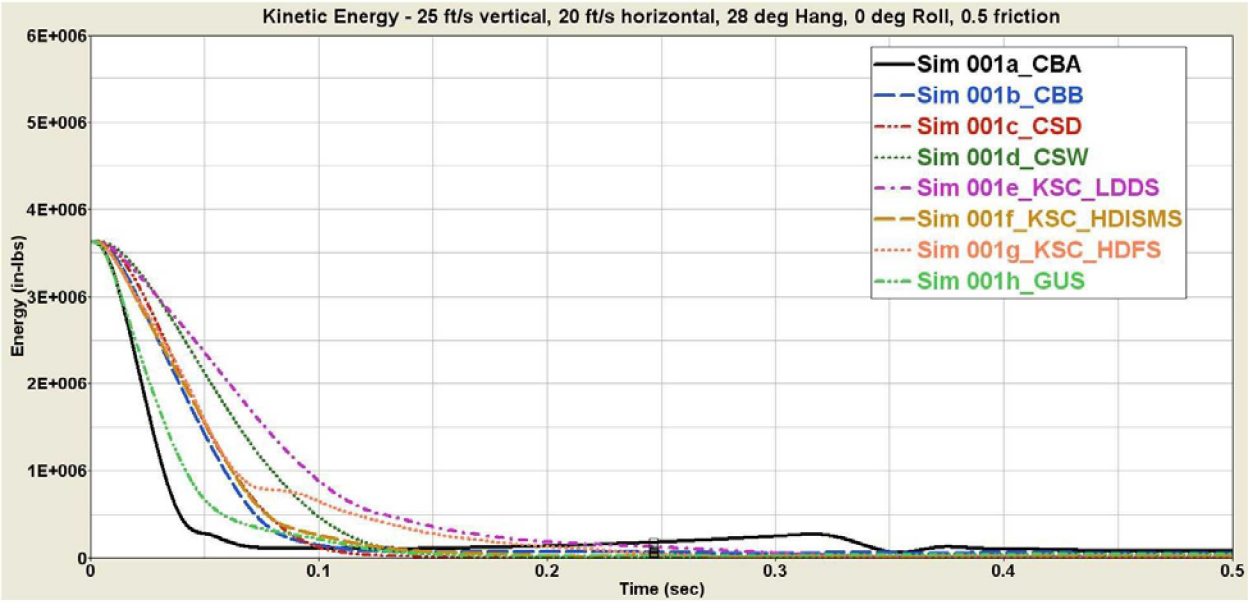

Figure 24. CM Kinetic Energy for Baseline Case

Figure 25 shows the soil internal energy versus time for the baseline case. The Cuddeback A soil gains the least internal energy, indicating a more elastic impact with a larger rebound. Although not shown here, the motion of the CM continues to 2 seconds after the initial impact. The Gantry Unwashed Sand initially absorbs energy almost as quickly as the Cuddeback A soil, and also eventually absorbs more overall energy due to its lower shear strength. The Carson Sink Wet soil eventually absorbs about the same amount of energy as the KSC High Density In-Situ Moisture Sand, but with a different time history.

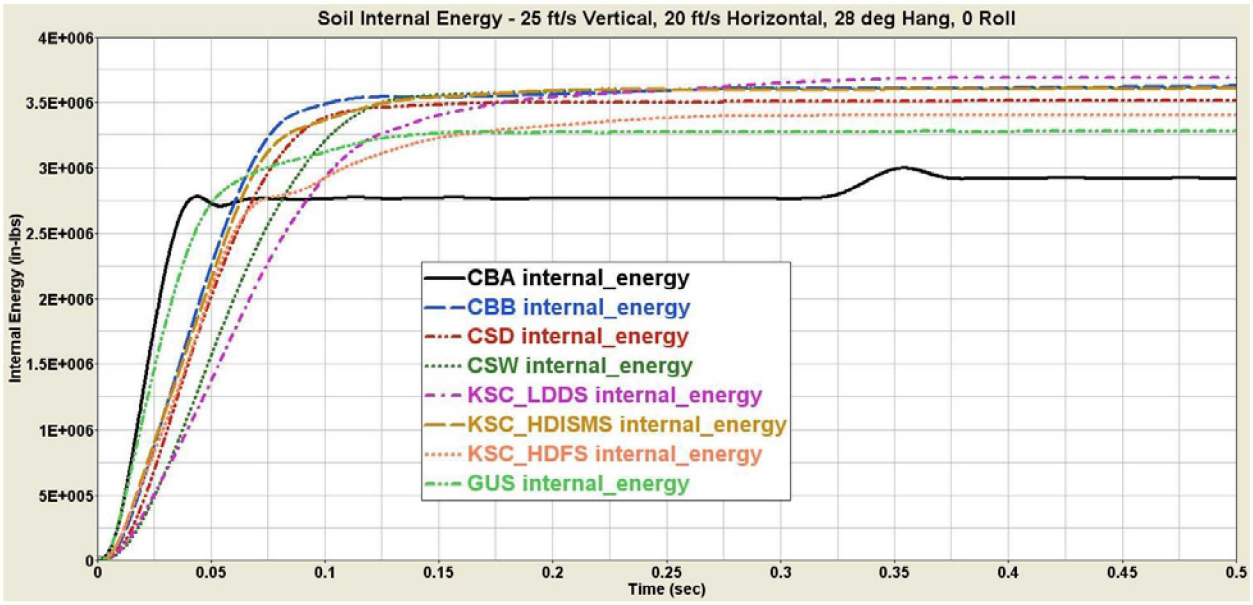

Figure 25. Soil Internal Energy for Baseline Case

Figure 26 shows the soil kinetic energy for the eight soils for the baseline case. The Cuddeback A soil is displaced the least, and thus has the lowest kinetic energy gained. Similarly, the KSC Low Density Dry Sand and Carson Sink Wet soil have the largest kinetic energy peaks. The soil kinetic energy plot indicates that the Carson Sink Wet soil gains more kinetic energy than the KSC High Density In-Situ Moisture Sand, suggesting that the CSW soil is more easily displaced, and thus absorbs more energy through conversion into kinetic energy.

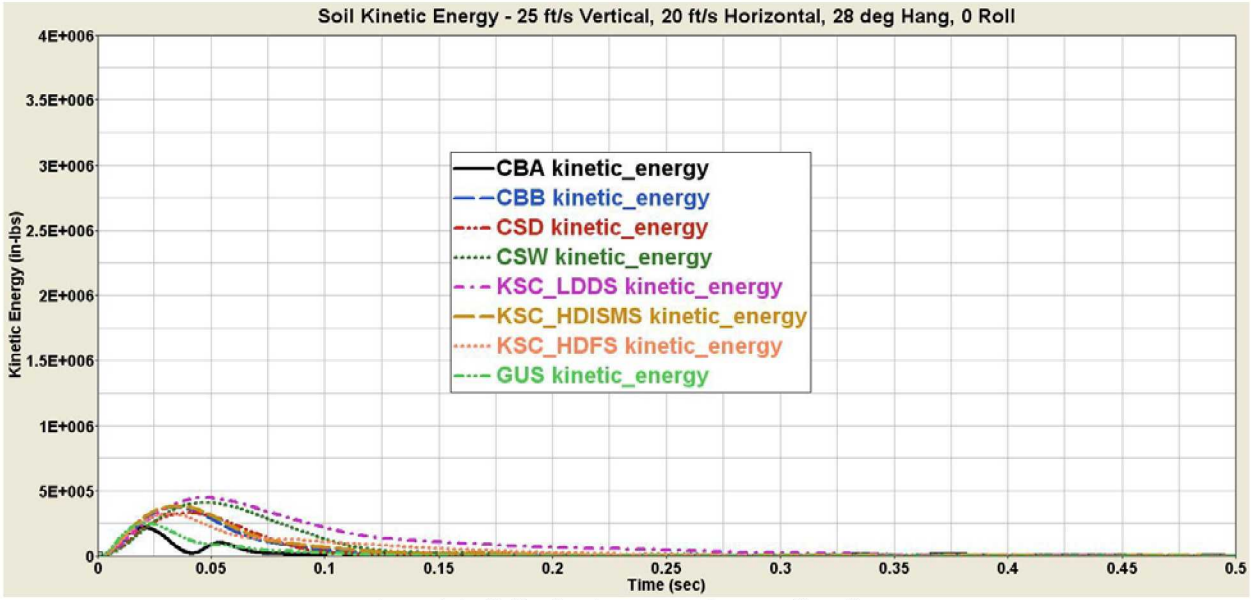

Figure 26. Soil Kinetic Energy for Baseline Case

5.2 18° Hang Angle Case

For the second simulation case, the impact hang angle was adjusted from the nominal 28° to 18°, and the simulation was rerun on all eight soil models. Figure 27 presents a sequence of simulation snapshots of the model illustrating the behavior of the 18° hang angle case on the Cuddeback B soil. The CM comes to rest quickly in a highly damped manner in this simulation run, slipping at the interface between the soil and the CM so that the CM can rotate to an even shallower pitch angle.

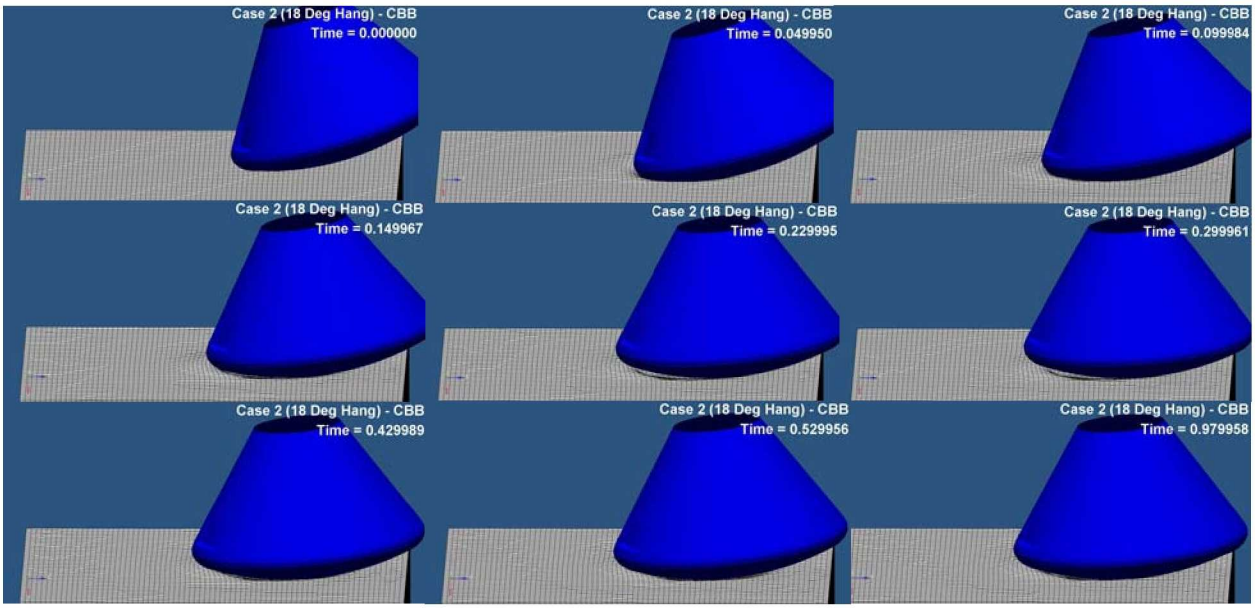

Figure 27. Animation Sequence of 18° Hang Angle Case on Cuddeback B

The CM X-, Y-, and Z-axis accelerations for the 18° hang angle case are shown in Figure 28, Figure 29, and Figure 30, respectively. In the simulations, Cuddeback A and the Gantry Unwashed Sand produce comparable maximum X- and Z-axis accelerations. However, the Gantry Unwashed Sand acceleration

peaks are of shorter duration. As mentioned in the summary, the reduction of the hang angle increases the severity of the impact along the CM X-axis.

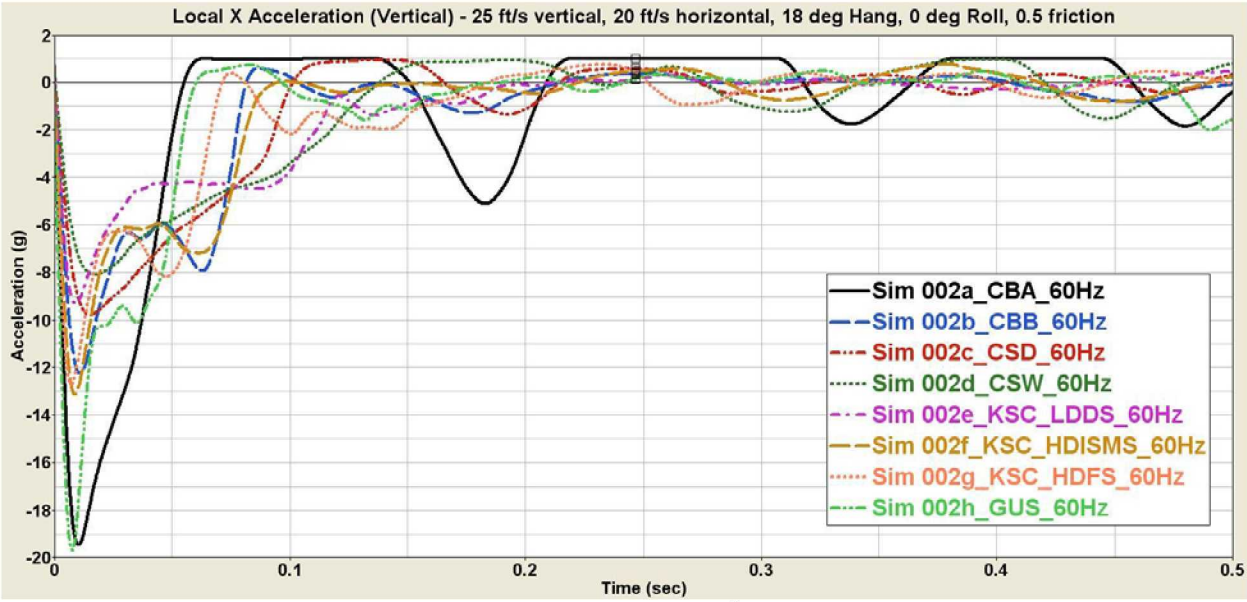

Figure 28. X-axis Accelerations for 18° Hang Angle Case

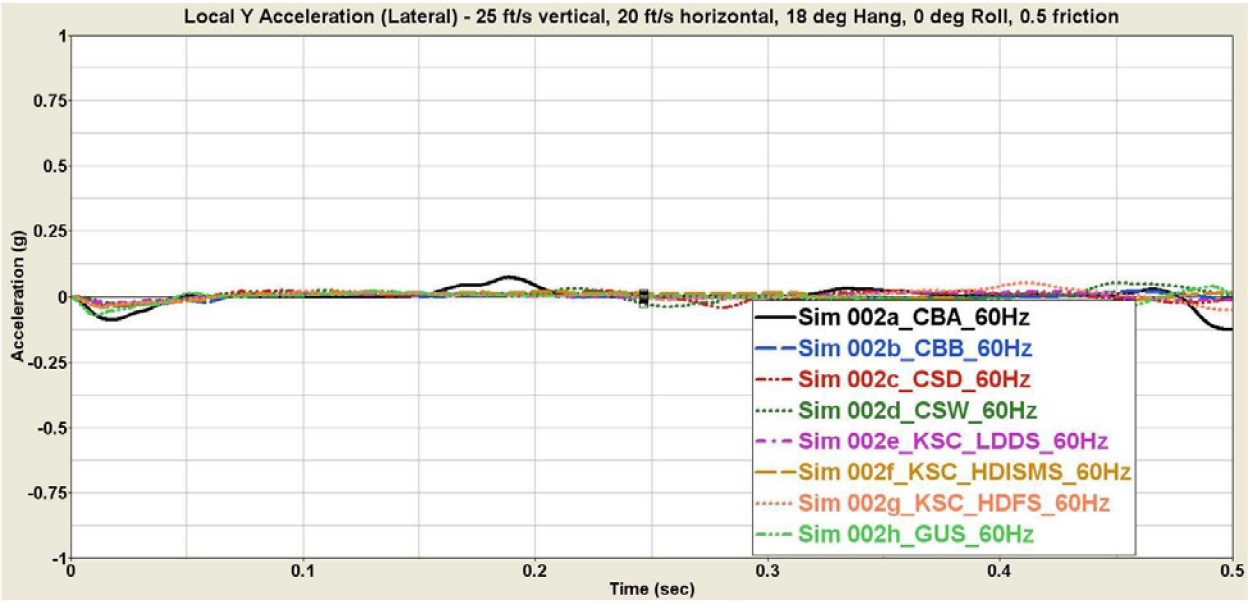

Figure 29. Y-axis Accelerations for 18° Hang Angle Case

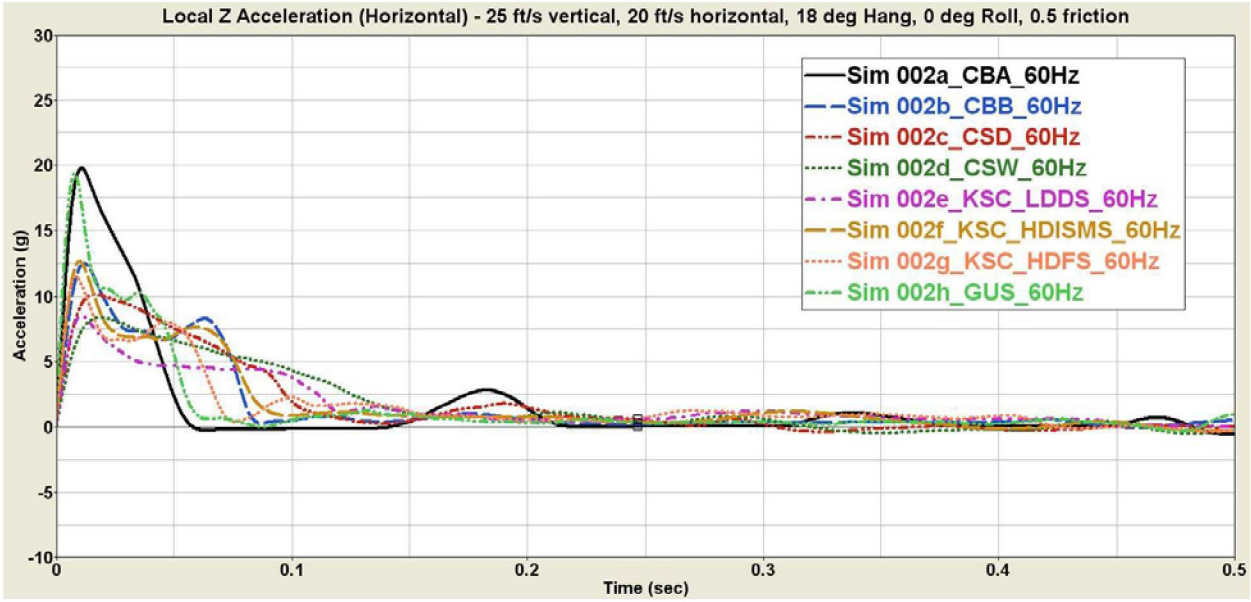

Figure 30. Z-axis Accelerations for 18° Hang Angle Case

Figure 31 shows the pitch angle time histories of the 18° hang angle case on the eight soil models. The largest pitch angle change occurs on the Cuddeback A soil, but this case is still relatively stable. Overall, the pitch angle response is very stable for the 18° hang angle case. There is less pitch angle change compared to the baseline case, and the CM comes to rest within the 2-second simulation period on all soils except Cuddeback A.

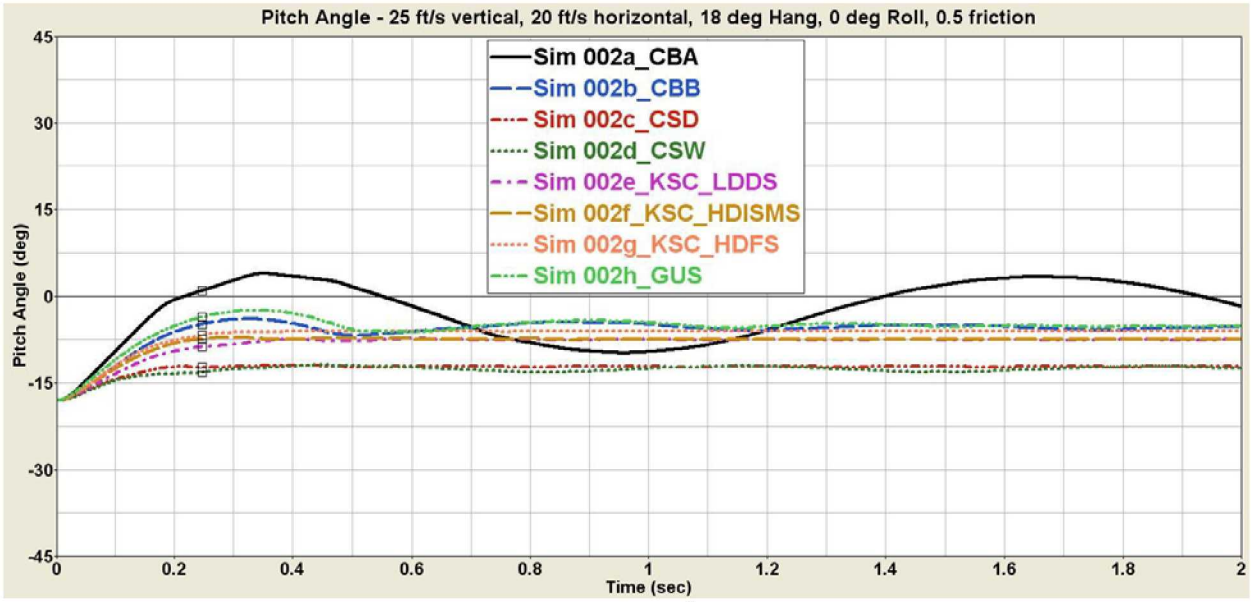

Figure 31. Pitch Angle for 18° Hang Angle Case

5.3 38° Hang Angle Case

For simulation case 3, the hang angle was then adjusted from the nominal 28° to 38°, keeping all other input variables at the baseline values. Figure 32 presents a sequence of simulation snapshots illustrating the behavior of the 38° hang angle case on the Carson Sink Dry soil. The CM digs into the Carson Sink

Dry soil with relatively little horizontal travel, and then rocks back as its translational momentum is converted to rotational momentum. Landing on the Carson Sink Dry soil produces a 17.3 inch deep depression, but only a 1.6 inch soil berm above the initial ground level.

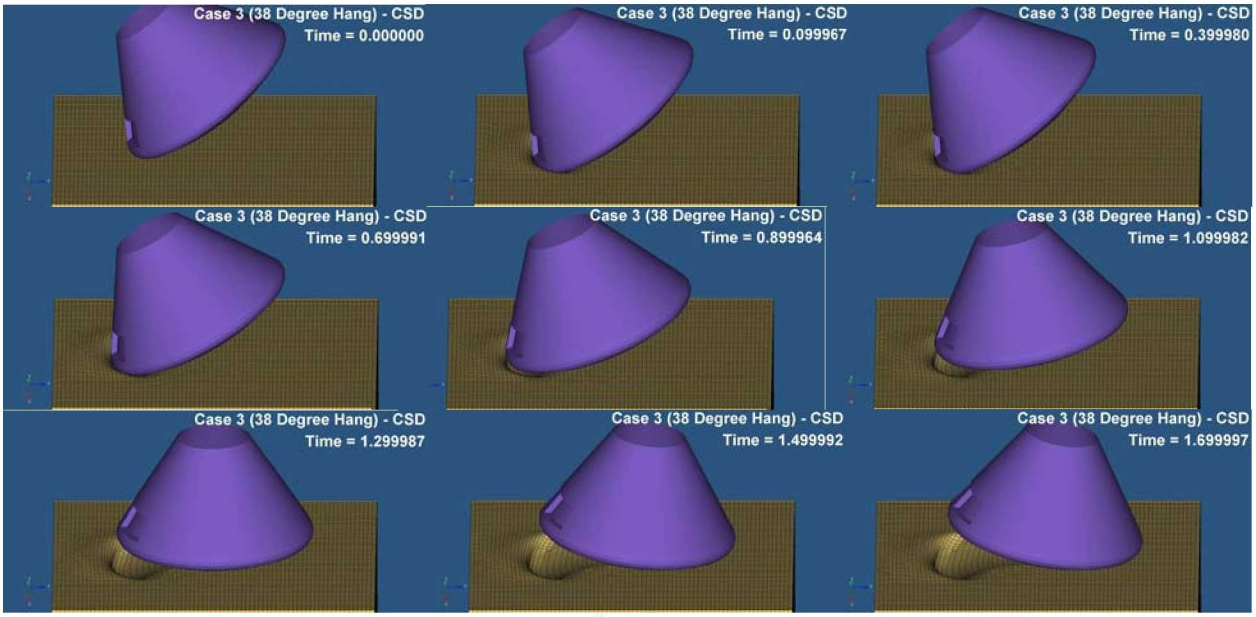

Figure 32. Animation Sequence of 38° Hang Angle Case on Carson Sink Dry Soil

The CM X-, Y-, and Z-axis accelerations for the 38° hang angle case are shown in Figure 33, Figure 34, and Figure 35, respectively. The KSC-High Density In-Situ Moisture Sand X- and Z-axis acceleration curves have the same overall shape as the Cuddeback B soil curves, characterized by the initial slope and the timing of the peak at approximately 0.07 seconds. The trends in the acceleration time-history curves for the Cuddeback A and Gantry Unwashed Sand cases are similar to each other, while being markedly different from the other soils; they have a steeper initial slope and an earlier peak at approximately 0.04 seconds. As seen in Figure 35, the Gantry Unwashed Sand Z-axis acceleration peak is the same as that on the Cuddeback B soil, although the time-histories are notably different. The KSC Low Density Dry Sand and Carson Sink Wet soils have the lowest X- and Z-axis acceleration peaks for this 38° hang angle case.

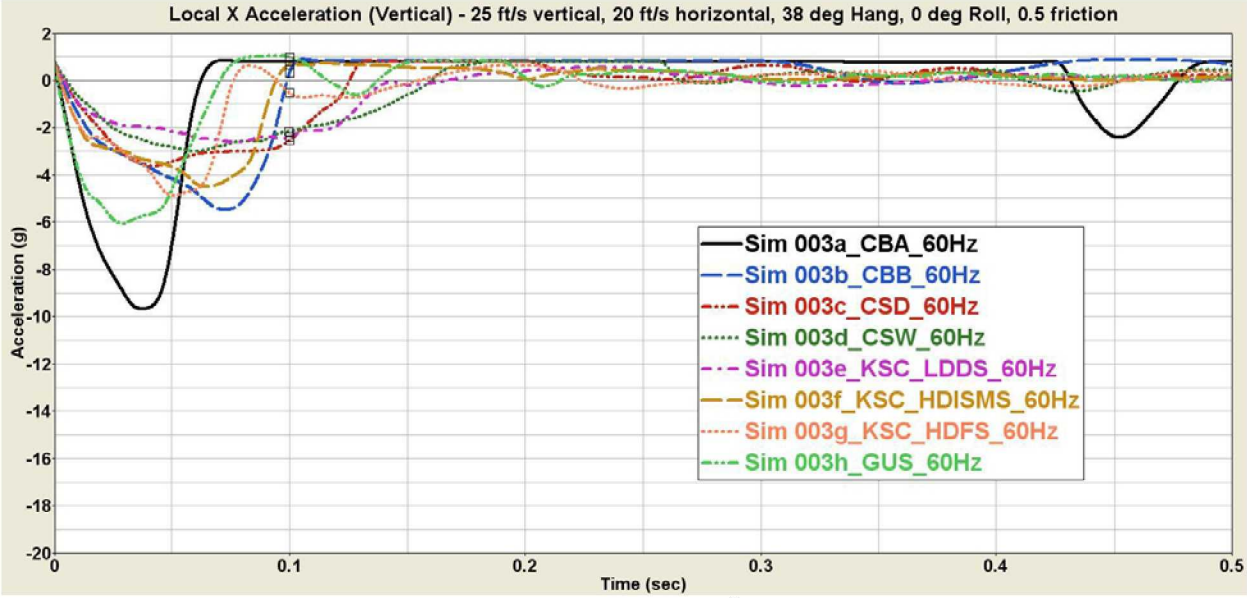

Figure 33. X-axis Accelerations for 38° Hang Angle Case

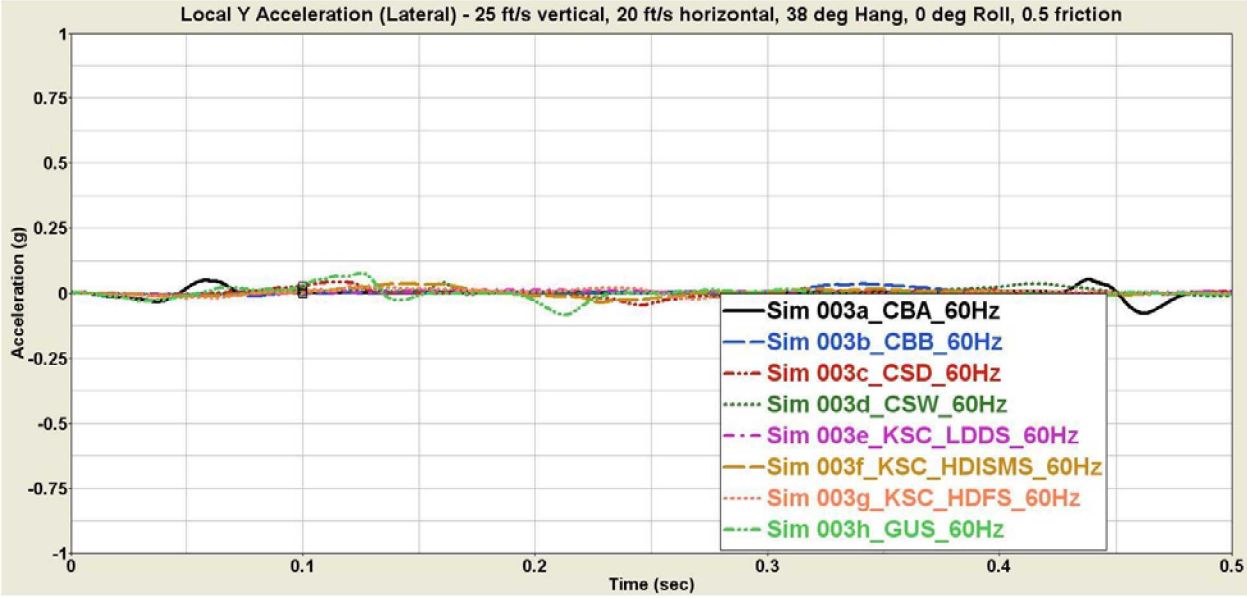

Figure 34. Y-axis Accelerations for 38° Hang Angle Case

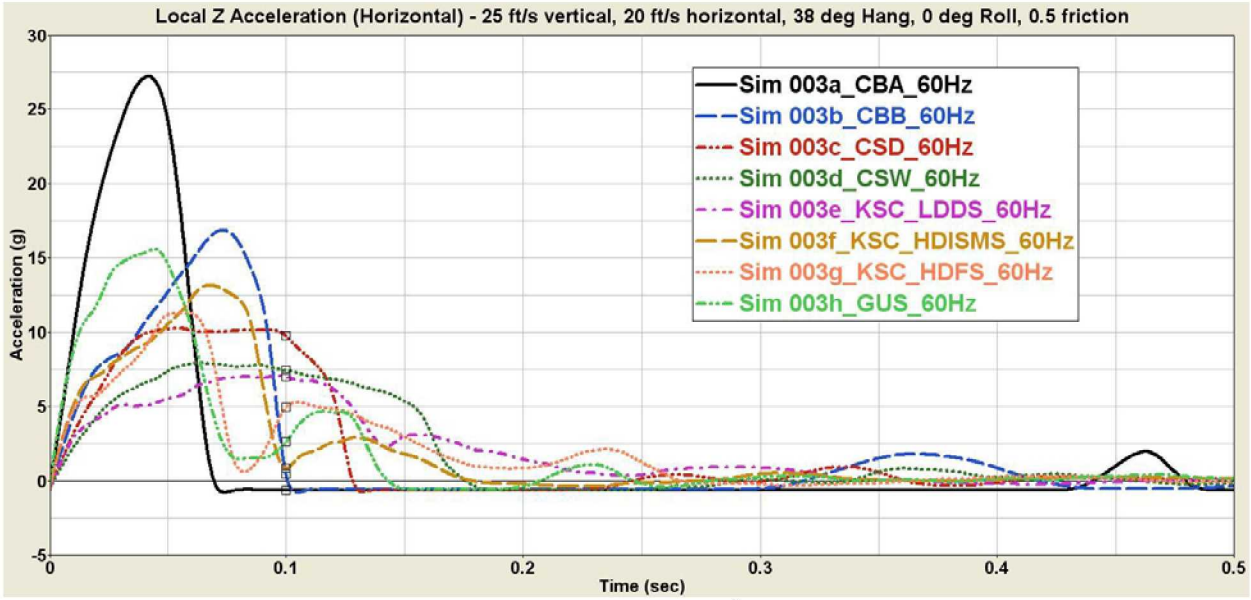

Figure 35. Z-axis Accelerations for 38° Hang Angle Case

Figure 36 shows the pitch angle time histories of the 38° hang angle case on the eight soil models. The largest pitch angle change again occurs for the Cuddeback A soil case, which also pitches forward initially and then bounces backwards after 0.45 seconds. The Carson Sink Dry soil case also pitches forward initially, but bounces backwards after only 0.25 seconds. Generally, the initial behavior for the 38° hang angle case is to displace the soil upon initial impact, and then either dig in and tilt forward, or slide out and tilt back, depending on the balance of friction and soil stiffness. The softness of the KSC Low Density Dry Sand damps out the CM pitching significantly, making it the most stable soil for this 38° hang angle case.

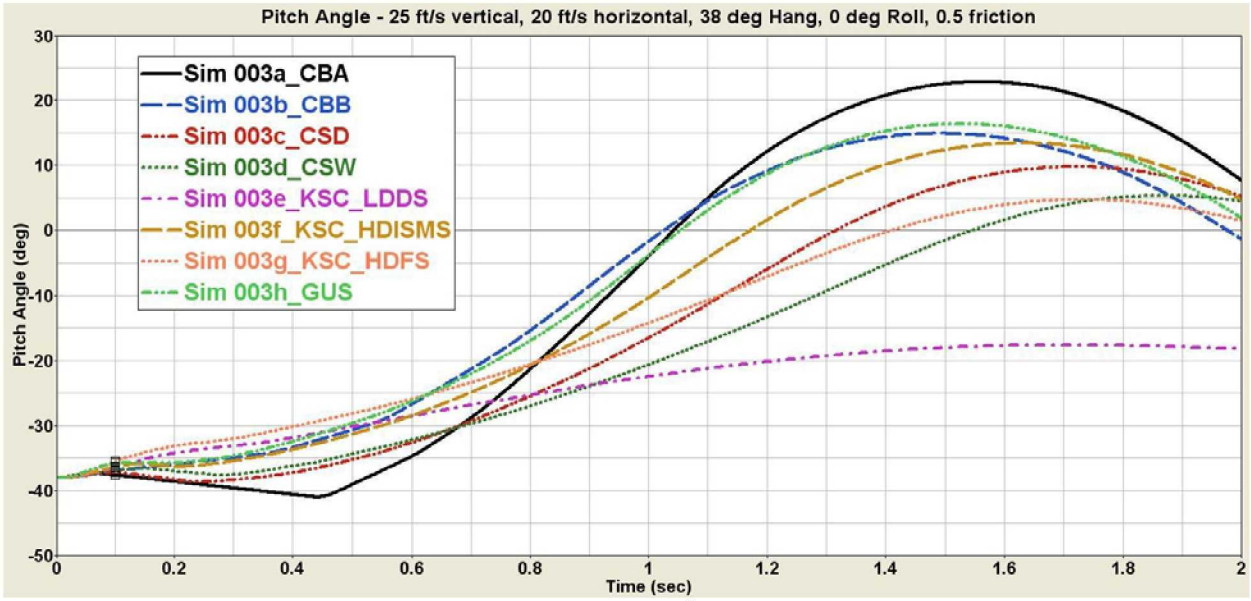

Figure 36. Pitch Angle for 38° Hang Angle Case

5.4 45° Roll Angle Case

For the fourth simulation case a roll angle was introduced, where roll is defined as a rotation about the global X-axis. The first roll angle case was a 45° roll, as illustrated in Figure 37. Figure 38 presents a sequence of simulation snapshots illustrating the behavior of the 45° roll angle case on Cuddeback A soil. After the initial impact, the CM bounces up, back, and to the side, away from the point of initial contact. With the second impact with the soil, the CM skips and rolls around, twisting counter-clockwise in the process. The 45° roll condition moves the initial contact point off the line of the CM initial velocity and to the side of the CG, so that the horizontal portion of the contact force drives the CM to rotate counter-clockwise about the X-axis.

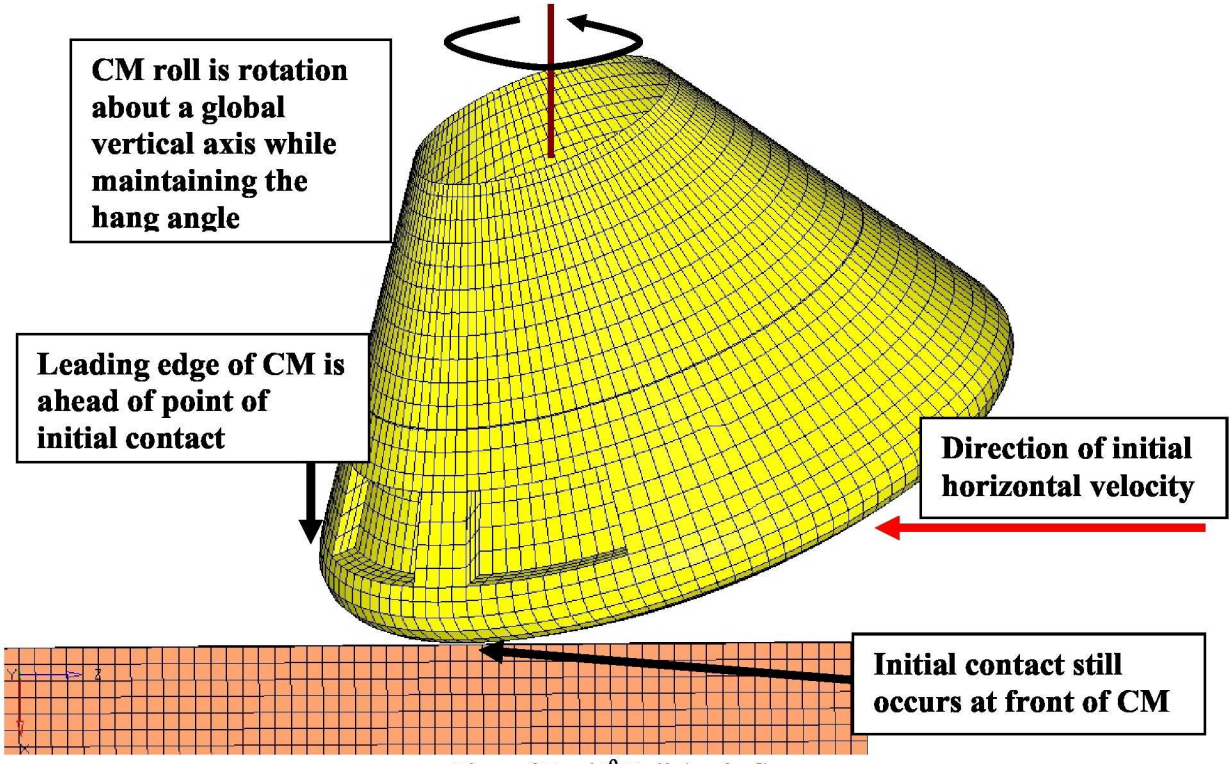

Figure 37. 45° Roll Angle Case

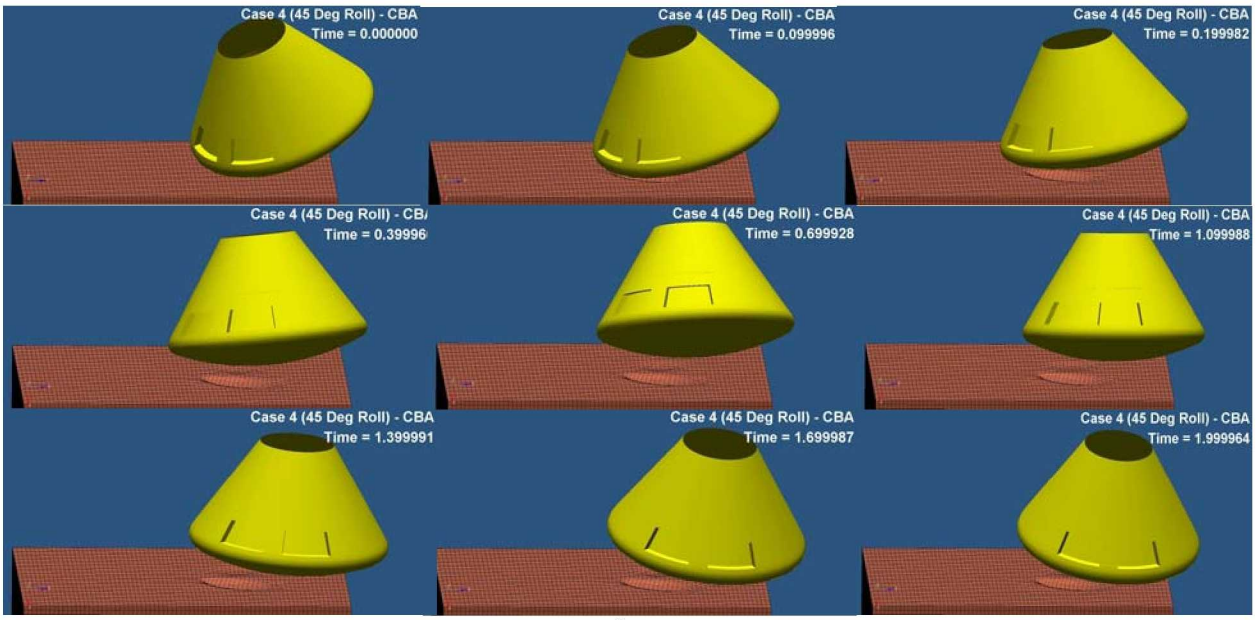

Figure 38. Animation Sequence of 45° Roll Angle Case on Cuddeback A Soil

The X-, Y-, and Z-axis accelerations for the 45° roll cases are plotted in Figure 39, Figure 40, and Figure 41, respectively. With 45° of roll introduced, the CM Y-axis (lateral) accelerations are no longer insignificant. However, the X- and Z-axis accelerations still dominate. For the Cuddeback A soil, the CM bounces such that the magnitude of the secondary impact is substantial for the X- and Y-axis accelerations. The peak Y-axis acceleration occurs at this second impact on the Cuddeback A soil. All the other soil models have peak CM X-, Y-, and Z-axis accelerations resulting from the initial impact. Trends are similar to the other cases, with the Cuddeback A soil and the Gantry Unwashed Sand cases having the highest accelerations, and the KSC Low Density Dry Sand the lowest. The Cuddeback B soil and KSC High Density In-Situ Moisture Sand acceleration time-histories are very similar.

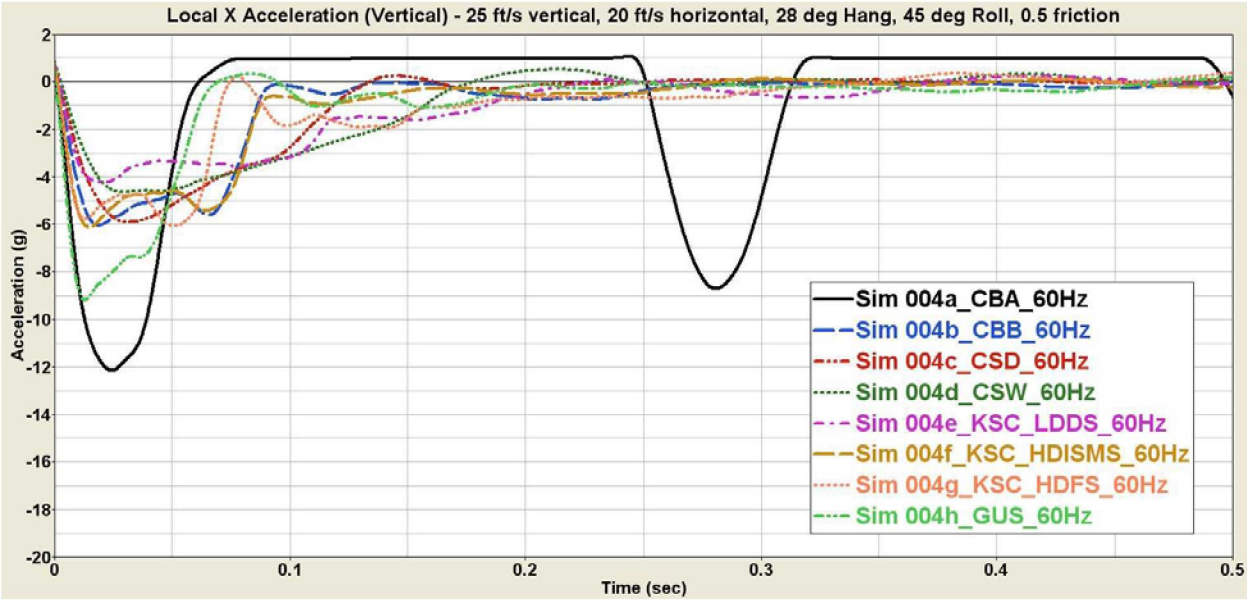

Figure 39. X-axis Accelerations for 45° Roll Angle Case

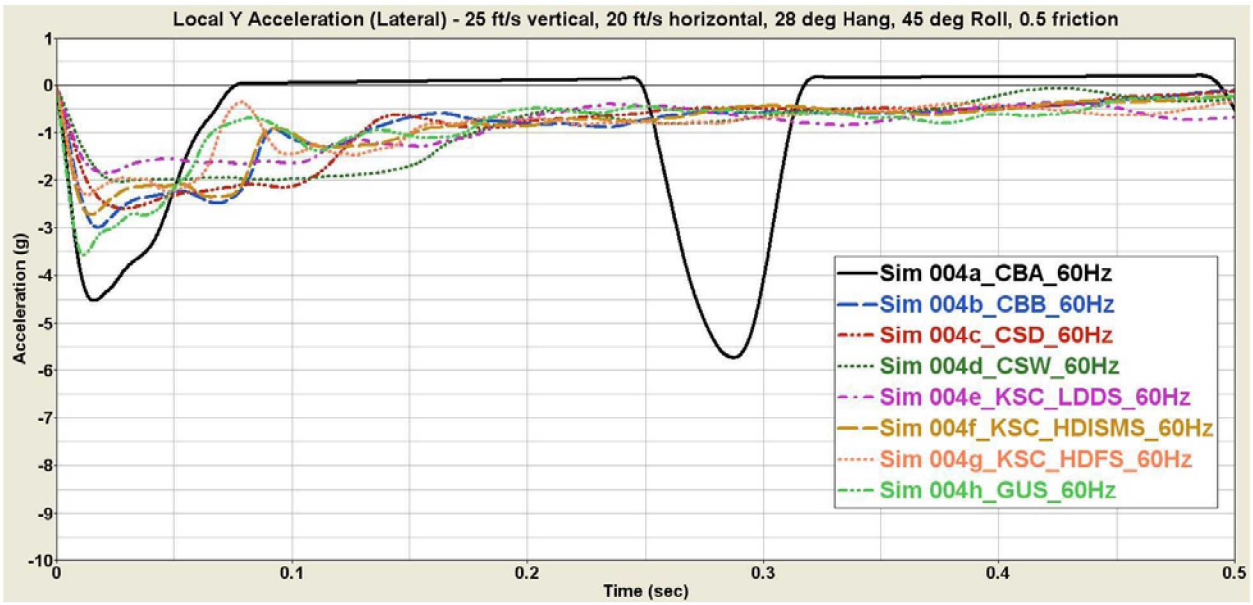

Figure 40. Y-axis Accelerations for 45° Roll Angle Case

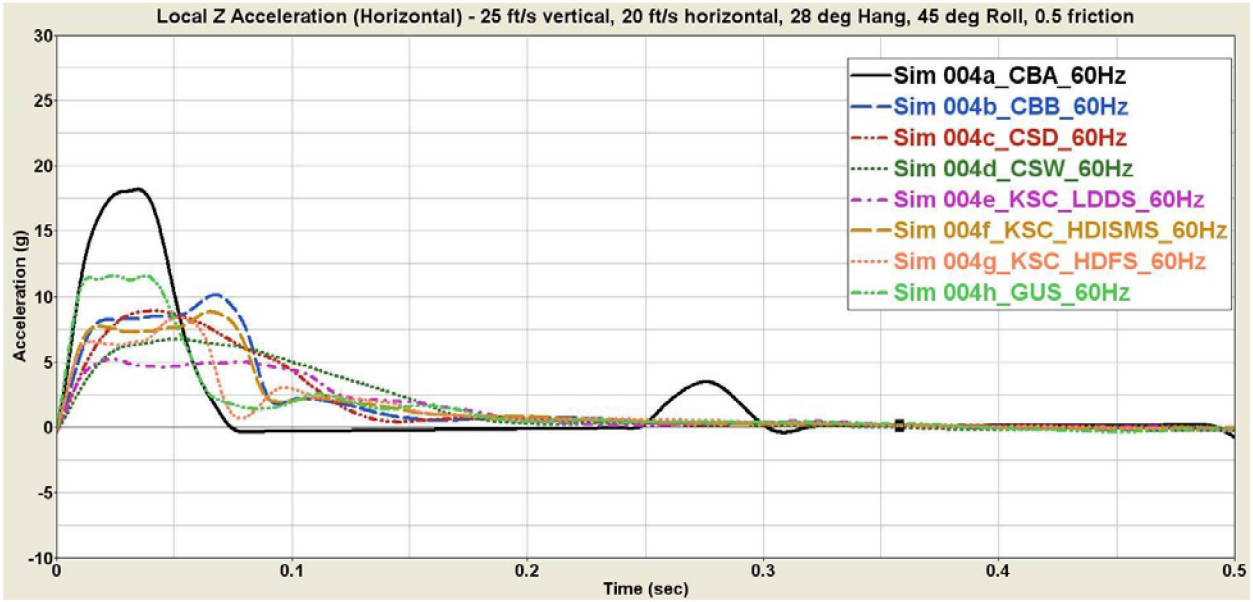

Figure 41. Z-axis Accelerations for 45° Roll Angle Case

Figure 42 shows the pitch angle time-histories for the eight soil cases for the 45° roll angle landing condition. The level of stability is again dependent on the soil model, but there is no rollover for any soil models in this landing scenario. The KSC Low Density Dry Sand and High Density Flooded Sand models reach a stationary pitch angle during the simulation.

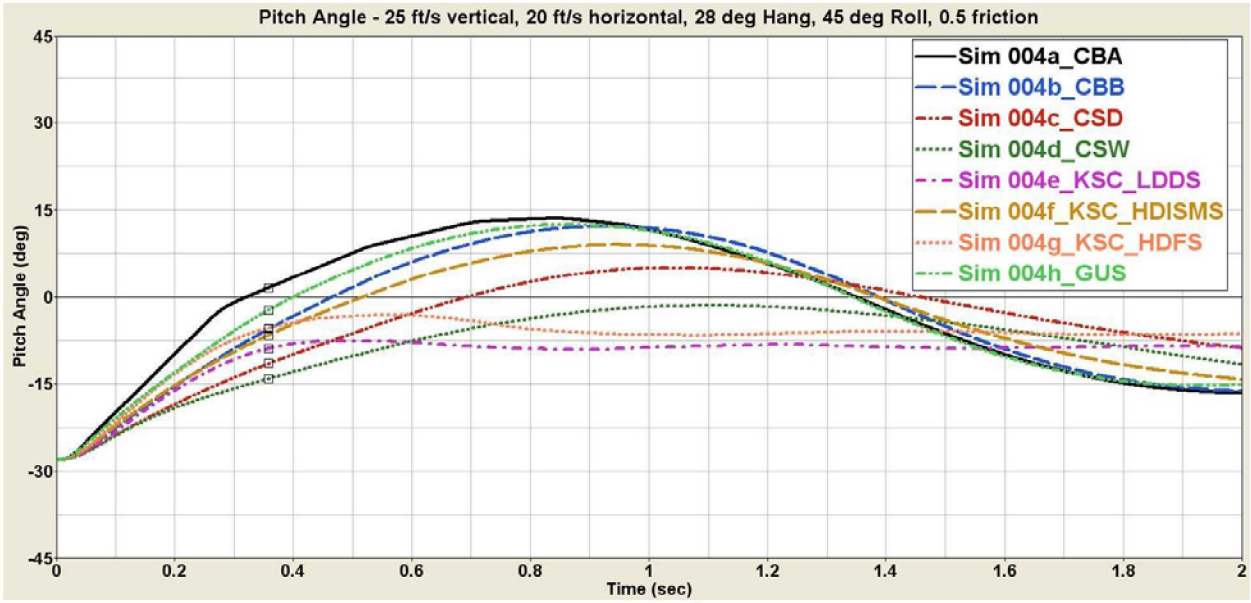

Figure 42. Pitch Angle for 45° Roll Angle Case

5.5 90° Roll Angle Case

For the fifth simulation case, the roll angle was increased to 90°, as illustrated in Figure 43, which shows the CM on the KSC High Density Flooded Sand at a time shortly after the initial impact. Figure 44 presents a sequence of simulation snapshots of the model illustrating the behavior of the 90° roll angle case on the KSC High Density In-Situ Moisture Sand. After the initial impact, the CM rolls clockwise along the outer circumferential edge of the heat shield, deforming the soil in the process, sliding slightly, and eventually rocking back downwards towards the direction of the windows on the CM. In addition to illustrating the landing attitude of the CM, Figure 43 allows a visual comparison of the deformation of the KSC High Density Flooded Sand with that of the KSC High Density In-Situ Moisture Sand shown in Figure 44.

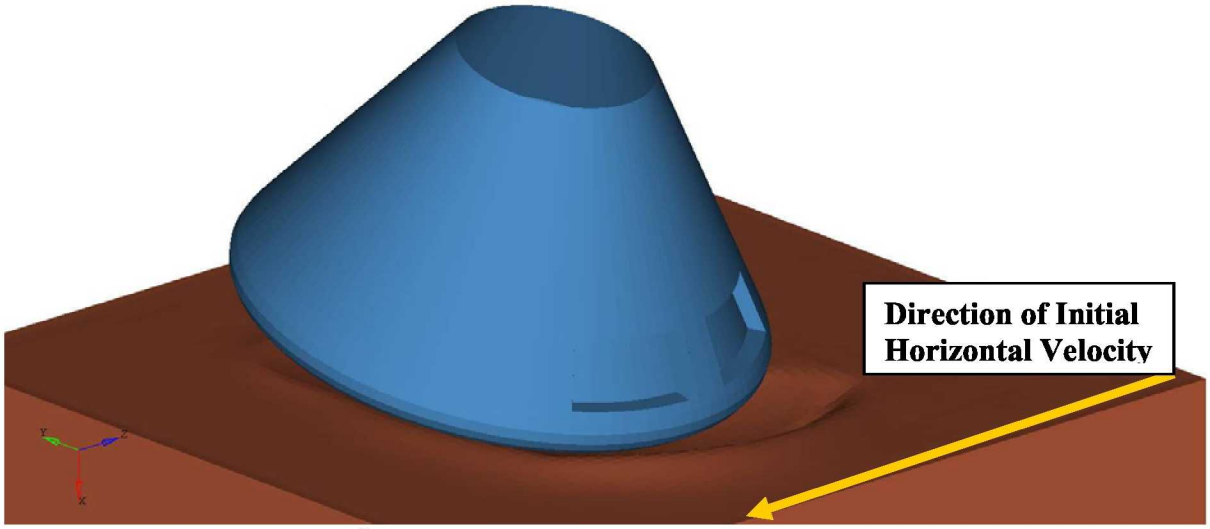

Figure 43. 90° Roll Angle Landing Case on KSC High Density Flooded Sand

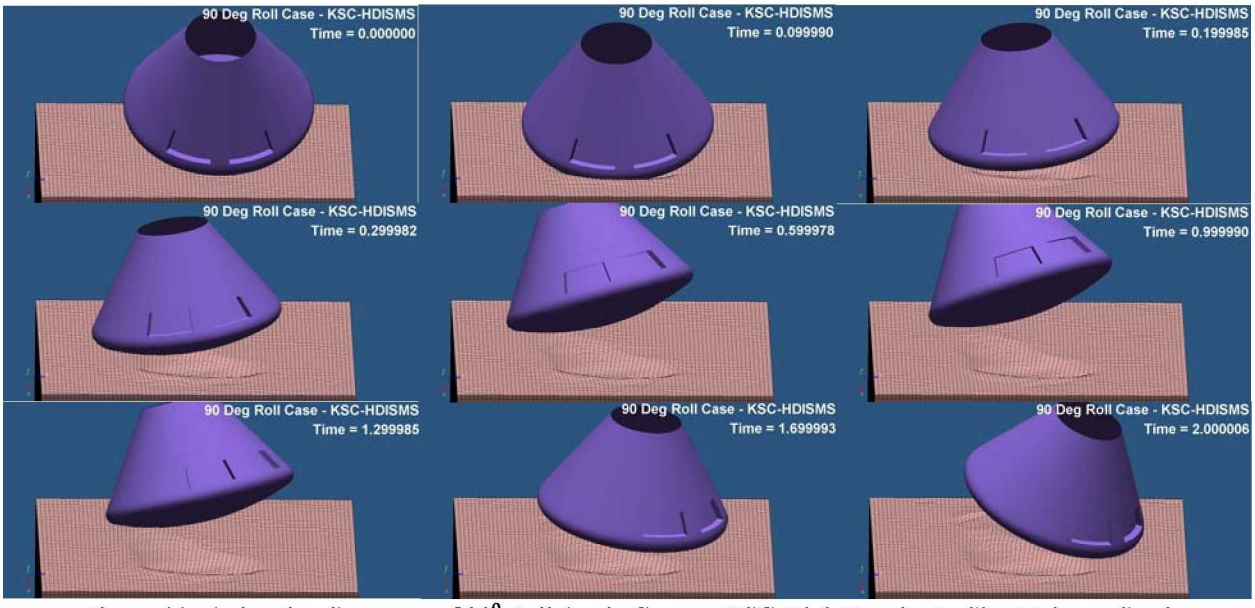

Figure 44. Animation Sequence of 90° Roll Angle Case on KSC-High Density In-Situ Moisture Sand

The X-, Y-, and Z-axis accelerations for the 90° roll case on all eight soils are shown in Figure 45, Figure 46, and Figure 47, respectively. For the 90° roll case, the peak Z-axis accelerations are lower than those of the baseline conditions case for all the soil models. The CM Y-axis accelerations are larger than the 45° roll case, but the X- and Z- axis acceleration peaks are still almost twice as large as the Y-axis peaks. As with the 45° roll case, on the Cuddeback A soil the Y-axis acceleration peak occurs at the second impact, when the CM is bouncing back onto the heat shield bottom. The trends of the Cuddeback B and KSC High Density In-Situ Moisture Sand accelerations are very similar.

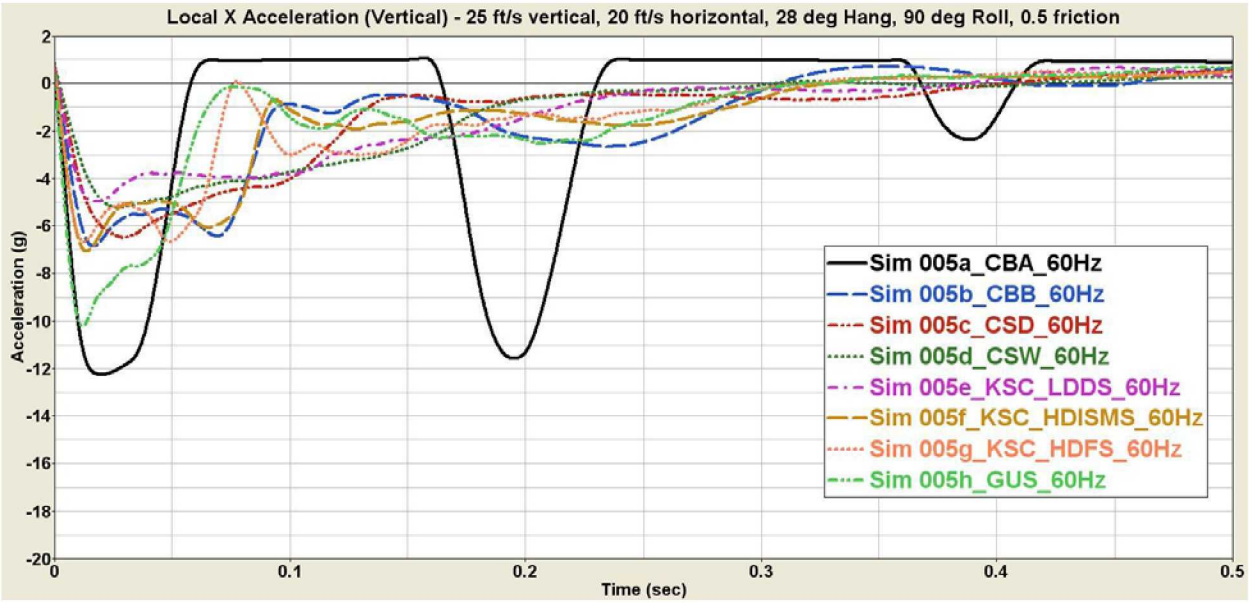

Figure 45. X-axis Accelerations for 90° Roll Angle Case

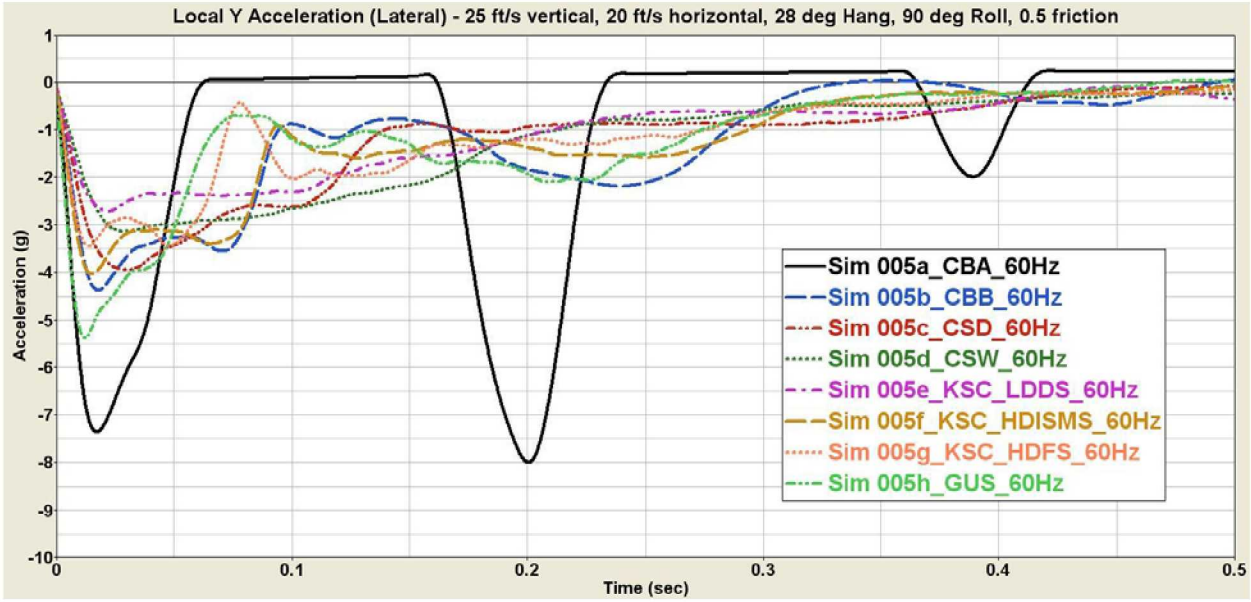

Figure 46. Y-axis Accelerations for 90° Roll Angle Case

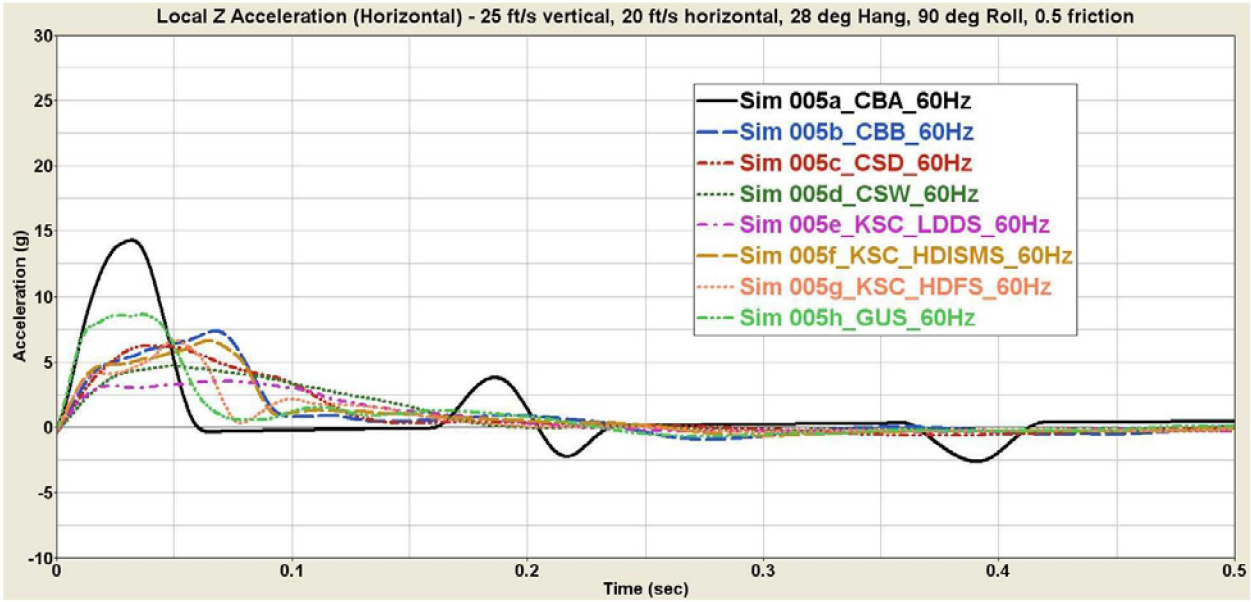

Figure 47. Z-axis Accelerations for 90° Roll Angle Case

Figure 48 shows the pitch angle time-histories for the 90° roll angle landing condition cases. The pitch responses for the Cuddeback A soil and the Gantry Unwashed Sand cases are very similar, as are the responses on the KSC High Density In-Situ Moisture Sand and Cuddeback B. The most stable response is on the KSC Low Density Dry Sand, as it gives the lowest pitch angle oscillation. While the Cuddeback A soil and the Gantry Unwashed Sand cases have larger pitch angle displacements and are less stable, extended time simulations indicated that they would not roll over.

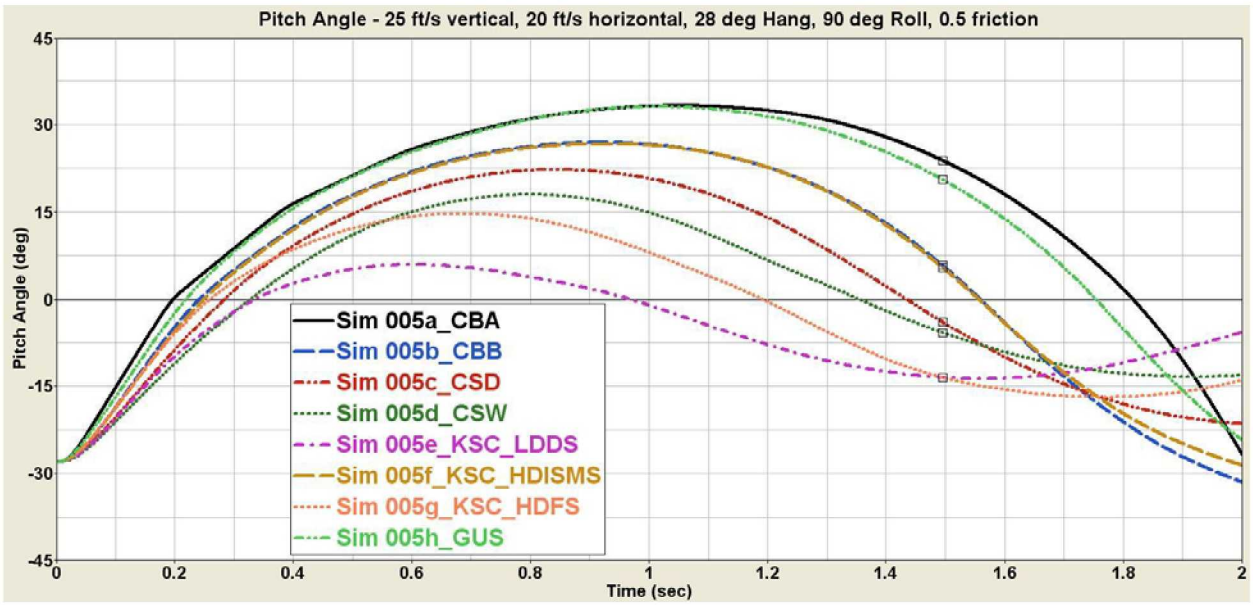

Figure 48. Pitch Angle for 90° Roll Angle Case

5.6 180° Roll Angle Case

The sixth simulation case was the 180° roll angle case. For this case, the CM lands facing backwards, as can be observed in Frame 1 of Figure 49. The figure shows a sequence of simulation animation snapshots illustrating the overall behavior of the 180° roll angle CM on the KSC High Density In-Situ Moisture Soil (note position of the airbag cutout areas; horizontal velocity is still from the right to the left in the figures). Upon initial impact, both the vertical and horizontal forces on the CM produce moments that drive the CM to pitch forward in the direction of the horizontal velocity. For the 0° roll cases with non-zero horizontal velocity, the moment resulting from the vertical contact force opposes the moment resulting from the horizontal contact force. Thus, for the 180° roll angle case, the stability is greatly reduced as there are no counter-balancing effects on the pitch rotation from the vertical and horizontal forces. Similar landing instability was found by McCullough during Apollo testing [ref. 7]. The rollover behavior shown in Figure 49 also occurred on all the other soils except the KSC Low Density Dry Sand and the Carson Sink Wet soil.

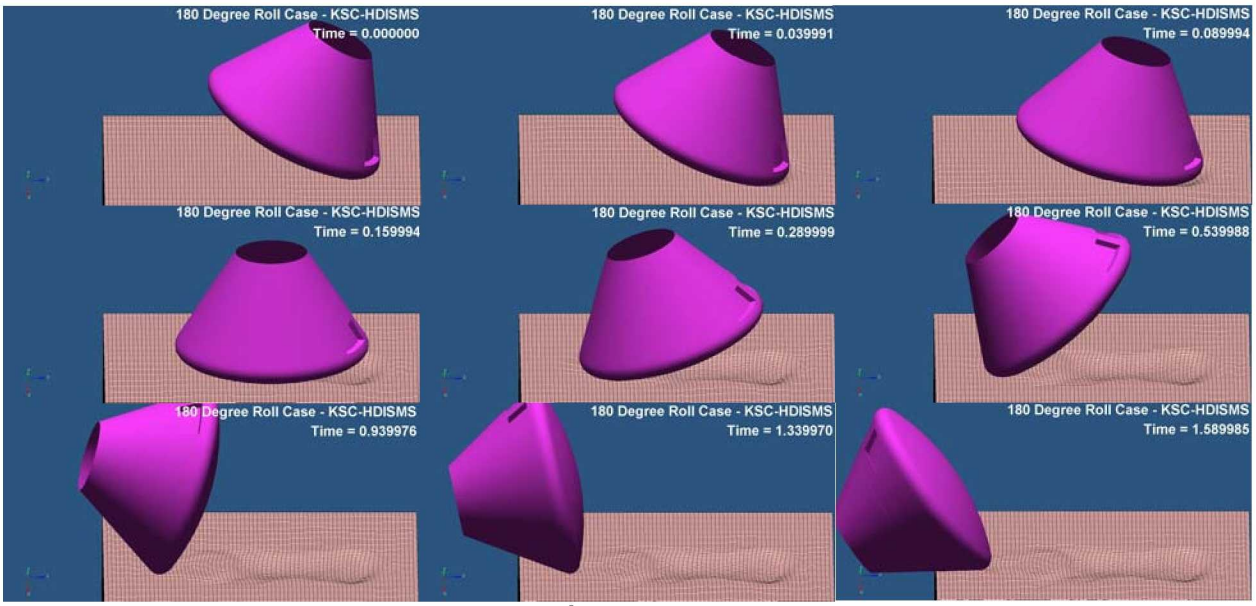

Figure 49. Animation Sequence of 180° Roll Angle Case on KSC High Density Dry Sand

Figure 50 shows a sequence of simulation snapshots for the 180° roll angle case on the KSC Low Density Dry Sand, which is the most stable case. The KSC Low Density Dry Sand and Carson Sink Wet soil cases are the only two that do not roll over. Similar to the other soils, the CM initially deforms the soil downwards, as shown in Frame 2 of Figure 50. The CM then rolls forward in the direction of its horizontal velocity, until the front edge pitches down and digs into the soil. The CM then plows ahead, building up a berm of soil ahead of it, and finally stops its horizontal motion and rocks backwards. Thus additional energy is dissipated as the CM plows through the soil. Figure 49 and Figure 50 illustrate the different behaviors possible for the CM landing on different soils.

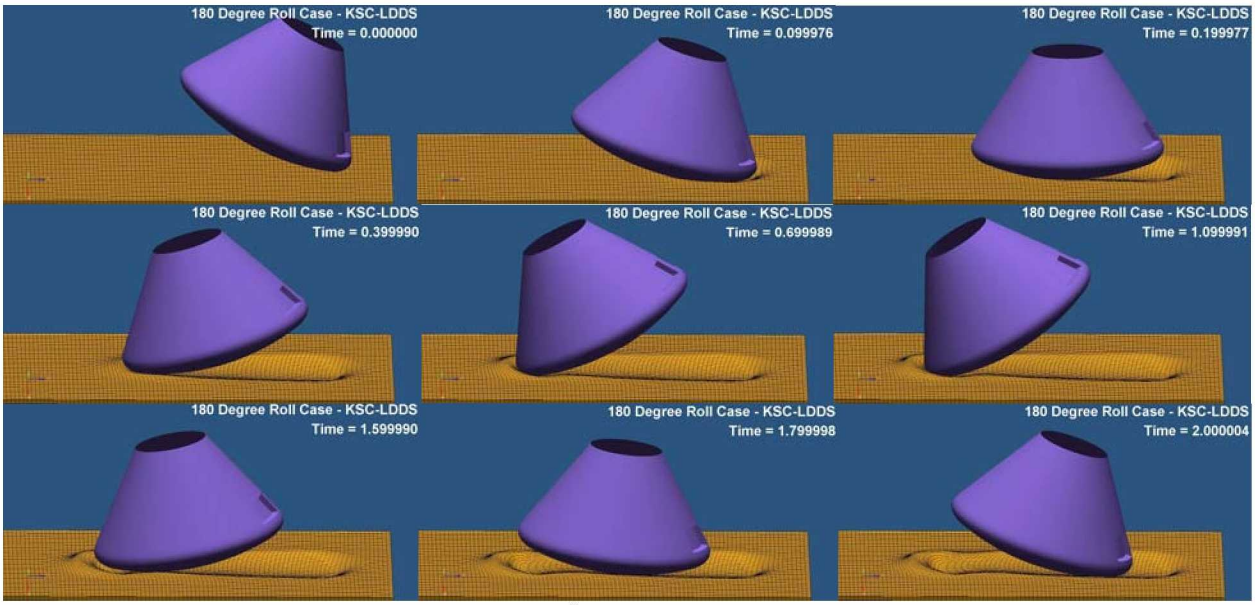

Figure 50. Animation Sequence of 180° Roll Angle Case on KSC Low Density Dry Sand

The X-, Y-, and Z-axis accelerations for the 180° roll case on all eight soils are shown in Figure 51, Figure 52, and Figure 53, respectively. For both Cuddeback A and the Gantry Unwashed Sand in the 180° roll case, the secondary X-axis acceleration peak is of the same order of magnitude as the first peak. The lowest accelerations are again for the KSC Low Density Dry Sand case, and no secondary acceleration peak is visible for this case, as the sand deforms sufficiently to cushion and capture the CM as it rolls.

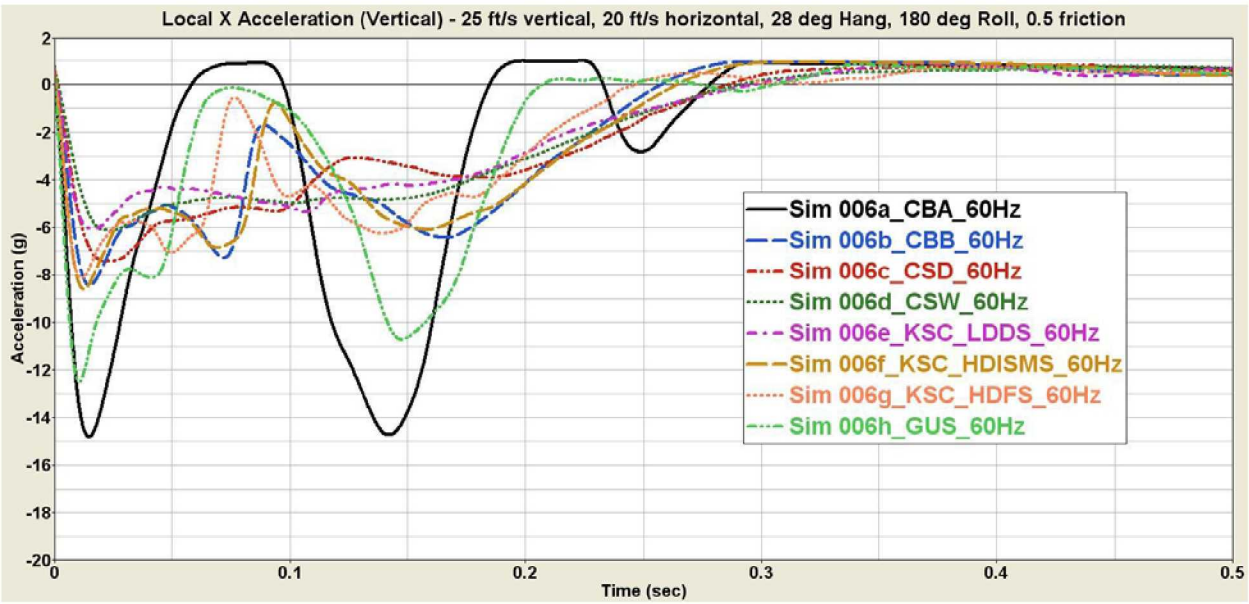

Figure 51. X-axis Accelerations for 180° Roll Angle Case

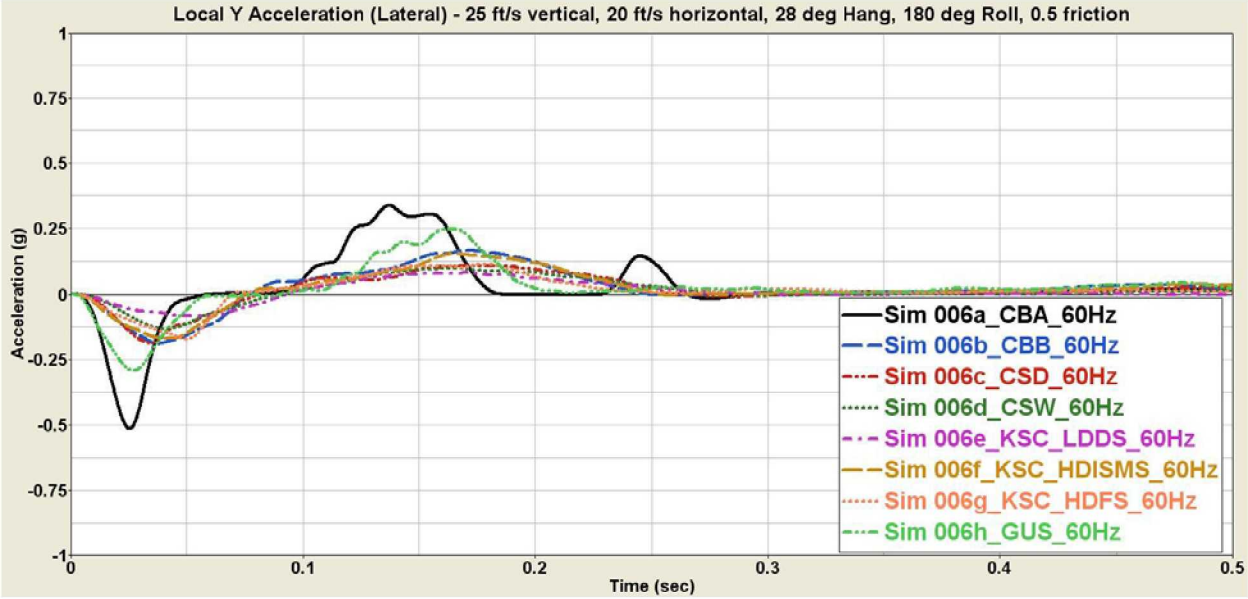

Figure 52. Y-axis Accelerations for 180° Roll Angle Case

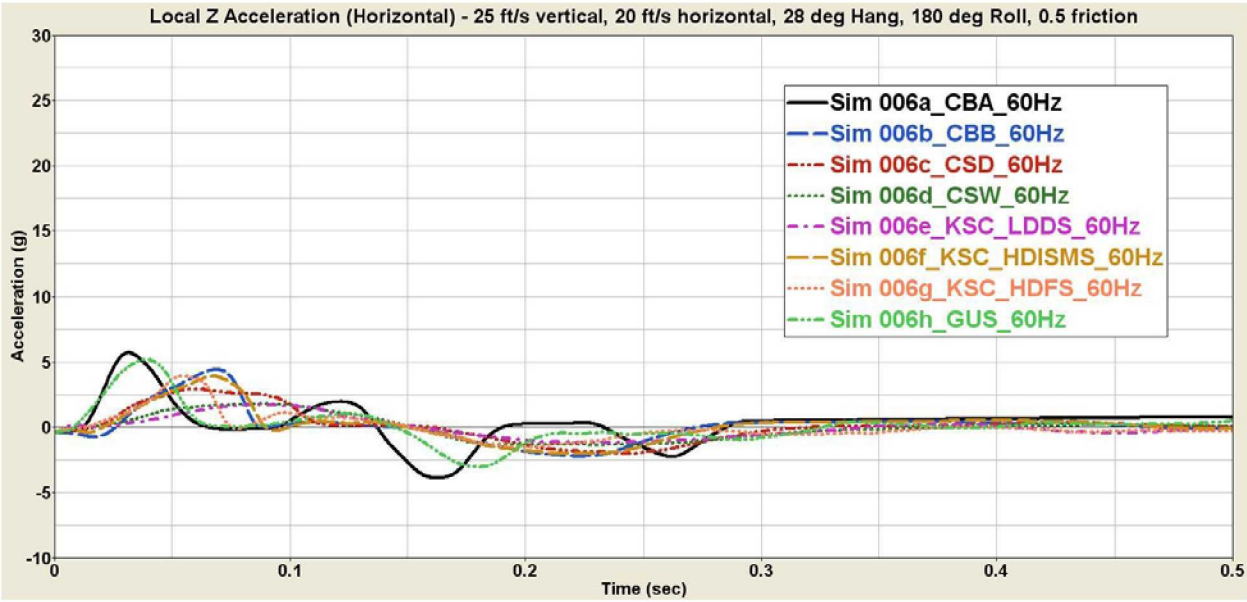

Figure 53. Z-axis Accelerations for 180° Roll Angle Case

Figure 54 shows the pitch angle time-histories for the eight soil cases for the 180° roll angle landing condition. The KSC Low Density Dry Sand produces a stable landing without rollover of the CM. The Carson Sink Wet soil case is near the stability limit, but does not roll over, as it begins rolling back to an upright position at 1.75 seconds. A maximum pitch angle of 45° or less is considered an indicator of a stable response. For a case where the pitch angle is larger than 45°, a small perturbation in the input parameters could result in rollover of the capsule.

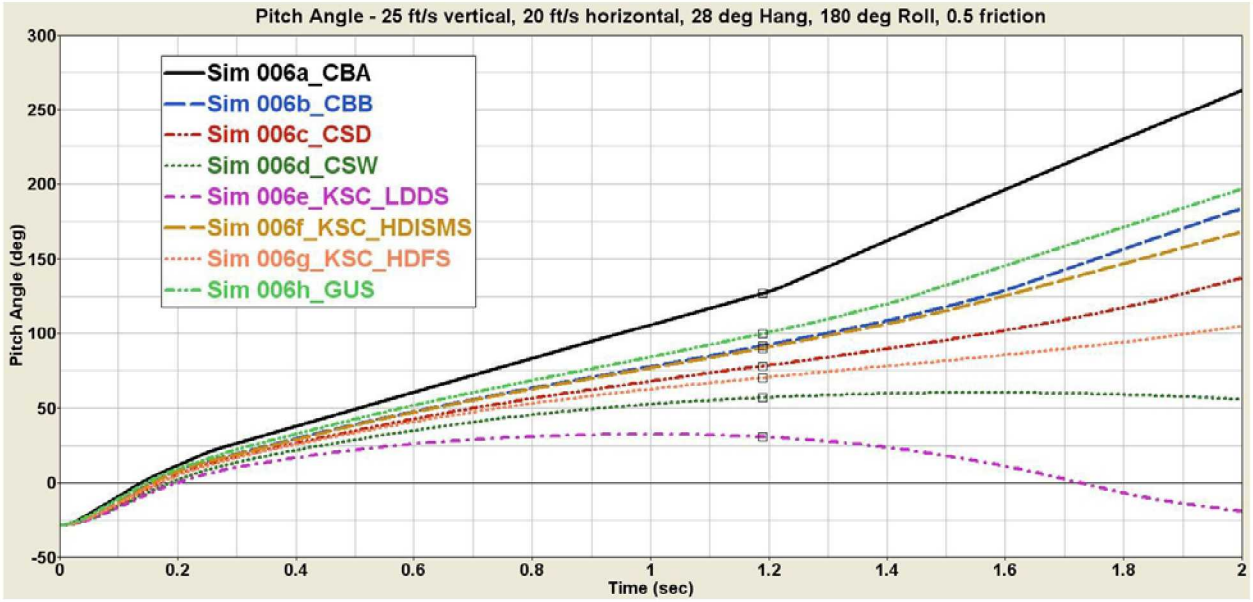

Figure 54. Pitch Angle for 180° Roll Angle Case

5.7 15 ft/s Vertical Velocity Case

For the seventh simulation case, the parameter varied was the vertical velocity, beginning with a reduction from the baseline 25 ft/s velocity to 15 ft/s. Again, all other input parameters were specified at the baseline values. Figure 55 shows a sequence of simulation snapshots illustrating the behavior of the 15 ft/s vertical velocity case on the KSC High Density In-Situ Moisture Soil. Similar to the baseline, the CM digs into the soil on initial impact, rocks back out of the crater created, and then rolls back forward partially into the depression created in the soil.

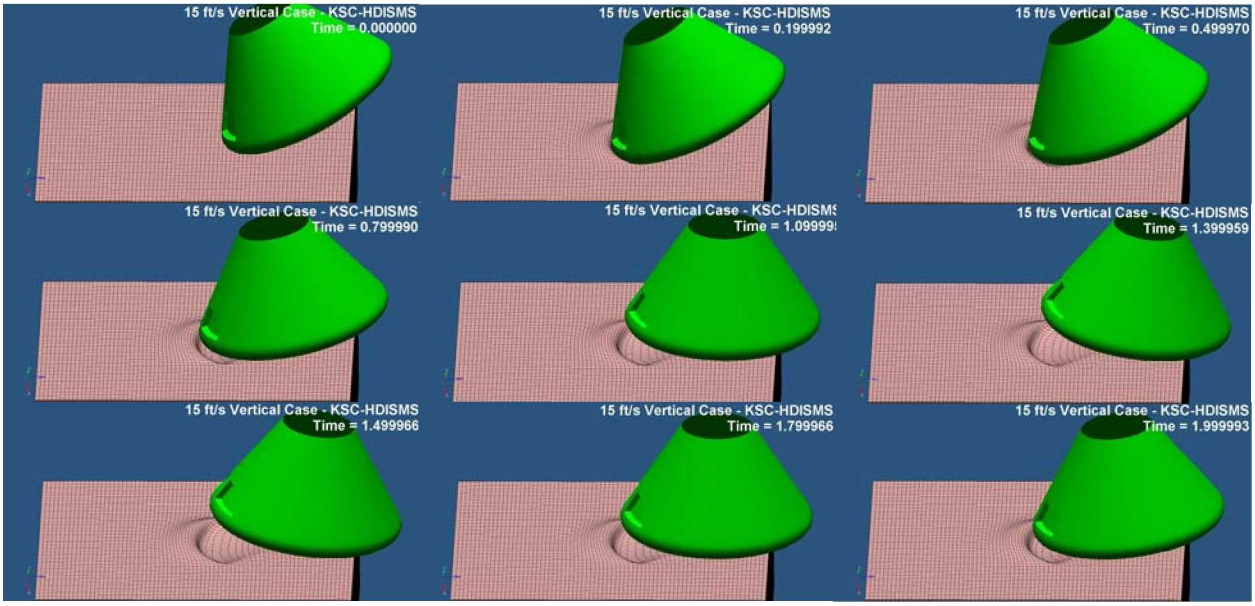

Figure 55. Animation Sequence of 15 ft/s Vertical Velocity Case on KSC High Density In-Situ Moisture Sand

The X-, Y-, and Z-axis accelerations for the 15 ft/s vertical velocity case on all eight soils are shown in Figure 56, Figure 57, and Figure 58, respectively. For this lower vertical velocity case, the second X-axis acceleration peak is higher than the first on Cuddeback A soil. This occurs in part because the second impact is more aligned with the local CM X-axis. The acceleration time-history trends are most similar for the Gantry Unwashed Sand and Cuddeback A soil, except that the Gantry Unwashed Sand case does not have a second peak for either the X- or Z-axis acceleration. The other soil models exhibit a softer response, characterized by a lower initial slope and a delayed peak.

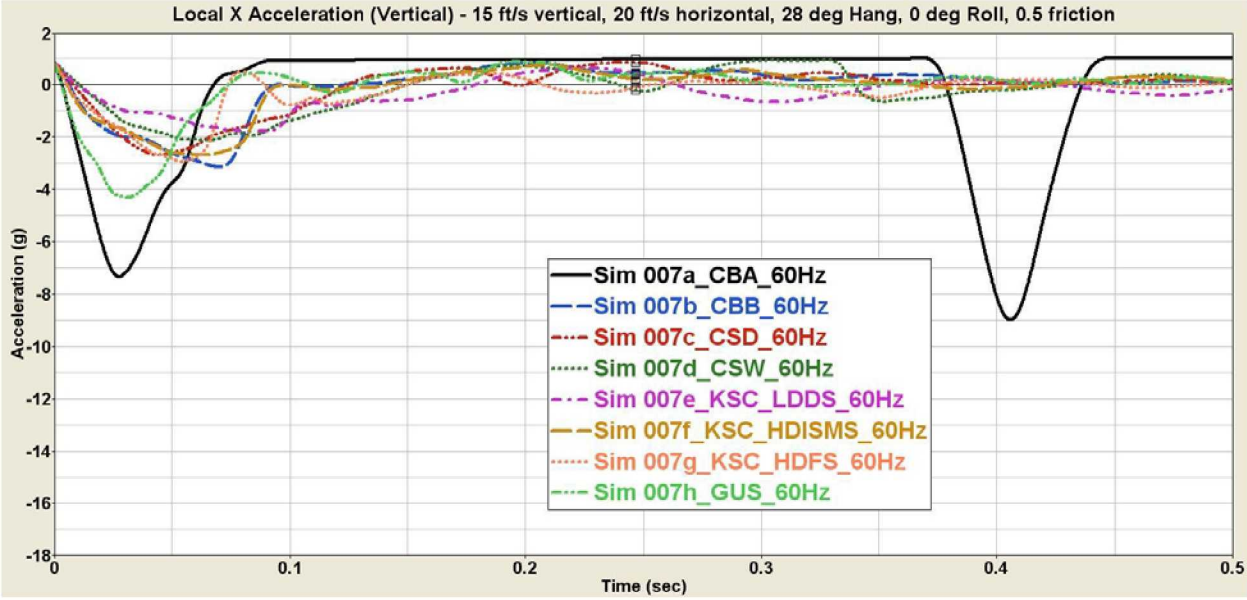

Figure 56. X-axis Accelerations for 15 ft/s Vertical Velocity Case

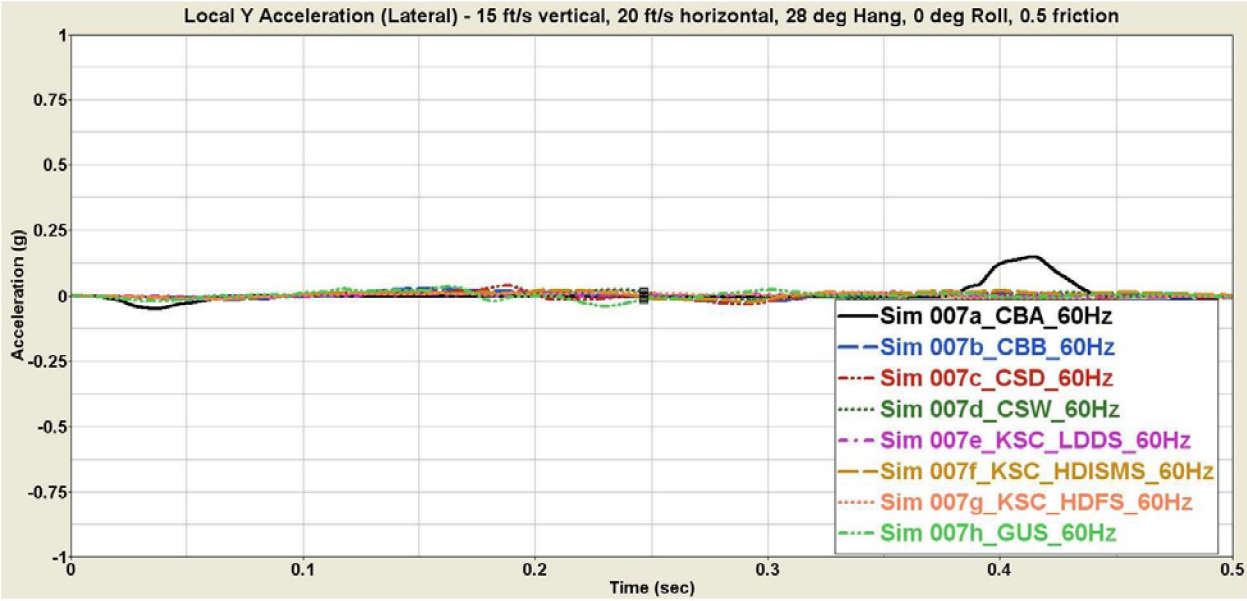

Figure 57. Y-axis Accelerations for 15 ft/s Vertical Velocity Case

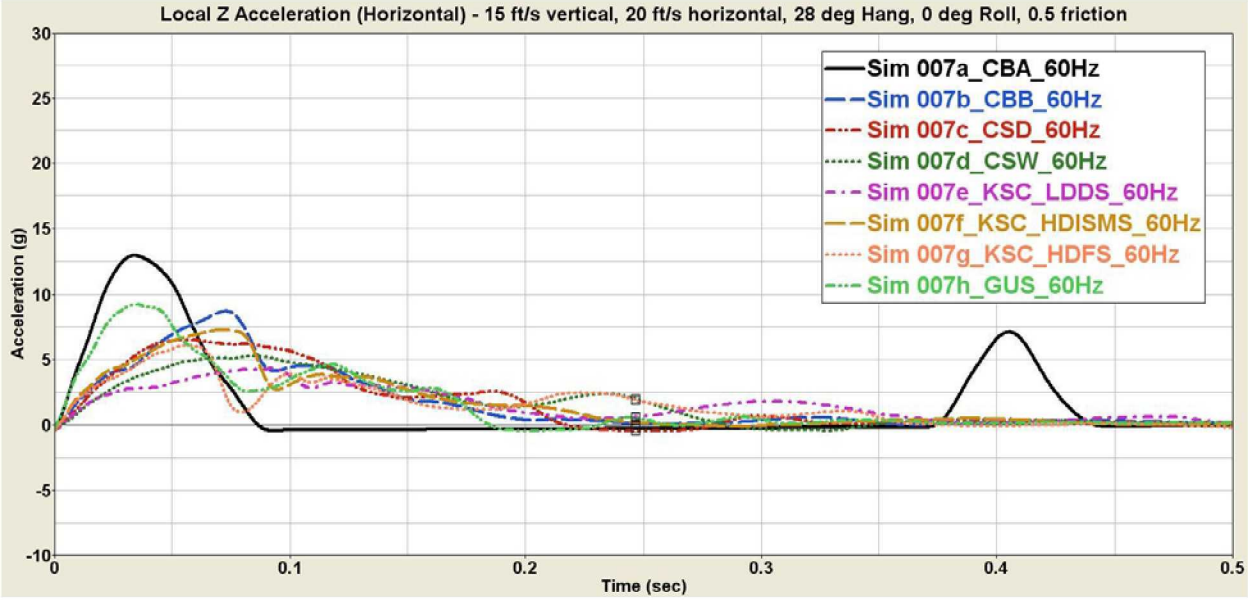

Figure 58. Z-axis Accelerations for 15 ft/s Vertical Velocity Case

Figure 59 shows the pitch angle time-histories for the eight soil cases for the 15 ft/s vertical velocity landing condition. The pitch behavior on the Cuddeback A soil stands apart from the other simulations, as the initial impact pitches the CM back earlier. The KSC High Density In-Situ Moisture Sand and High Density Flooded Sand cases exhibit the same pitch behavior, which also differs from all the other soil models. In the 15 ft/s vertical velocity simulations for these two soils, the CM becomes embedded in the soil and does not roll backwards after impact.

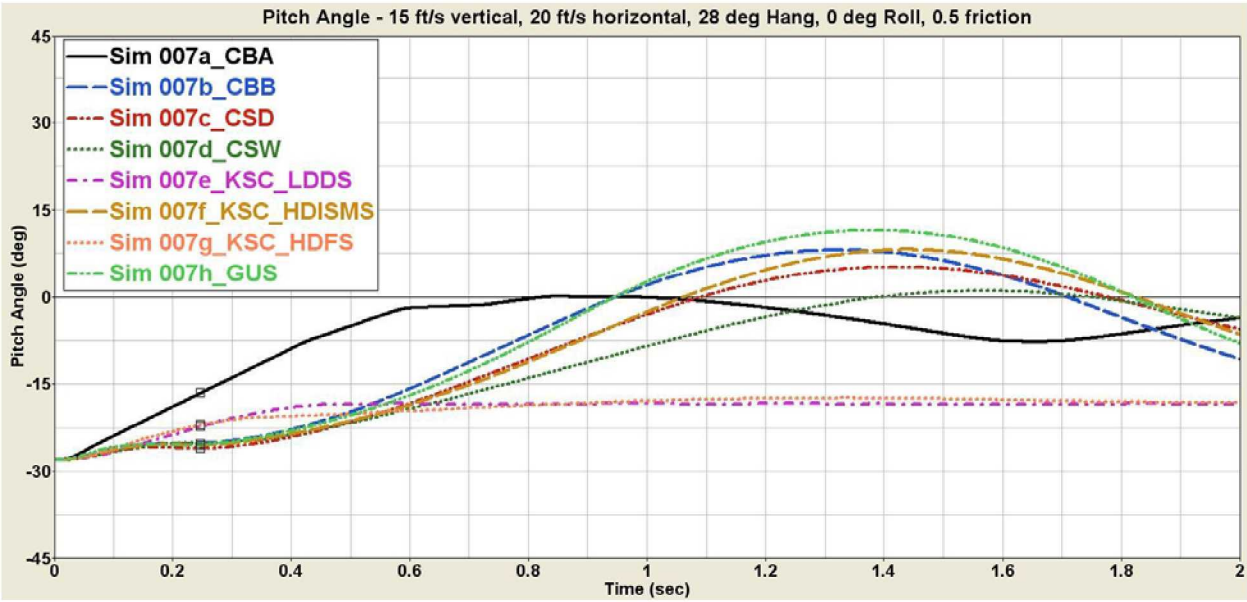

Figure 59. Pitch Angle for 15 ft/s Vertical Velocity Case

5.8 35 ft/s Vertical Velocity Case

For the eighth simulation case, the initial vertical velocity was increased to 35 ft/s, holding all other input parameters at the baseline values. Figure 60 shows a sequence of animation images that illustrate the behavior of the CM landing for the 35 ft/s vertical velocity case on the Gantry Unwashed Sand. The CM digs into the soil initially, and then bounces up and out of the crater that is created, only to eventually rock forward again and come to rest in the same hole.

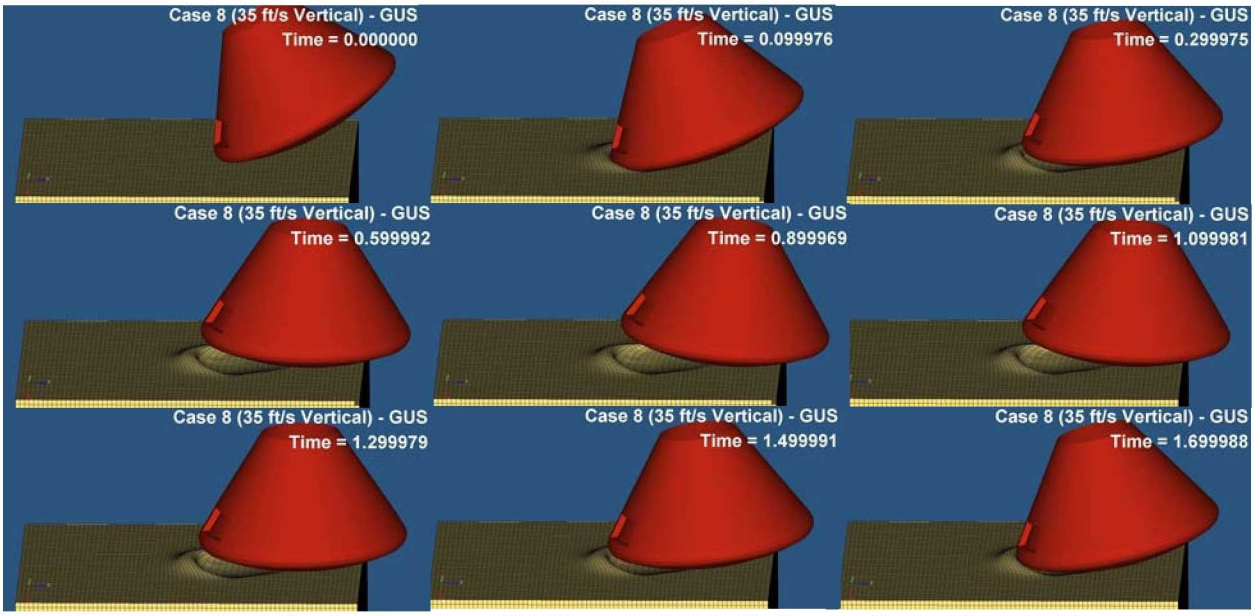

Figure 60. Animation Sequence of 35 ft/s Vertical Velocity Case on Gantry Unwashed Sand

The X-, Y-, and Z-axis accelerations for the 35 ft/s vertical velocity case on all eight soils are shown in Figure 61, Figure 62, and Figure 63, respectively. The peak X-axis acceleration on the Gantry Unwashed Sand approaches that of Cuddeback A, but is much shorter in duration. The Gantry Unwashed Sand Z-axis acceleration peak is only approximately 80% of the Cuddeback A peak. With a vertical impact speed of 35 ft/s, the X-axis acceleration peaks all occur earlier (at approximately 0.01 seconds), with the partial exception of the Carson Sink soils (which occur at approximately 0.025 seconds). For the Z-axis accelerations, the peak values also occur early.

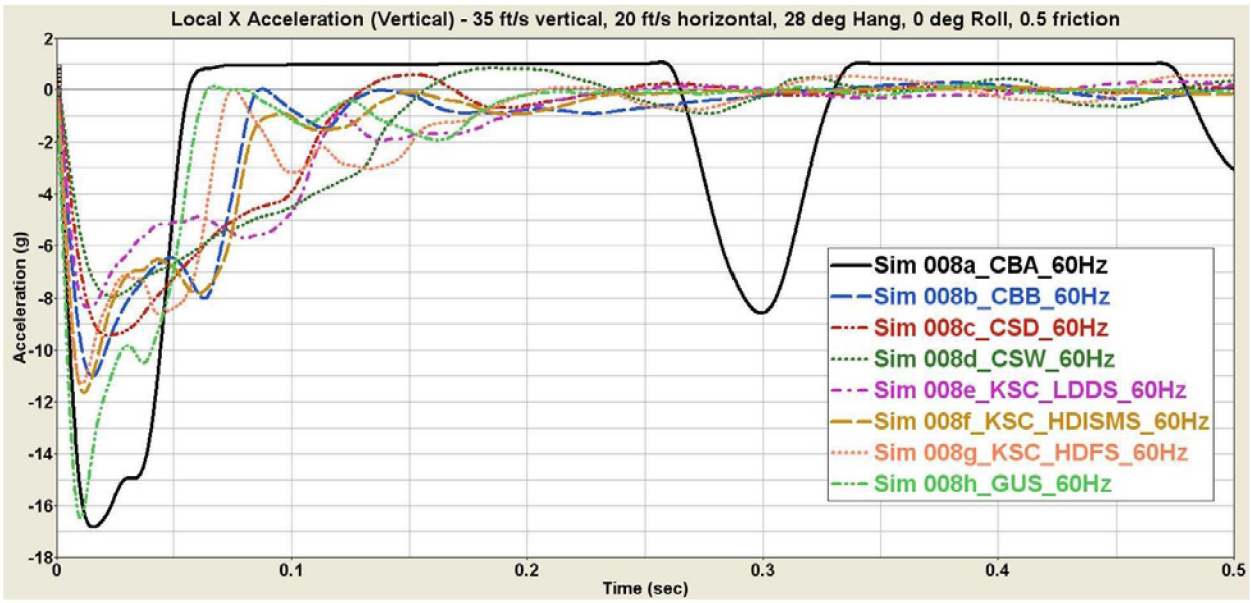

Figure 61. X-axis Accelerations for 35 ft/s Vertical Velocity Case

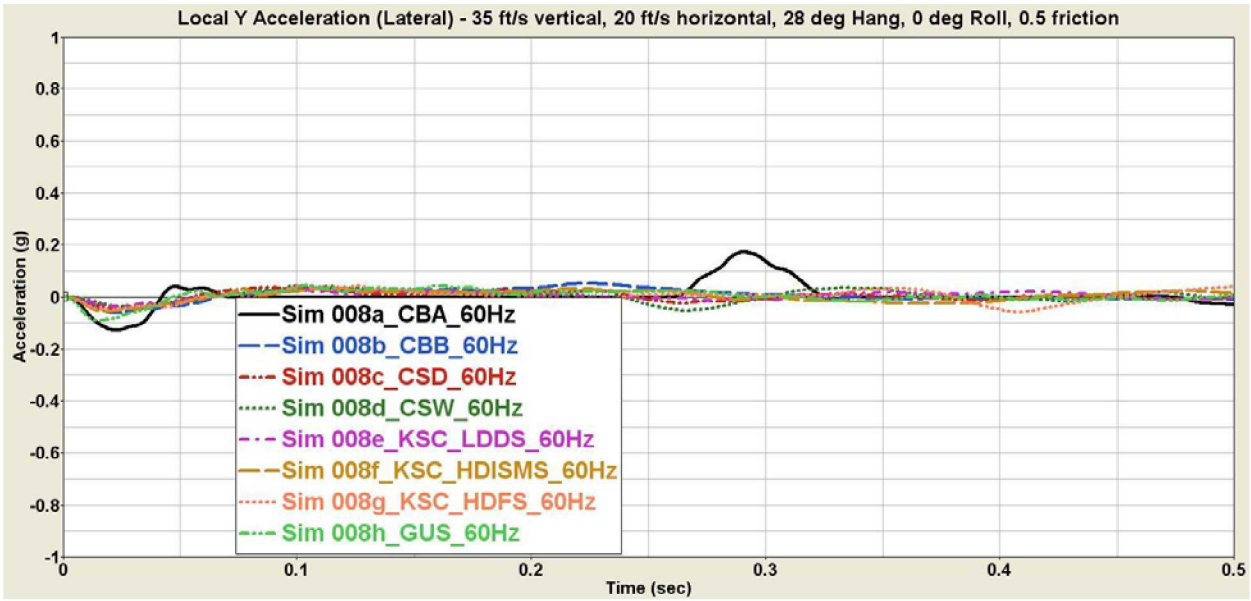

Figure 62. Y-axis Accelerations for 35 ft/s Vertical Velocity Case

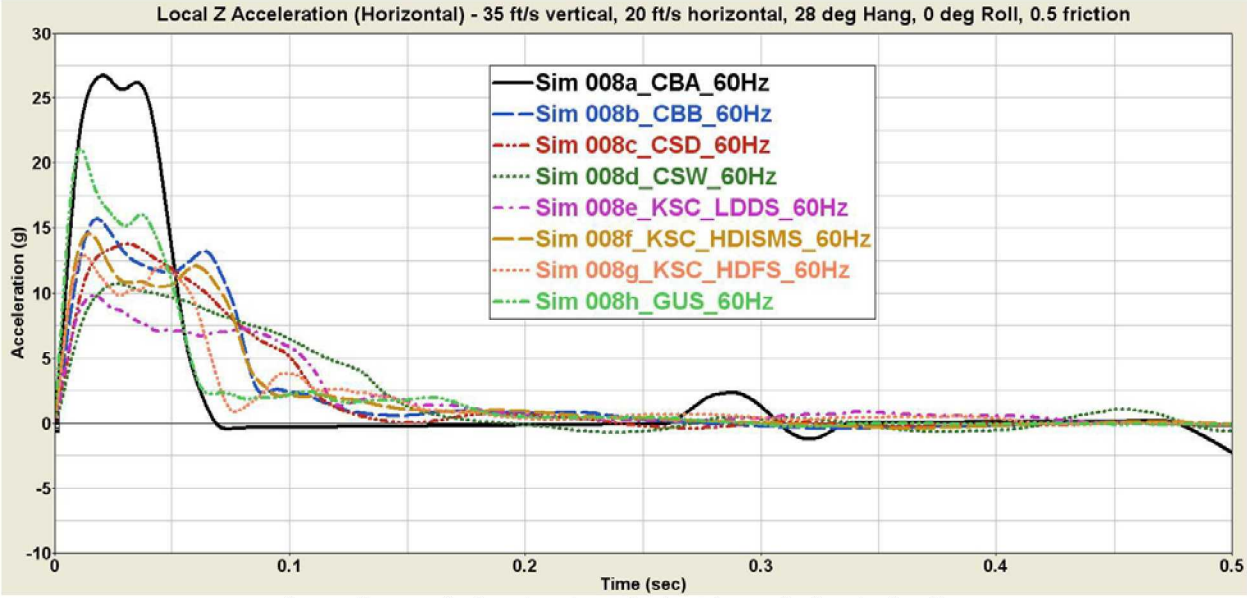

Figure 63. Z-axis Accelerations for 35 ft/s Vertical Velocity Case

Figure 64 shows the pitch angle time-histories for the eight soil cases for the 35 ft/s vertical velocity landing condition. There is a smooth distribution of these curves, with the same general pitch behavior exhibited by half of the soils, but to different levels according to the soil stiffness. The soils that do not produce this pitch behavior are the Carson Sink Wet and Dry soils, the KSC Low Density Dry Sand, and the KSC High Density Flooded Sand, on which the CM essentially comes to rest by 0.3 seconds, as indicated by the unchanging pitch angle in Figure 64.

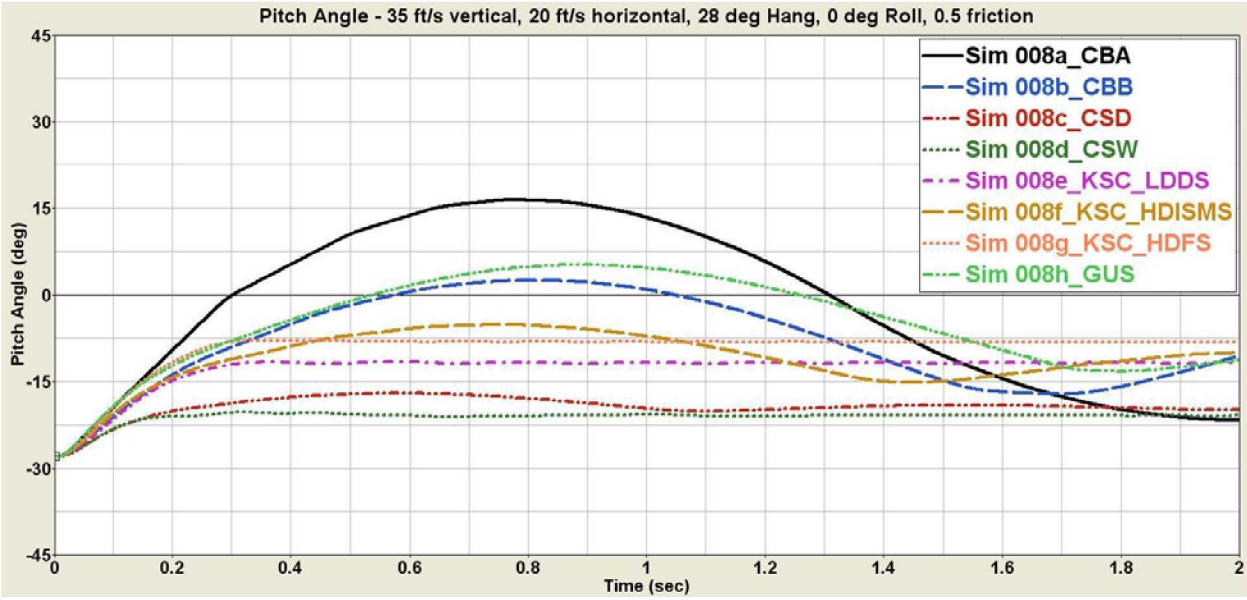

Figure 64. Pitch Angle for 35 ft/s Vertical Velocity Case

5.9 0 ft/s Horizontal Velocity Case

For the ninth simulation case, the next parameter to be varied was the horizontal velocity, while holding all other input parameters at the baseline values. Setting the horizontal velocity to 0 ft/s creates a pure vertical drop landing scenario, removing the effect of plowing into the soil and building up a berm. The Z-axis accelerations for this case result from the combination of the inclination of the CM coordinate system and the movement of the CG as the CM rolls along the bottom of the heat shield. Figure 65 shows a sequence of animation images that illustrate the behavior of the CM landing for the 0 ft/s horizontal velocity case on the Cuddeback A soil. A (second) crater is left under the center of the heat shield when the CM bounces backwards after the initial impact.

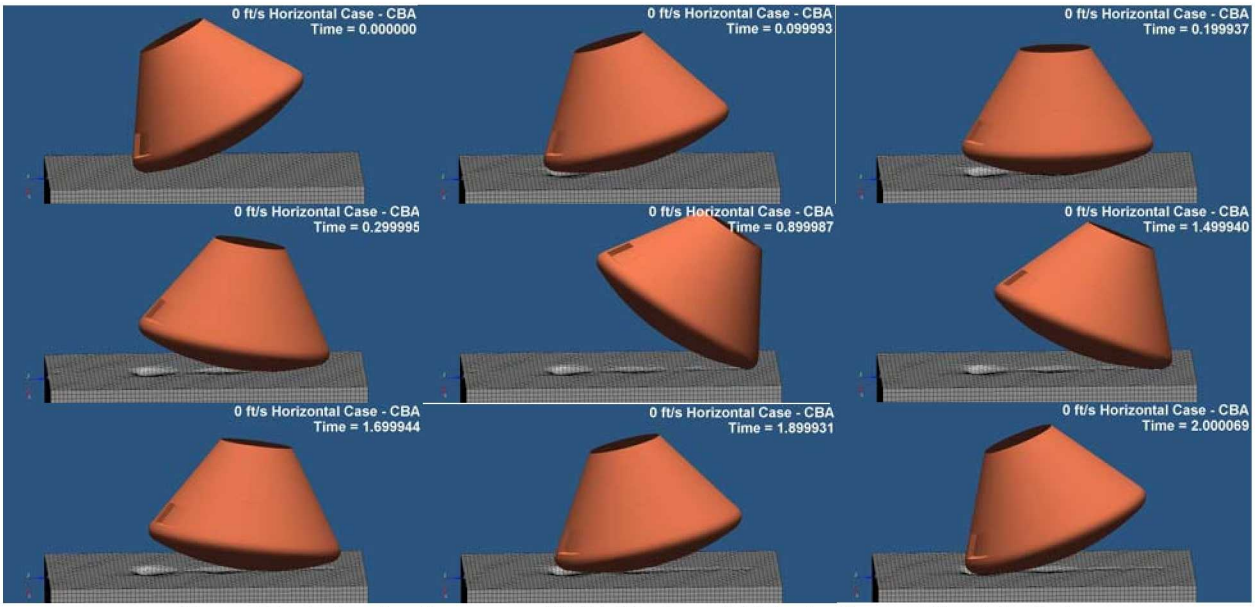

Figure 65. Animation Sequence of 0 ft/s Horizontal Velocity Case on Cuddeback A

Figure 66, Figure 67, and Figure 68 show the X-, Y-, and Z-axis accelerations, respectively, for the 0 ft/s horizontal velocity case on all eight soils. The secondary impact X-axis acceleration peak only occurs on the Cuddeback A soil, as seen in Figure 66. At the time of the second peak (0.2 seconds), the CM local coordinate system is aligned with the global system, so the accelerations are primarily along the X-axis. The Gantry Unwashed Sand approaches the initial X-axis acceleration peak of the Cuddeback A soil, but does not impart enough force to the CM to make it bounce as it rotates backwards, so there is no secondary spike. Instead, the secondary spike is much lower in peak magnitude (27% versus 86%) and spans approximately twice the time period.

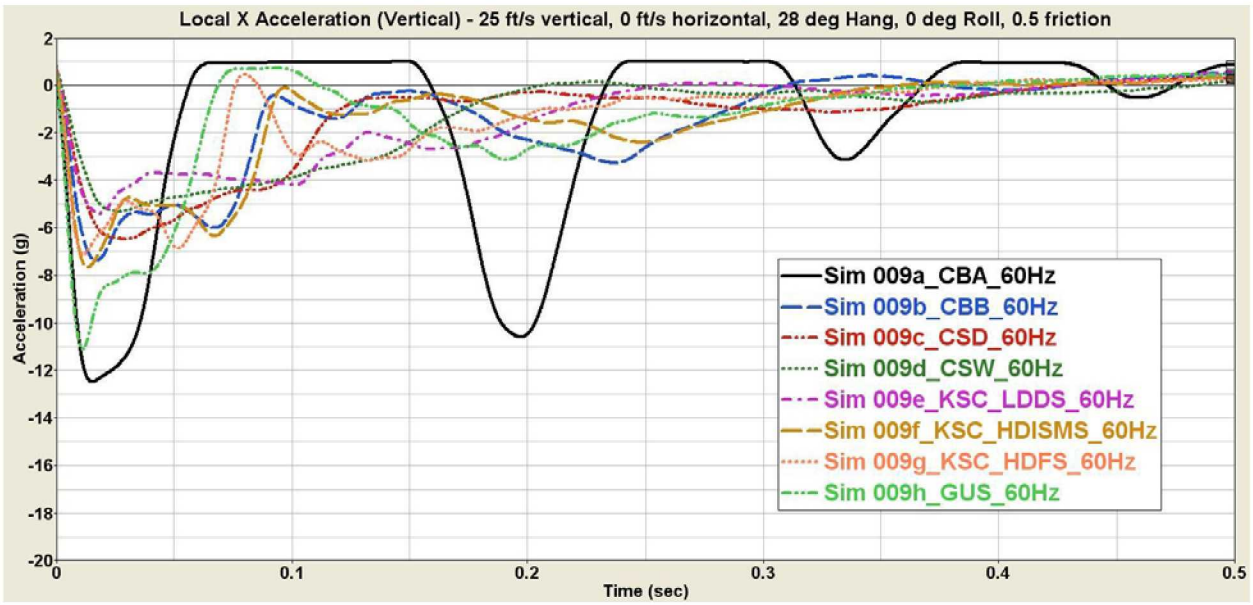

Figure 66. X-axis Accelerations for 0 ft/s Horizontal Velocity Case

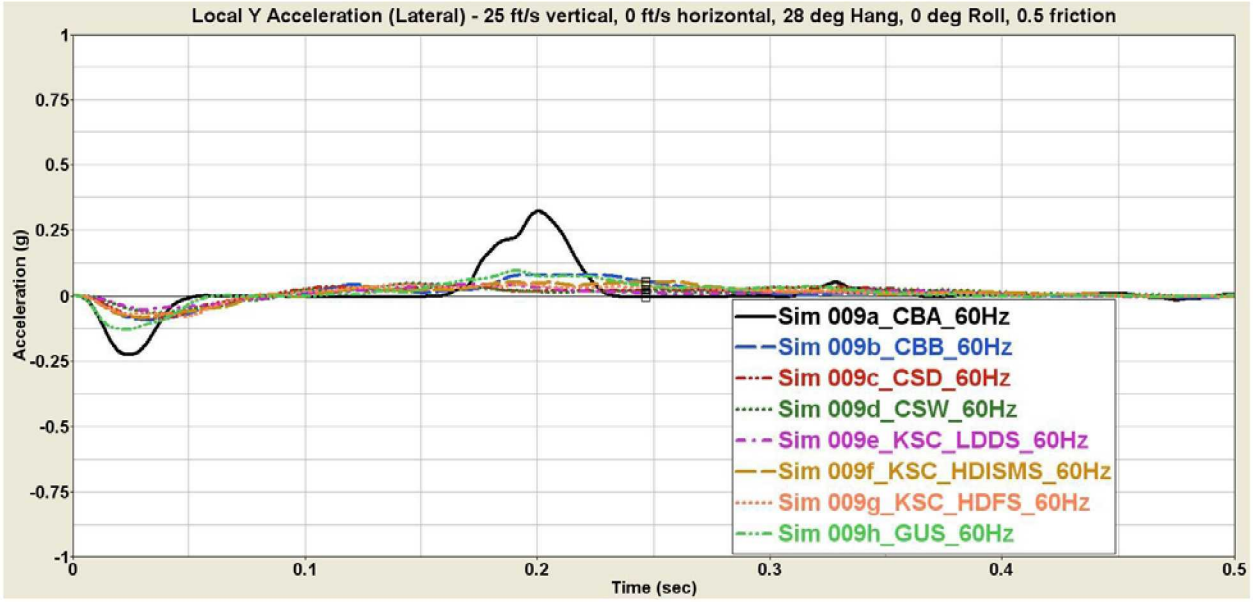

Figure 67. Y-axis Accelerations for 0 ft/s Horizontal Velocity Case

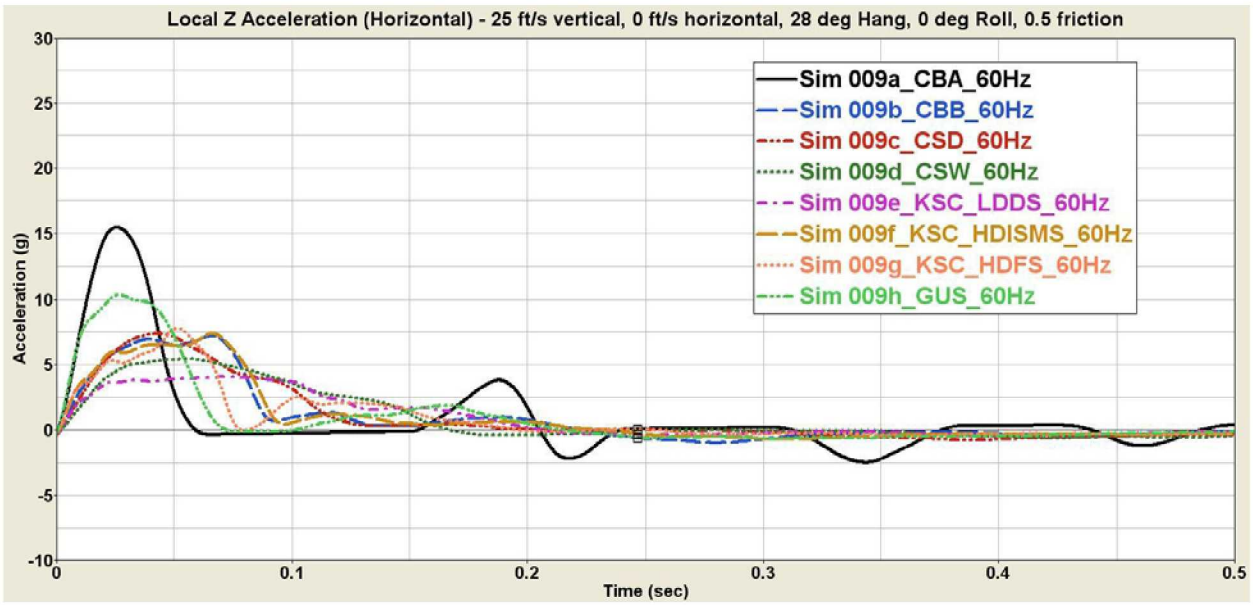

Figure 68. Z-axis Accelerations for 0 ft/s Horizontal Velocity Case

Figure 69 shows the pitch angle time-histories for the eight soil cases for the 0 ft/s horizontal velocity landing condition. The pitch behavior of the vehicle shows the same trends on all the soil models, but has larger displacements on the stiffer soils.

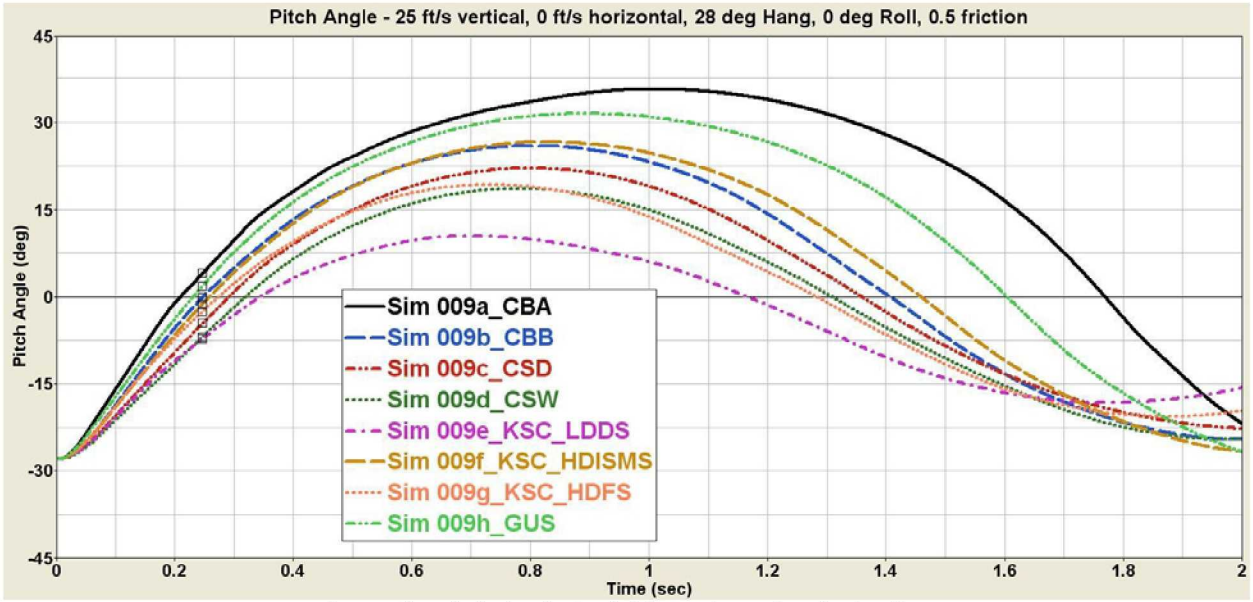

Figure 69. Pitch Angle for 0 ft/s Horizontal Velocity Case

5.10 40 ft/s Horizontal Velocity Case

For the tenth and final simulation case, the horizontal velocity was set to 40 ft/s, and all other input parameters were set to the baseline values. Figure 70 shows a sequence of animation images that illustrate the behavior of the CM landing for the 40 ft/s horizontal velocity case on the KSC Low Density Dry Sand. For this highest impact velocity case, the CM embeds itself into the sand, displacing the sand in front. After 0.7 seconds it rocks back, but eventually tilts forward again slightly, into the hole. The soil is highly deformed and settles downwards under gravity, as evident in the last frame image. However, even with this large soil deformation the model remains stable.

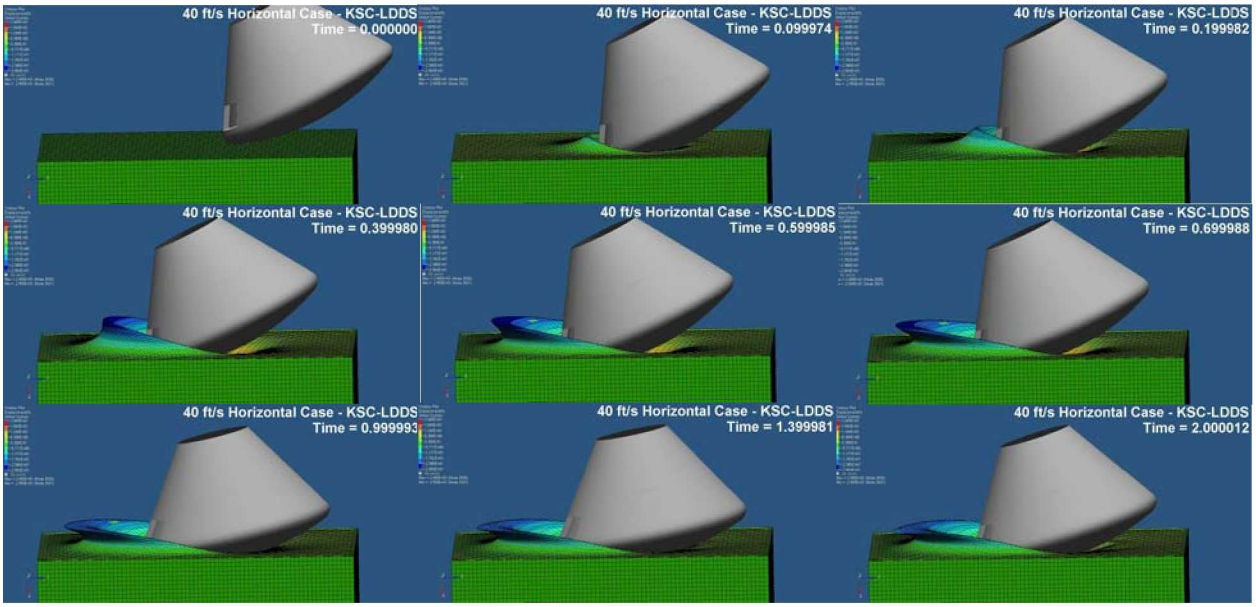

Figure 70. Animation Sequence of 40 ft/s Horizontal Velocity Case on KSC Low Density Dry Sand

Figure 71, Figure 72, and Figure 73 show the X-, Y-, and Z-axis accelerations, respectively, for the 40 ft/s horizontal velocity case on all eight soils. For the 40 ft/s horizontal velocity case, the CM X-axis acceleration peaks are lower than those of the baseline. However, the 40 ft/s horizontal velocity case has the highest CM (combined X and Z) velocity. The Z-axis accelerations are higher for this landing scenario than for any other. The X-axis acceleration for the Gantry Unwashed Sand case drops off earlier than the Cuddeback A case, resulting in a lower acceleration peak. The other six soils all have comparable peak X-axis accelerations. However, the peak Z-axis acceleration is much higher for Cuddeback A than any of the other soils. Cuddeback B and the Gantry Unwashed Sand have comparable Z-axis acceleration peak values, but very different time-history curves, demonstrating that different soil behavior can still result in the same peak acceleration values.

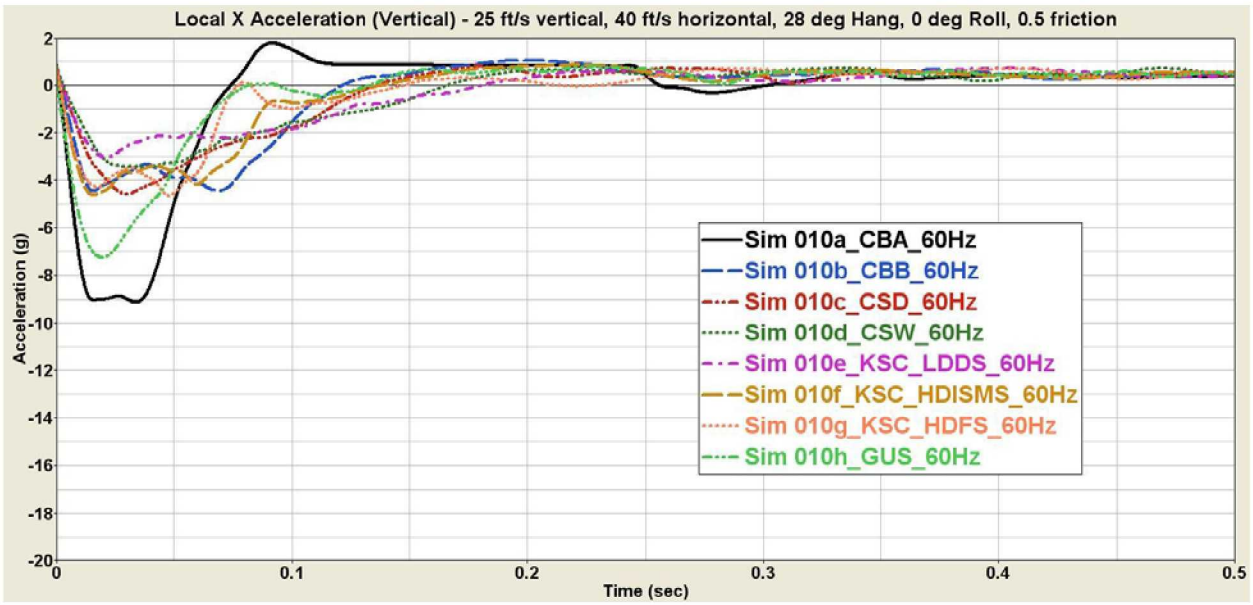

Figure 71. X-axis Accelerations for 40 ft/s Horizontal Velocity Case

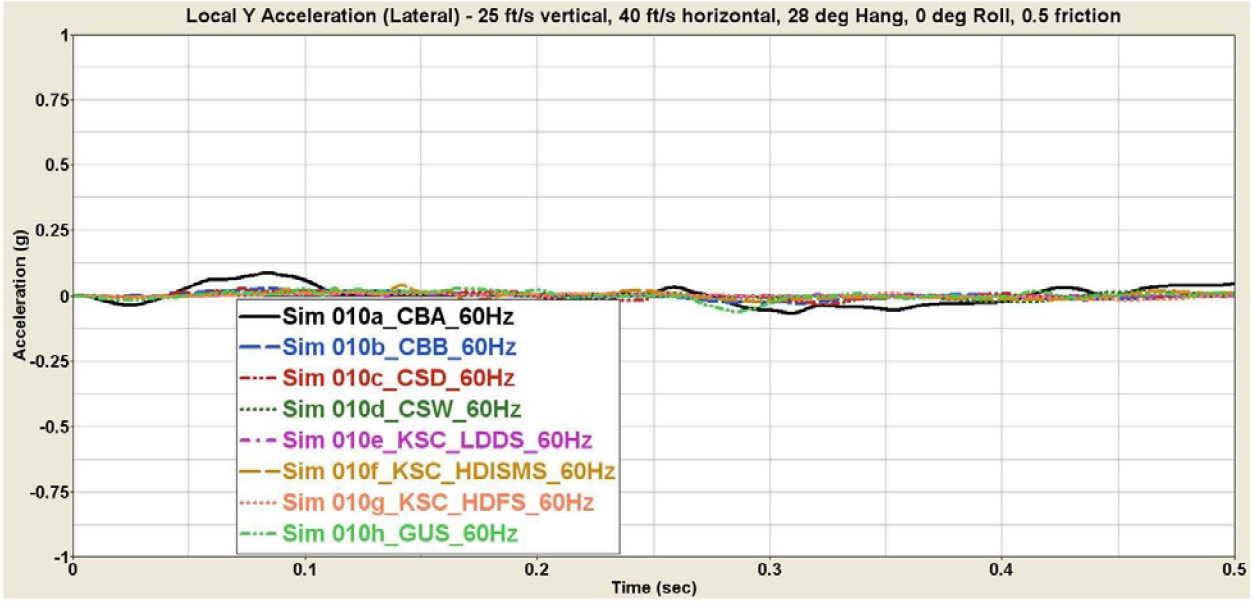

Figure 72. Y-axis Accelerations for 40 ft/s Horizontal Velocity Case

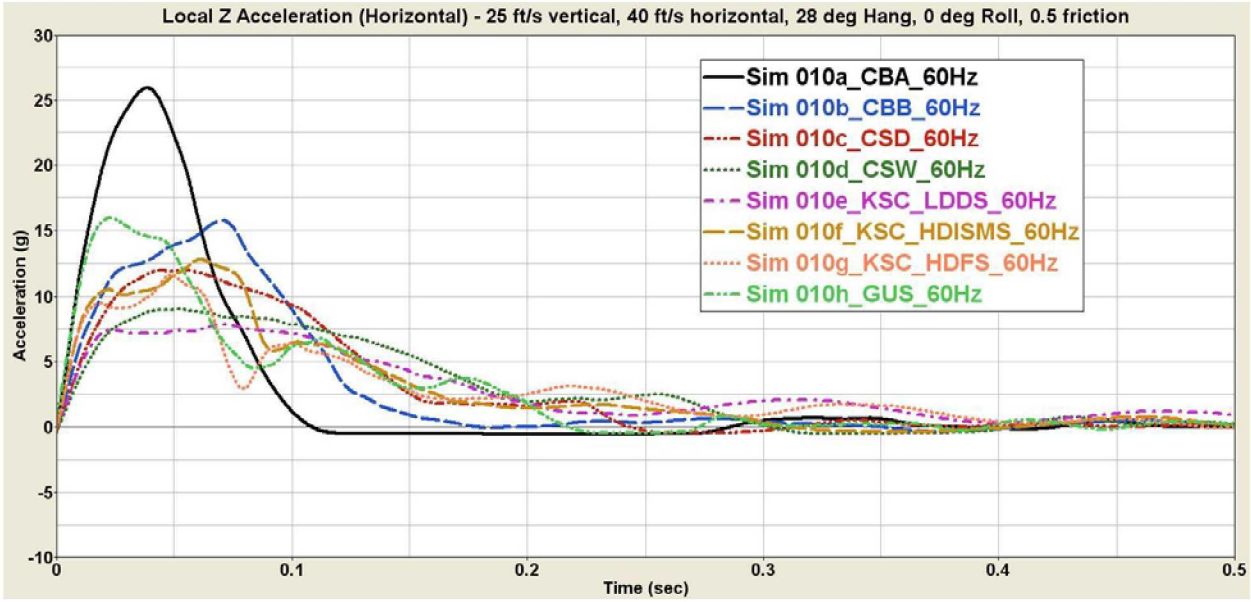

Figure 73. Z-axis Accelerations for 40 ft/s Horizontal Velocity Case

Figure 74 shows the pitch angle time-histories for the eight soil cases for the 40 ft/s horizontal velocity landing condition. The CM pitch angle change is less severe for the KSC Low Density Dry Sand and the High Density Flooded Sand. The change in the pitch angle after 0.1 seconds is in the opposite direction for the other six soils.

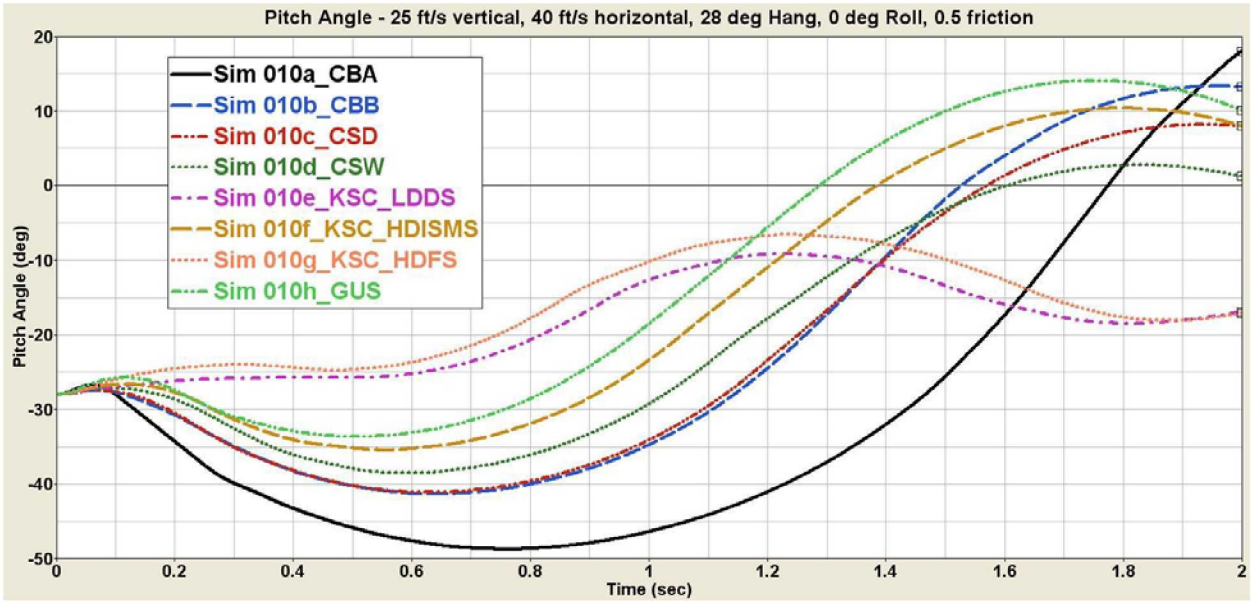

Figure 74. Pitch Angle for 40 ft/s Horizontal Velocity Case

6.0 Conclusions

The soil model response is very complicated and is not controlled by a single material input parameter or curve. In addition, different combinations of soil material properties can produce the same peak CM accelerations. However, the soils analyzed in this study can be roughly categorized as soft, medium, or hard, according to the relative levels of CM landing accelerations. The soft group is comprised of the

Carson Sink Wet soil and the KSC Low Density Dry Sand. The medium group includes the Carson Sink Dry soil, the KSC High Density In-Situ Moisture Sand, the High Density Flooded Sand, and the Cuddeback B soil. The Carson Sink Dry soil is the softest soil categorized as medium, and would have been classified as soft if X-axis accelerations only were considered, but the consideration of the Z-axis accelerations led to its classification as medium. The hard soils are Cuddeback A and the Gantry Unwashed Sand.

The following conclusions were derived from the results of this study:

1. Accelerations experienced by the CM are dependent on the combination of the impact conditions and the soil model used for the simulation. Different soil models have varying sensitivities to the different initial conditions. Lower hang angles result in higher X-axis accelerations on all soils, but the softer soil models have less sensitivity to the hang angle. Although classified as a medium soil, Carson Sink Dry soil also shares this relatively lower sensitivity to the hang angle.

2. The harder the soil, the more sensitive the acceleration peaks are to the input conditions. This conclusion was reached by comparing the change in the peak acceleration values among the different simulation cases.

3. Although the impact conditions have a large effect on the accelerations on the hard soils, the peak accelerations on the softer soils for the most severe impact conditions are still lower than the acceleration peaks on the hard soils for the baseline landing conditions.

4. The softer the soil, the less likely the CM is to roll over since the pitch behavior is more damped and controlled. The KSC Low Density Dry Sand produced a stable landing and the lowest Z-axis accelerations for the 180° roll case.

5. The Cuddeback A soil stands out as much harder than any of the other soils. Although the Gantry Unwashed Sand has comparable acceleration peaks for some landing conditions, the duration of these accelerations is shorter than those of Cuddeback A. Further, the Gantry Unwashed Sand is not from an expected landing zone, but instead is an available area at which tests may be performed, leaving Cuddeback A as the only soil in the hard category. If Cuddeback A could be avoided in a land landing, substantial reductions in the envelope of expected impact accelerations would be achieved.

6. As the roll angle is increased, the Z-axis acceleration peak is reduced, although the X-axis peak acceleration is increased. In the CM, the astronauts will be seated lying on their backs, with their spines oriented roughly in line with the CM Z-axis [ref. 4]. The human tolerance for accelerations is about half as much along the axis of the spine, as compared with the direction perpendicular to the spine through a person's back [ref. 5]. Thus, if the CM Z-axis accelerations can be reduced even while increasing the X-axis accelerations a nominal amount, there will be a net benefit to reducing the potential for injuries to the crew. Therefore, since increasing the roll angle is simultaneously beneficial to crew survivability and detrimental to vehicle landing stability in terms of rollover, a balance between these factors is needed to optimize the overall design of the CM for land landings.

7. The KSC Low Density Dry Sand produces both the lowest relative accelerations and the most stable pitch behavior. Choosing from the eight soils, this would be the ideal soil for a land landing. The KSC High Density Flooded Sand and the Carson Sink soils also have very stable pitch behavior and relatively low accelerations, and so would be good second choices for a land

landing. The Carson Sink Wet soil gives better performance in these areas than the Carson Sink Dry soil, which is comparable to the KSC High Density Flooded Sand.

References

1. Fasanella, Edwin L., "Multi-Terrain Earth Landing Systems Applicable for Manned Space Capsules" Proceedings of the 11th American Society of Civil Engineers (ASCE) Earth and Space Conference, Special Symposium on Ballistic Impact and Crashworthiness of Aerospace Structures, Long Beach, CA, March 3-5, 2008.

2. Applied Research Associates, Inc., "Constitutive Soil Properties for Cuddeback Lake, CA and Carson Sink, NV", NASA CR-2008-215345, August 2008.

3. Applied Research Associates, Inc., "Constitutive Soil Properties for Unwashed Sand and Kennedy Space Center", NASA CR-2008-215334, July 2008.

4. Vassilakos, G. J., Mark S. D., "Orion Contingency Land Landing Passive Attenuation Study", NASA CR-2009-215716, Langley Research Center, April 2009.

5. Eiband, A. Martin, "Human Tolerance to Rapidly Applied Accelerations: A Summary of the Literature", NASA Memorandum 5-19-59E, June 1959.

6. Hallquist, John O., "LS-DYNA Keyword User's Manual", Version 971, Livermore Software Technology Company, Livermore, CA, August 2006.

7. McCullough, J. E., Lands, J. F., Jr., "Apollo Command Module Land-Impact Tests", NASA TN D-6979, National Aeronautics and Space Administration, Manned Spacecraft Center, Houston, TX, October 1972.

Appendix A: Soil Material Input Values

Table 5 contains the primary input parameters for the eight soil models. The KSC-LDDS soil has the lowest density and shear modulus, and the highest bulk unloading modulus. Cuddeback A has the largest A0 value, which is related to the tensile strength due to cohesion of the soil. Typically, clays have the highest cohesion, and dry sands have no cohesion. The Gantry Unwashed Sand has the highest density and shear modulus.

Table 5. Primary Input Parameters for Soil Models

	CBA	CBB	CSD	CSW	KSC-LDDS	KSC-HDISMS	KSC-HDFS	GUS
Density (lb-s2/in4)	0.000136	0.000121	0.000129	0.000135	0.00012	0.00015	0.000135	0.000196
Shear Modulus (psi)	2500	460	1590	500	201	472	525	3340
Bulk Unloading Modulus (psi)	17400	24400	19400	12600	22437	16080	19075	19370
A0 Yield Surface Coefficient	77.52	0.13	0.281	1.968	0	1.371	0.1406	6.326
A1 Yield Surface Coefficient	15.26	0.746	0.961	1.858	0	1.869	0.5397	3.707
A2 Yield Surface Coefficient	0.751	1.068	0.822	0.439	0.5042	0.6368	0.518	0.5432
Pressure Cutoff (psi)	-2	0	0	-1	0	0	0	-1

Table 6 and Table 7 show the stress-strain data for the material models. There is a large variation in the range of strain values that were tested for the different soils. The soils were tested by applying pressure and measuring the strain, and the harder soils do not strain as much as the softer ones. Ten points were manually chosen from the test data in order to adequately capture all slope changes of this curve [ref. 2, 3], and it is known that LS-DYNA will linearly interpolate both between the defined points and to extrapolate the curve past the final point [ref 6].

Table 6. Stress-Strain Values for CBA, CBB, CSD, and CSW

CBA		CBB		CSD		CSW	
eps	P (psi)	eps	P (psi)	eps	P (psi)	eps	P (psi)
0	0	0	0	0	0	0	0
0.0089	30	0.02	18	0.001	2.4	0.007	4.5
0.0104	35	0.0317	25	0.002	3.56	0.0102	5.36
0.012	40	0.0379	30	0.004	4.8	0.013	6
0.0138	45	0.0436	35	0.005	5.72	0.019	7
0.0155	50	0.0491	40	0.01	7.37	0.063	12
0.019	60	0.0592	50	0.076	20	0.125	19.6
0.0226	70	0.0683	60	0.111	30	0.185	32
0.0263	80	0.0766	70	0.15	50	0.22	47
0.0291	87.8	0.0827	78	0.18	71	0.259	67

Table 7. Stress-Strain Values for KSC-LDDS, KSC-HDISMS, KSC-HDFS, and GUS

KSC_LDDS		KSC_HDISMS		KSC_HDFS		GUS	
eps	P (psi)	eps	P (psi)	eps	P (psi)	eps	P (psi)
0	0	0	0	0	0	0	0
0.0118	5.88	0.0044	3.37	0.002	2	0.00252	10
0.0284	6.02	0.0087	7.65	0.004	4.93	0.00479	20
0.0302	12.18	0.0125	13.15	0.006	9.2	0.00703	30
0.0333	19.29	0.0175	20.8	0.008	14.4	0.00917	40
0.0376	29.14	0.0214	27.99	0.01	22.67	0.0103	45
0.0401	33.25	0.0264	39.01	0.012	33.33	0.01143	50
0.0444	45.15	0.031	51.09	0.014	45.73	0.01254	55
0.0478	54.46	0.0335	59.04	0.016	60.13	0.01362	60
0.0512	67.05	0.0357	65.77	0.0172	70.4	0.01599	71.15

Appendix B: Additional Contact Force Results

The following sections present the contact forces for all the simulation cases.

B.1 Baseline Case: 28° Hang Angle, 0° Roll Angle, 25 ft/s Vertical, 20 ft/s Horizontal

The vertical, lateral, and longitudinal contact forces between the CM and the soil are shown in Figure 75, Figure 76, and Figure 77, respectively.

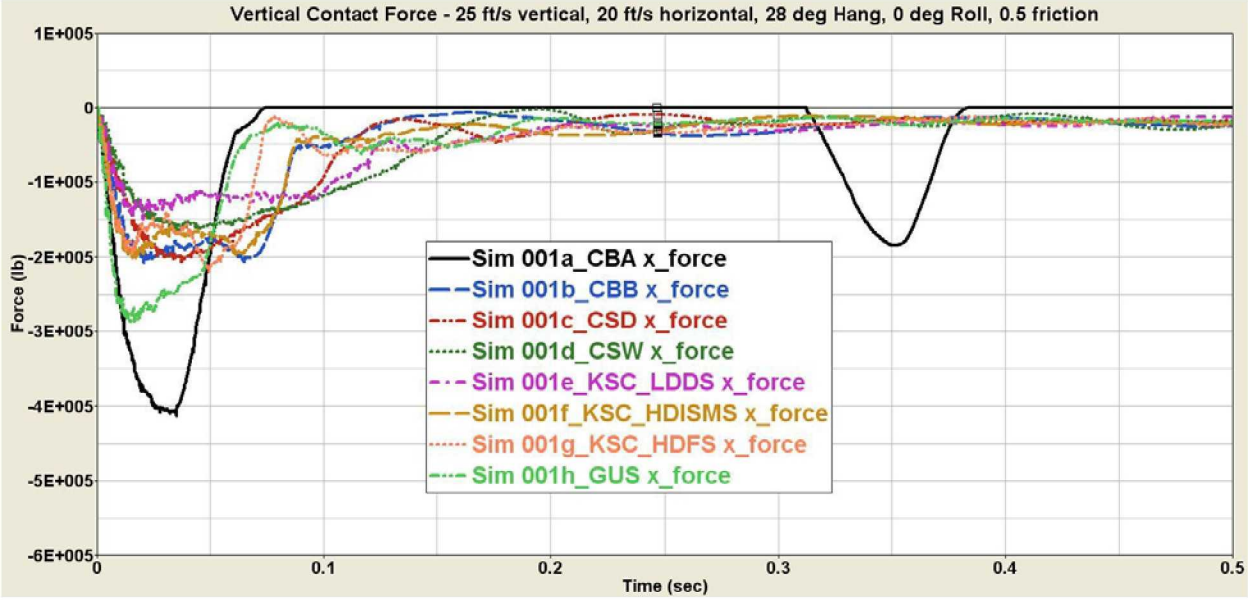

Figure 75. X (Vertical) Contact Force for Baseline Case

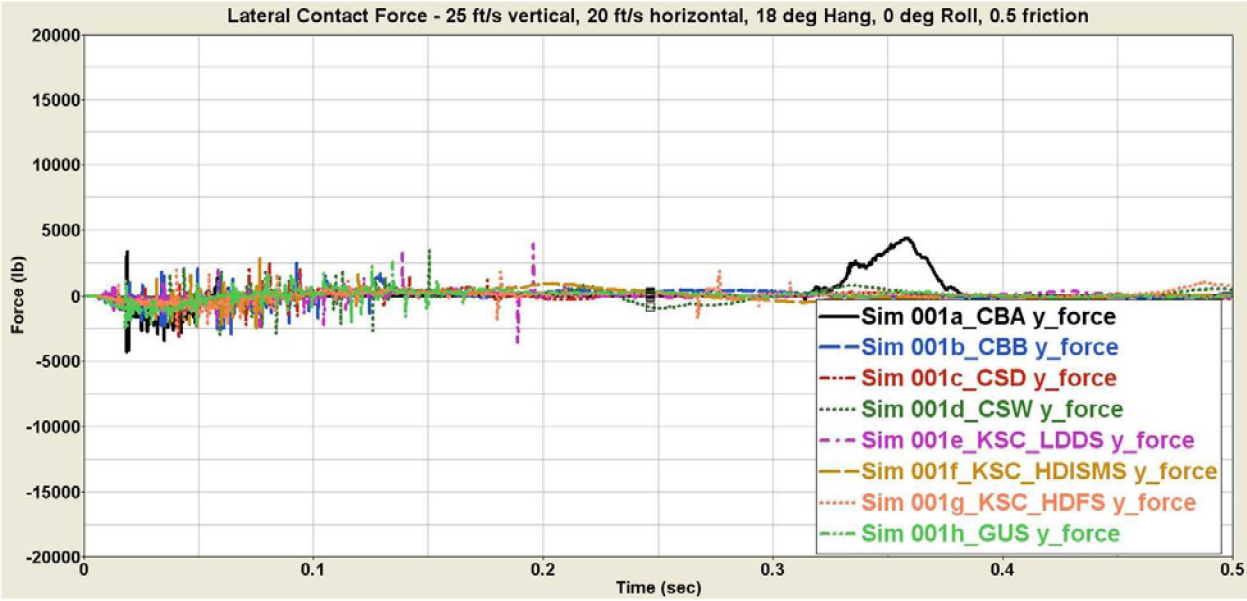

Figure 76. Y (Lateral) Contact Force for Baseline Case

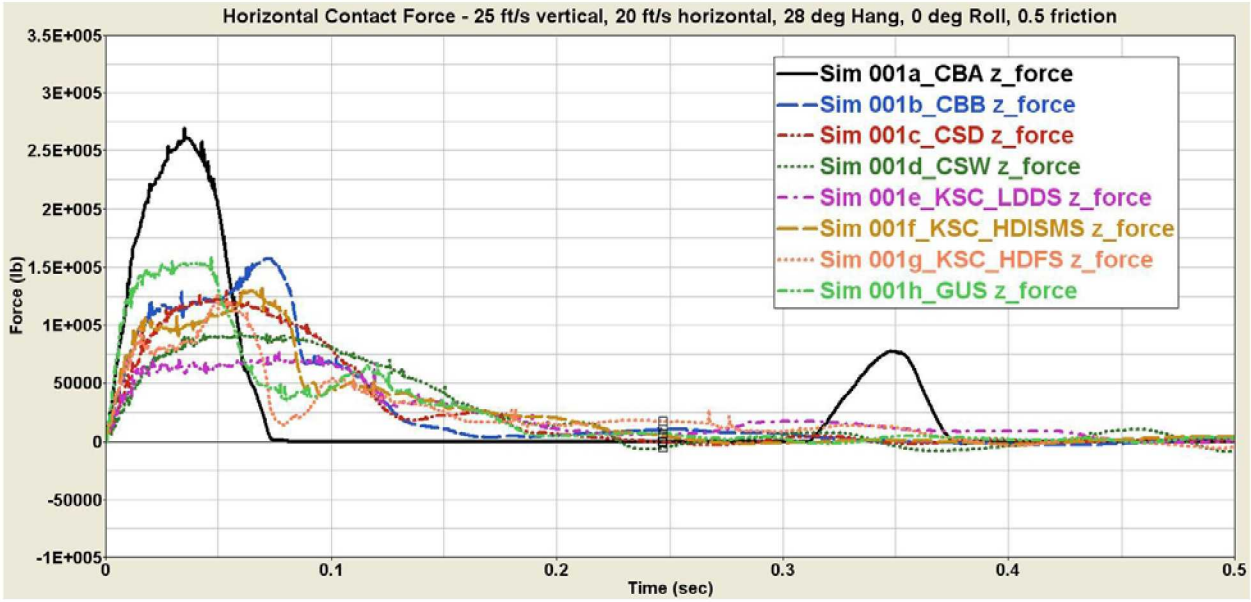

Figure 77. Z (Longitudinal) Contact Force for Baseline Case

B.2 18° Hang Angle Case

The vertical, lateral, and longitudinal contact forces for the 18° hang angle cases are shown in Figure 78, Figure 79, and Figure 80, respectively. The peak contact forces for the Gantry Unwashed Sand actually exceed those of the Cuddeback A soil, although for a much shorter duration, resulting in less area under the force curve for the Gantry Unwashed Sand.

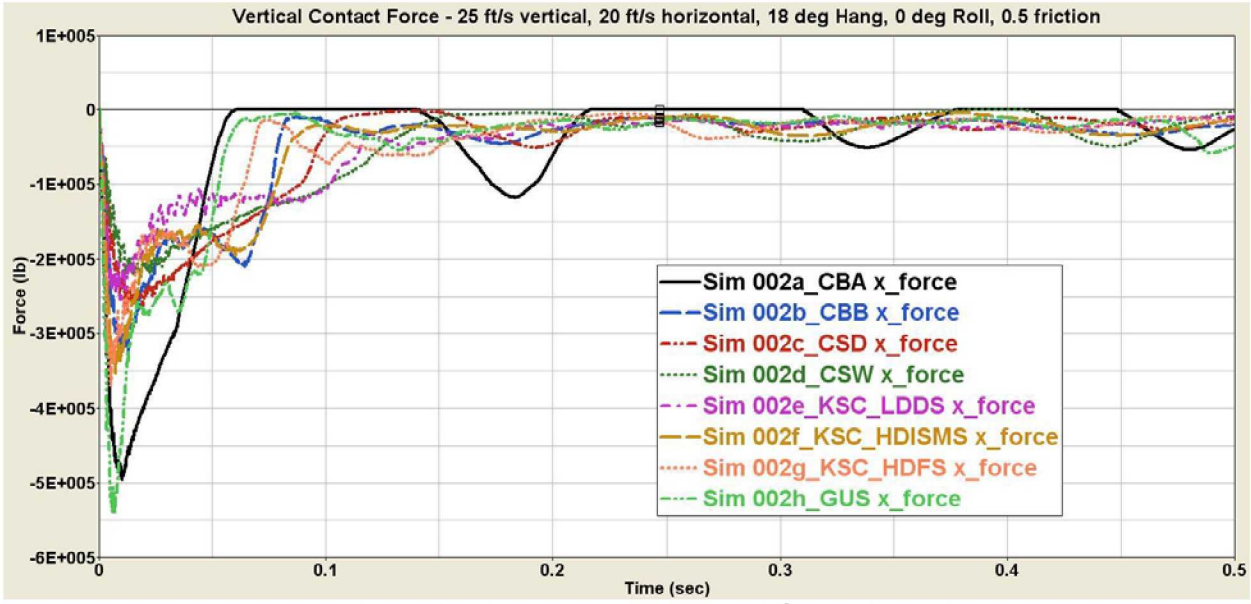

Figure 78. Vertical (global X-axis) Force for 18° Hang Angle Case

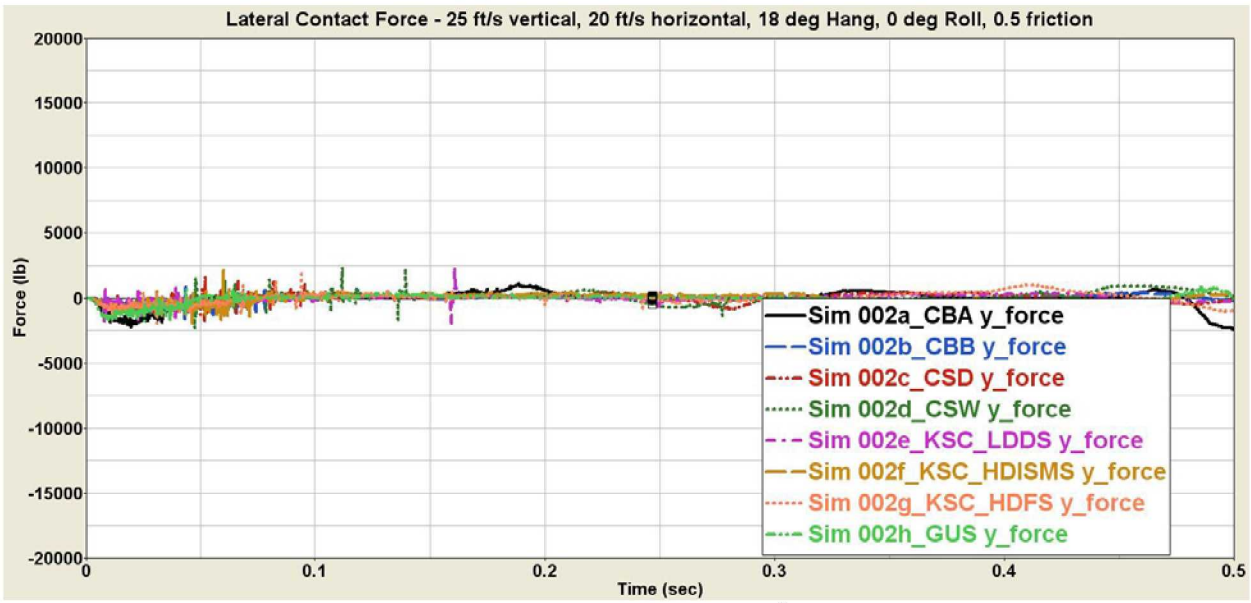

Figure 79. Lateral (global Y-axis) Force for 18° Hang Angle Case

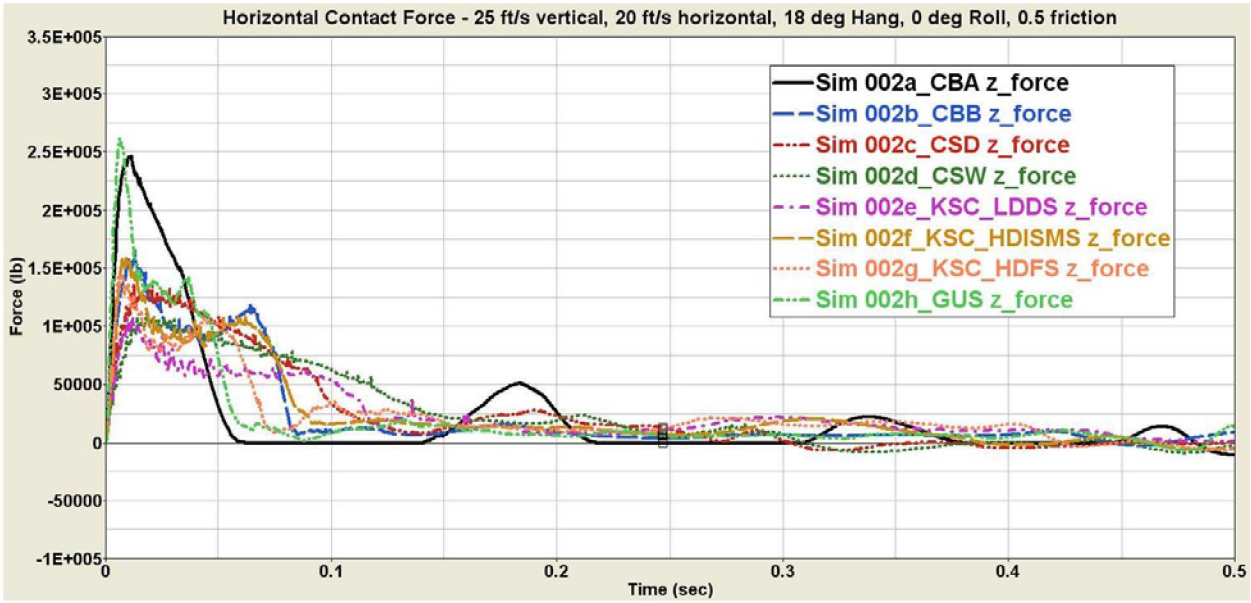

Figure 80. Longitudinal (global Z-axis) Force for 18° Hang Angle Case

B.3 38° Hang Angle Case

The vertical, lateral, and longitudinal contact forces for the 38° hang angle case on the eight soil models are plotted in Figure 81, Figure 82, and Figure 83, respectively. Even at this higher hang angle, the contact forces still follow the trends of the accelerations for all the soils despite the 38° difference in the orientations of the coordinate systems.

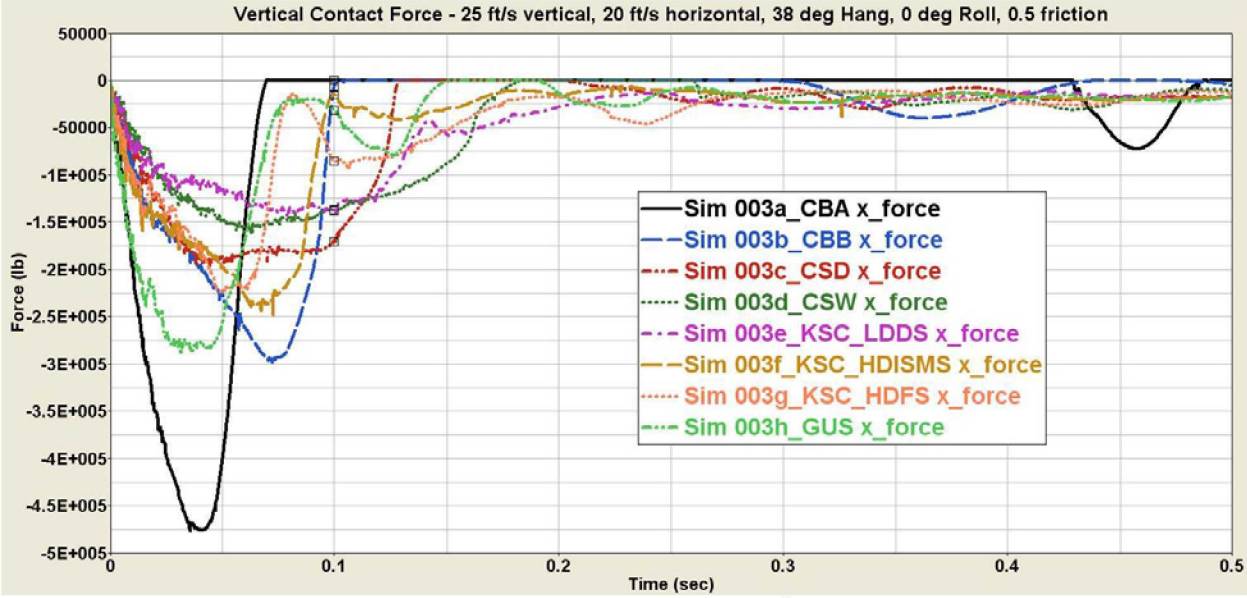

Figure 81. Vertical (global X-axis) Force for 38° Hang Angle Case

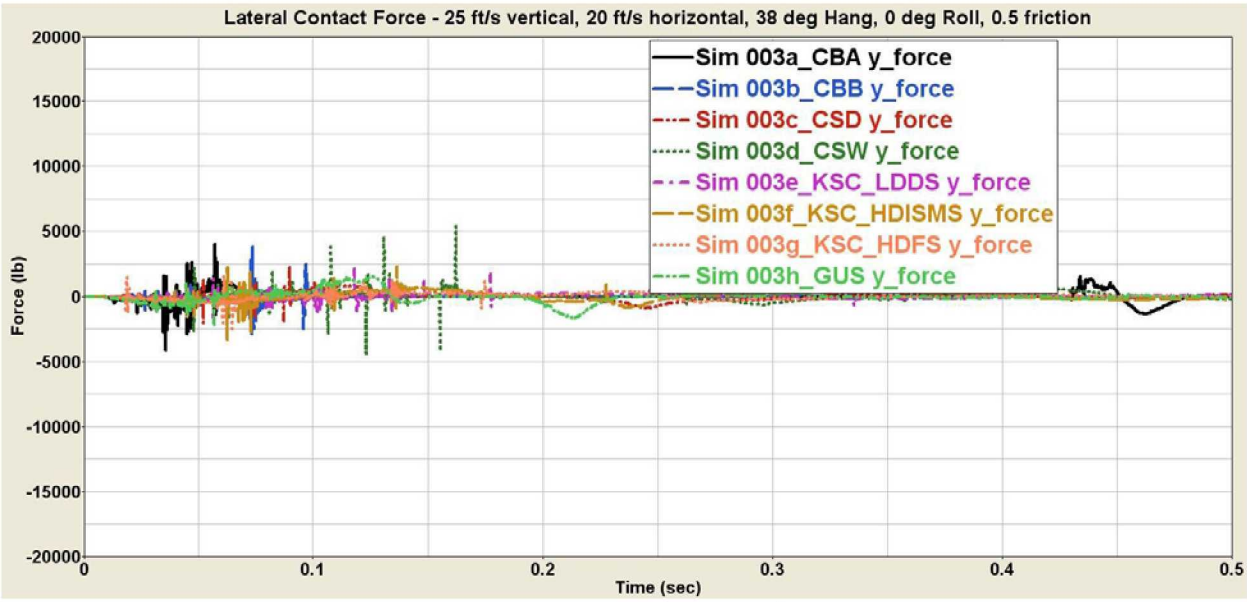

Figure 82. Lateral (global Y-axis) Force for 38° Hang Angle Case

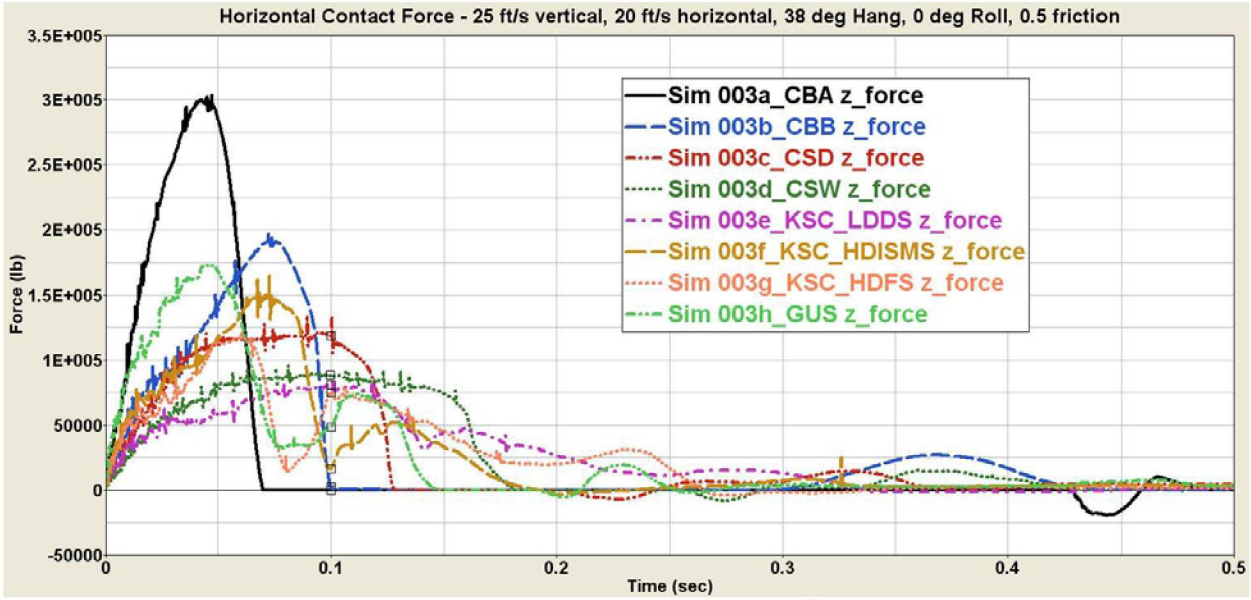

Figure 83. Longitudinal (global Z-axis) Force for 38° Hang Angle Case

B.4 45° Roll Angle Case

The vertical, lateral, and longitudinal contact forces for the 45° roll angle case on the eight soil models are plotted in Figure 84, Figure 85, and Figure 86, respectively. The lateral contact force is only about 28% of the vertical, while the longitudinal contact force is 50% of the vertical. The Cuddeback A soil and the Gantry Unwashed Sand simulations have higher peak values that occur earlier than the other soils. The difference in the initial slope of the contact force is most pronounced in the lateral direction, where Cuddeback A soil and the Gantry Unwashed Sand have the steepest slope and Carson Sink Wet soil and the KSC Low Density Dry Sand have the lowest.

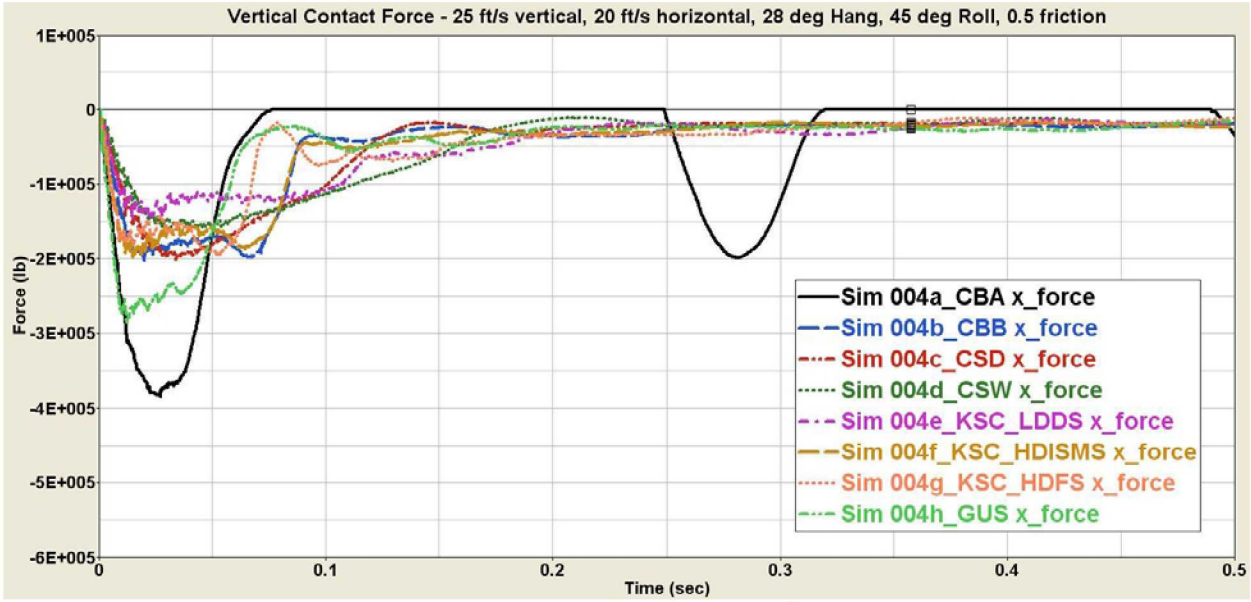

Figure 84. Vertical (global X-axis) Force for 45° Roll Angle Case

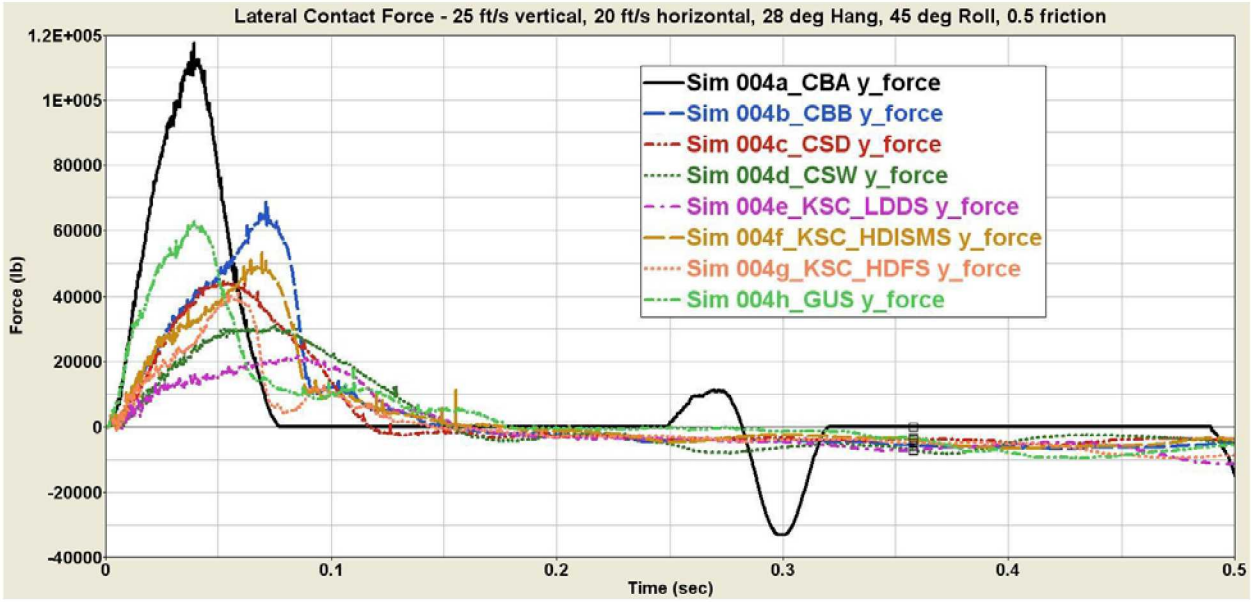

Figure 85. Lateral (global Y-axis) Force for 45° Roll Angle Case

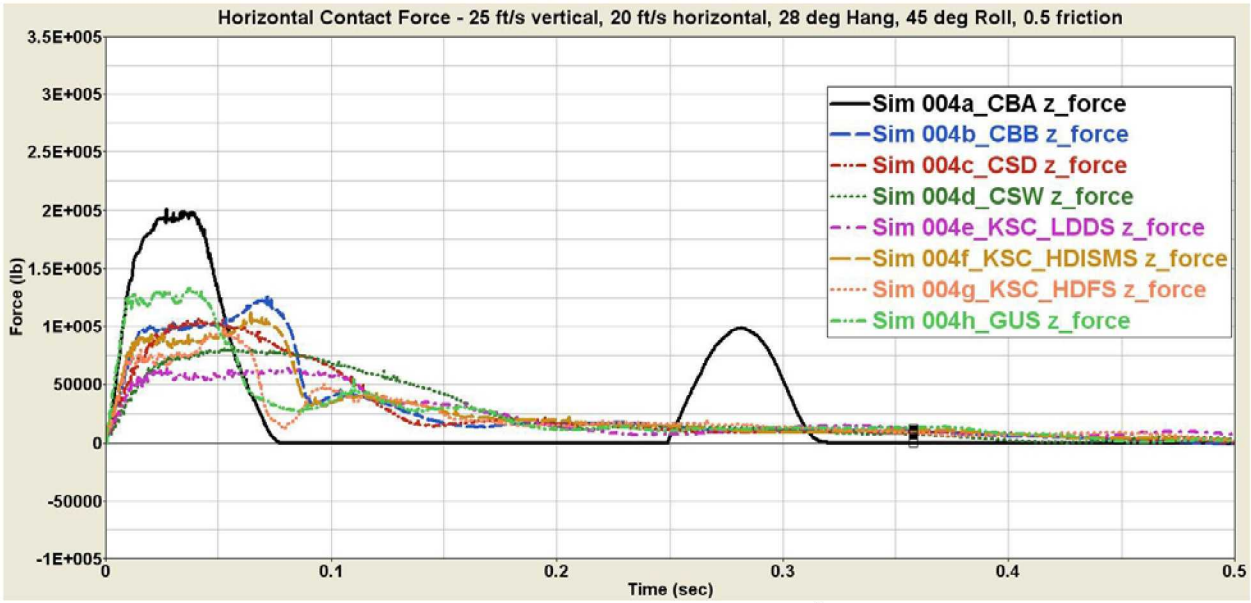

Figure 86. Longitudinal (global Z-axis) Force for 45° Roll Angle Case

B.5 90° Roll Angle Case

The vertical, lateral, and longitudinal contact forces for the 90° roll angle case on the eight soil models are plotted in Figure 87, Figure 88, and Figure 89, respectively. The second spike in the lateral contact force on the Cuddeback A soil is smaller than the first, indicating that the orientation of the CM Y-axis in the direction of the horizontal velocity is driving the Y-axis acceleration peak. For the Cuddeback A case, the lateral and longitudinal forces are both less than half of the vertical force. The lateral and horizontal contact force curves do not parallel the shape of the vertical forces. Both of these factors are indications that the soil is being displaced initially, which is also visible in the simulation animations.

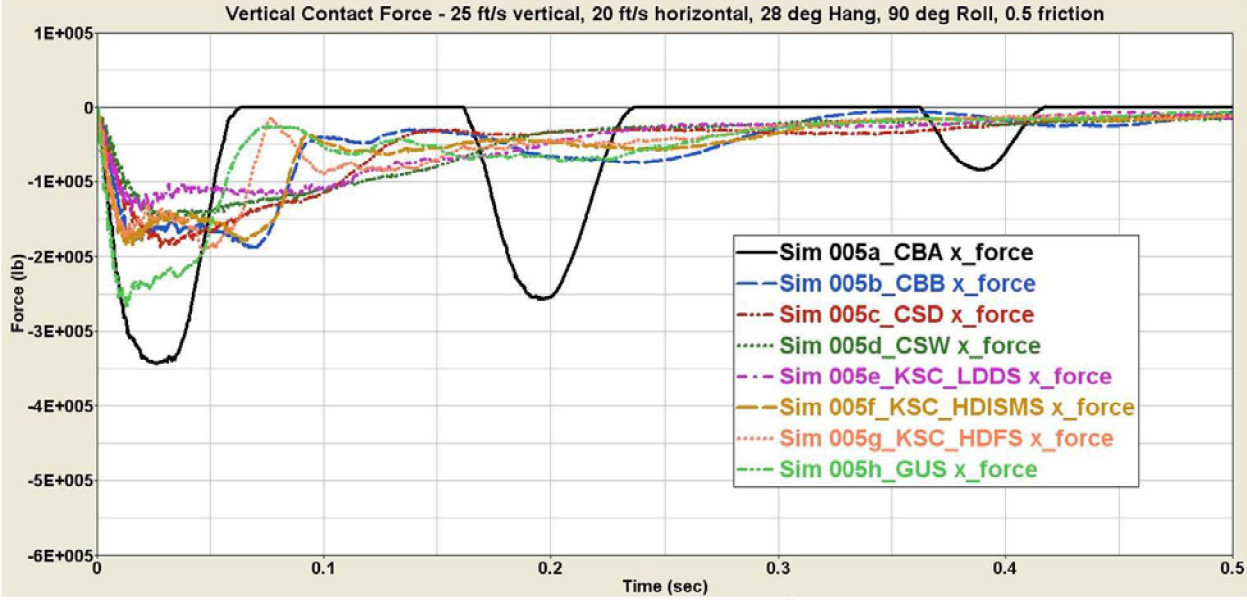

Figure 87. Vertical (global X-axis) Force for 90° Roll Angle Case

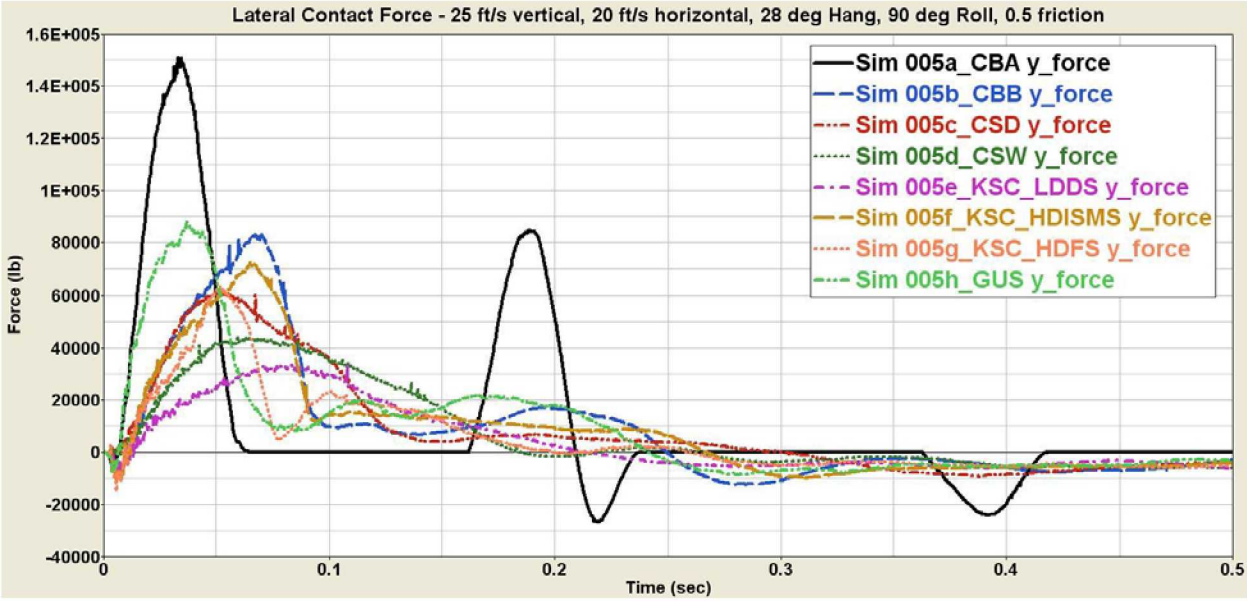

Figure 88. Lateral (global Y-axis) Force for 90° Roll Angle Case

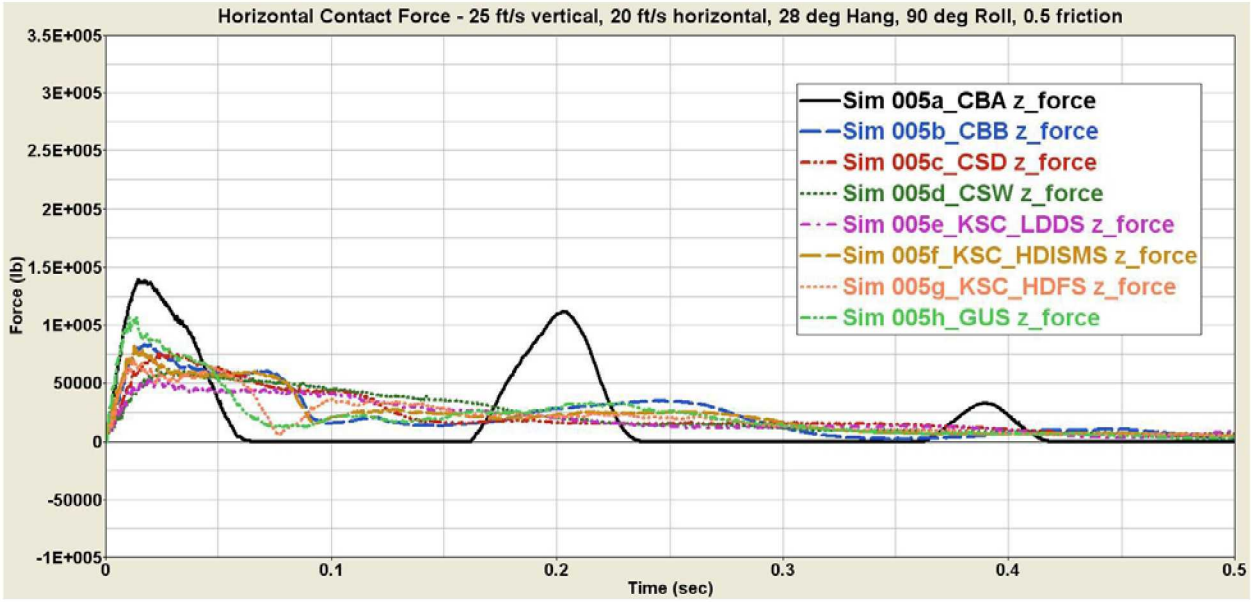

Figure 89. Longitudinal (global Z-axis) Force for 90° Roll Angle Case

B.6 180° Roll Angle Case

The vertical, lateral, and longitudinal contact forces for the 180° roll angle case on the eight soil models are plotted in Figure 90, Figure 91, and Figure 92, respectively. The contact forces for the 180° roll case are lower than those of the baseline case. The relative ratios of the contact forces among the different soil models follow the same trends as the accelerations. The lateral forces are less than 10% of the longitudinal forces.

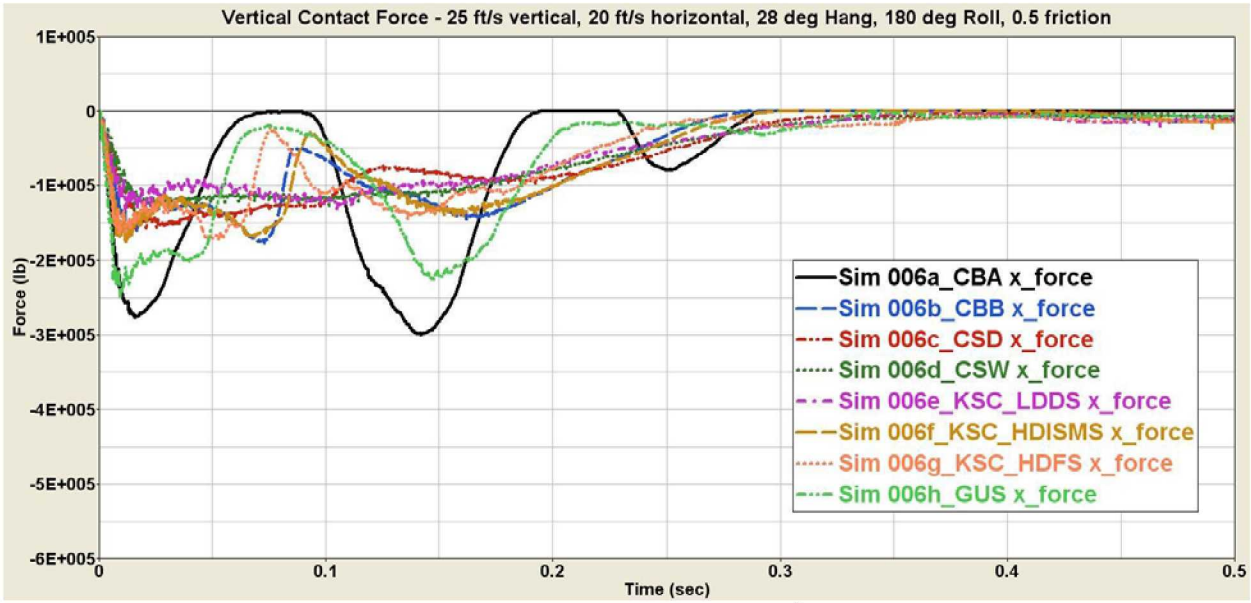

Figure 90. Vertical (global X-axis) Force for 180° Roll Angle Case

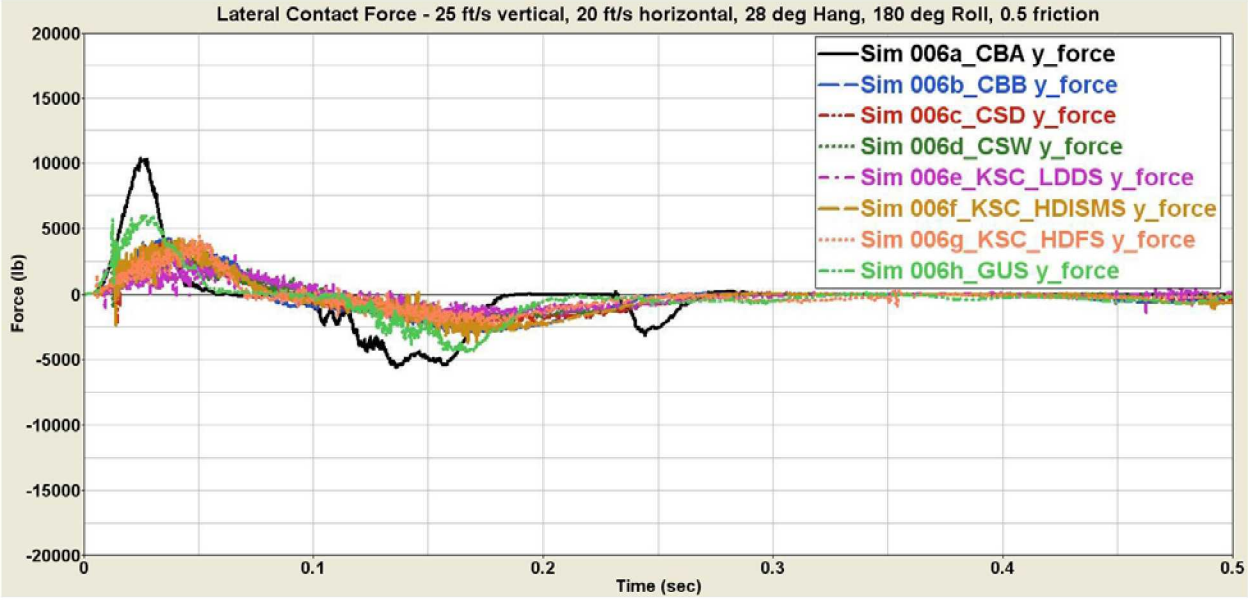

Figure 91. Lateral (global Y-axis) Force for 180° Roll Angle Case

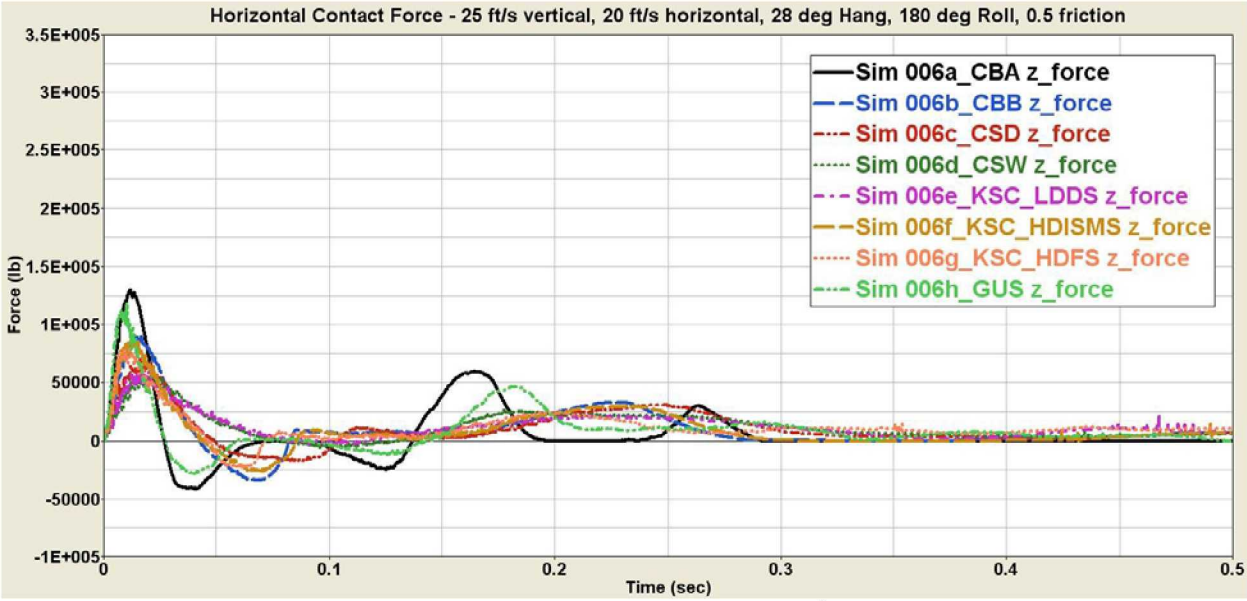

Figure 92. Longitudinal (global Z-axis) Force for 180° Roll Angle Case

B.7 15 ft/s Vertical Velocity Case

The vertical, lateral, and longitudinal contact forces for the 15 ft/s vertical velocity case on the eight soil models are plotted in Figure 93, Figure 94, and Figure 95, respectively. The trends of the forces track those of the accelerations.

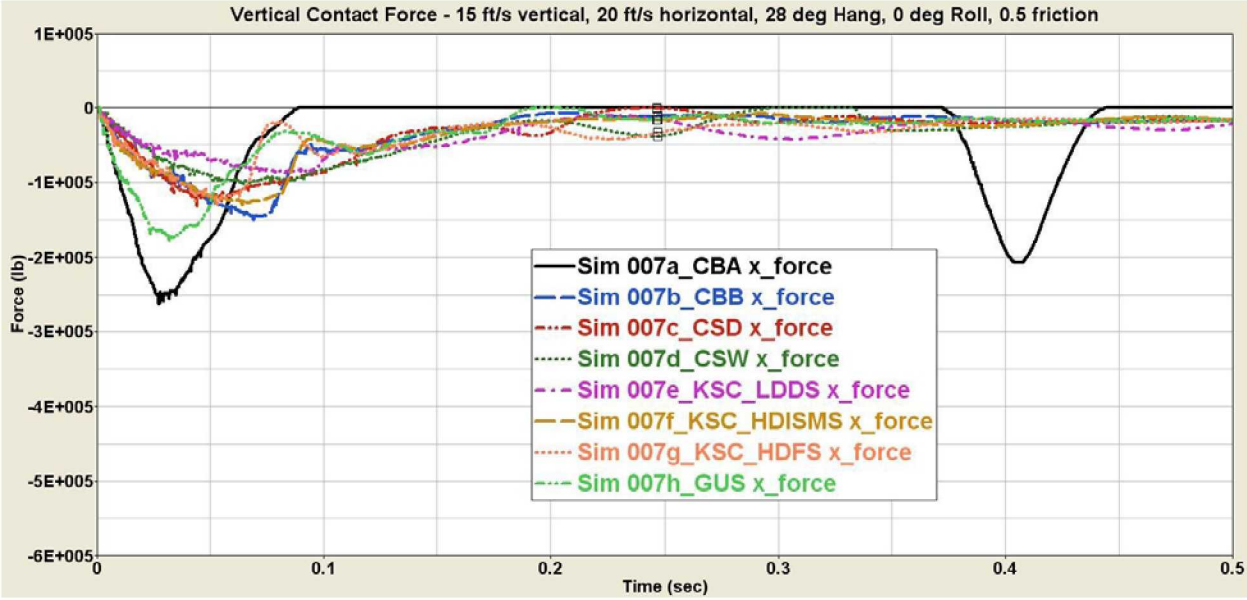

Figure 93. Vertical (global X-axis) Force for 15 ft/s Vertical Velocity Case

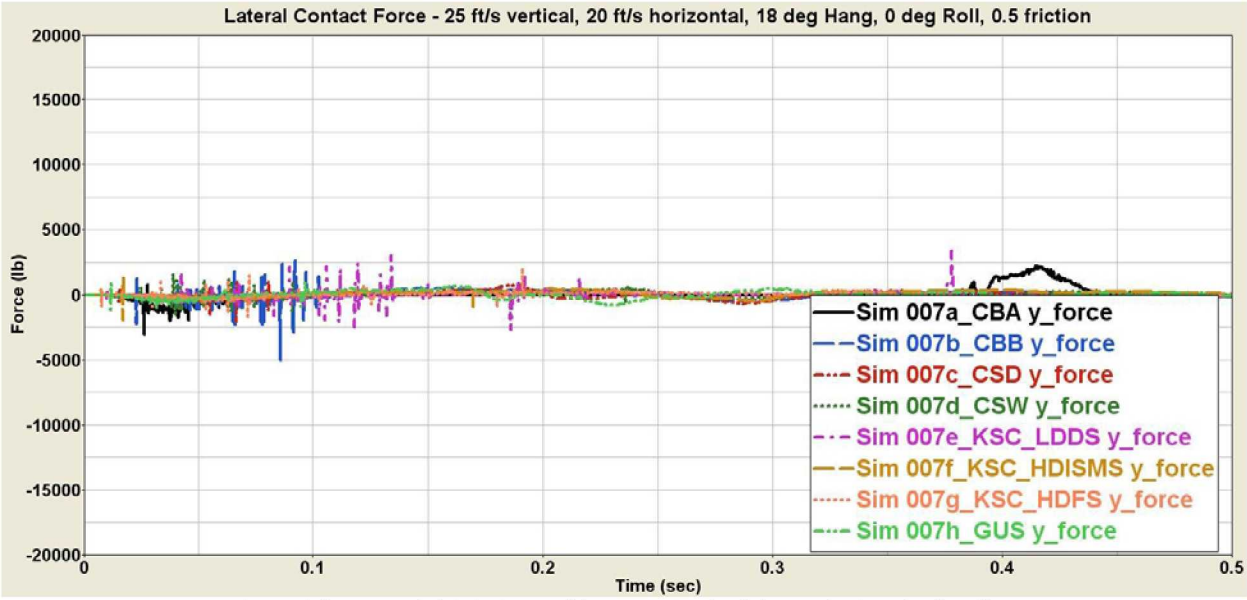

Figure 94. Lateral (global Y-axis) Force for 15 ft/s Vertical Velocity Case

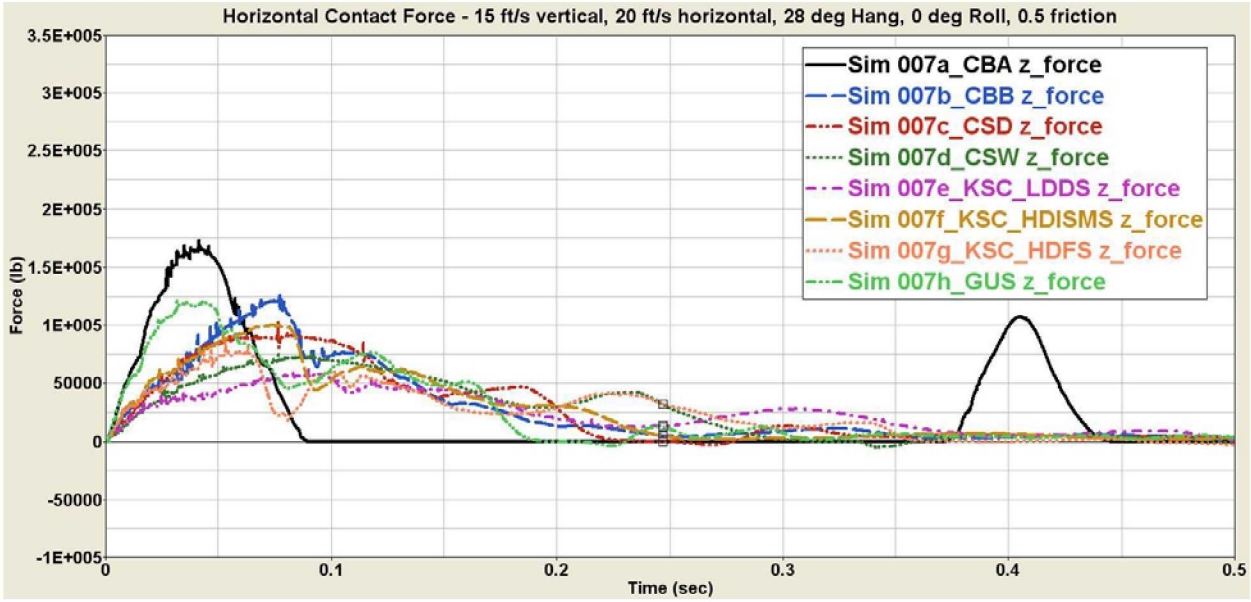

Figure 95. Longitudinal (global Z-axis) Force for 15 ft/s Vertical Velocity Case

B.8 35 ft/s Vertical Velocity Case

The vertical, lateral, and longitudinal contact forces for the 35 ft/s vertical velocity case on the eight soil models are plotted in Figure 96, Figure 97, and Figure 98, respectively. The contact force trends parallel those of the accelerations.

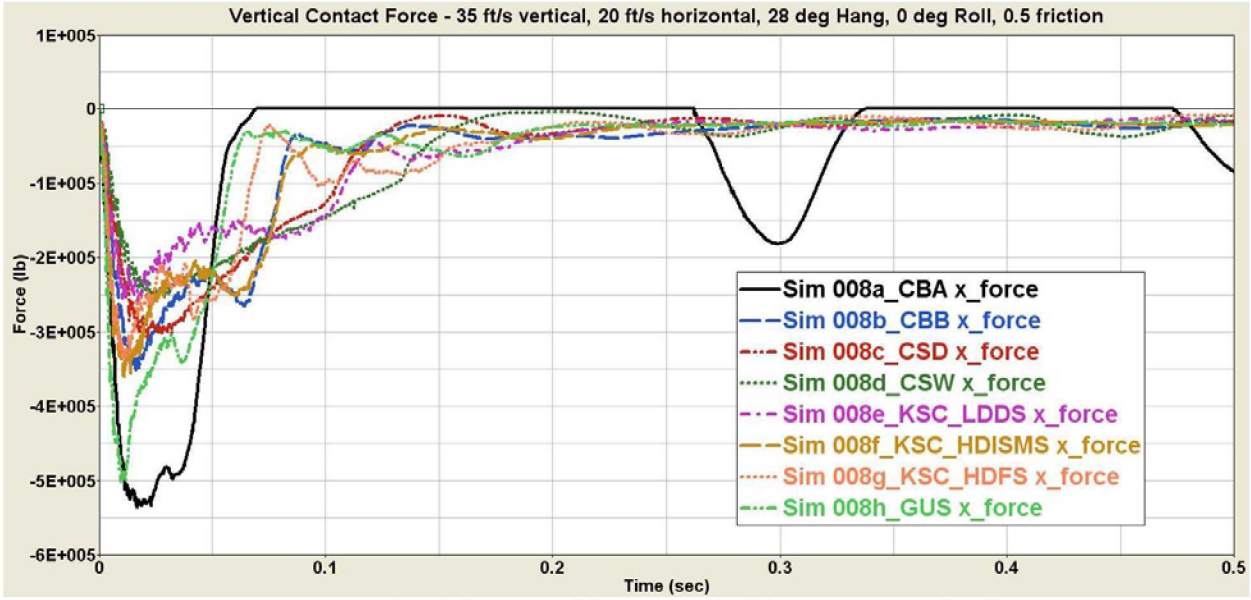

Figure 96. Vertical (global X-axis) Force for 35 ft/s Vertical Velocity Case

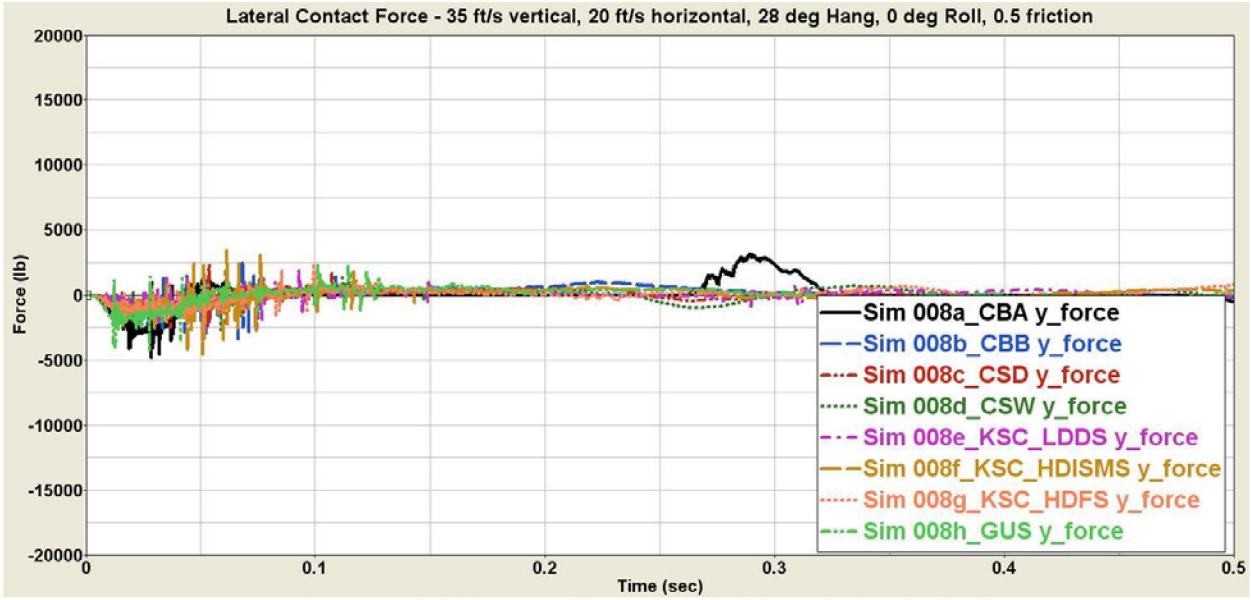

Figure 97. Lateral (global Y-axis) Force for 35 ft/s Vertical Velocity Case

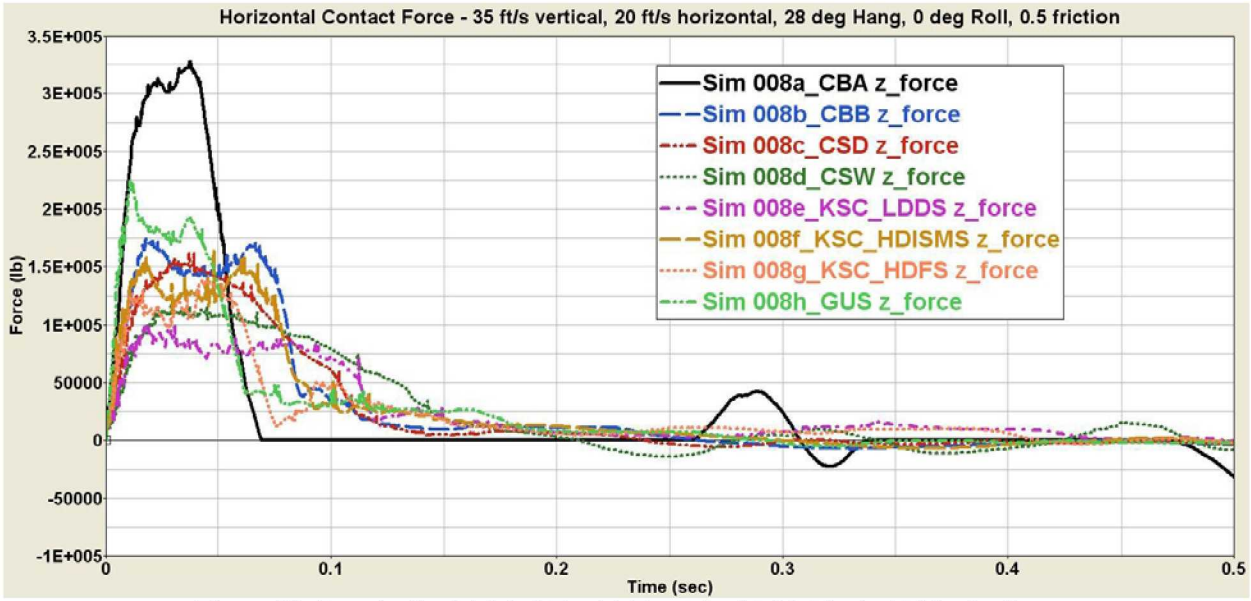

Figure 98. Longitudinal (global Z-axis) Force for 35 ft/s Vertical Velocity Case

B.9 0 ft/s Horizontal Velocity Case

The vertical and longitudinal contact forces for the 0 ft/s horizontal velocity case on the eight soil models are plotted in Figure 99, Figure 100, and Figure 101. The contact forces generally follow the same trends as the accelerations, despite the initial 28° angle difference between the coordinate systems. The local coordinate system aligns with the global system between 0.2-0.3 seconds, which corresponds to the peak value for most soil cases.

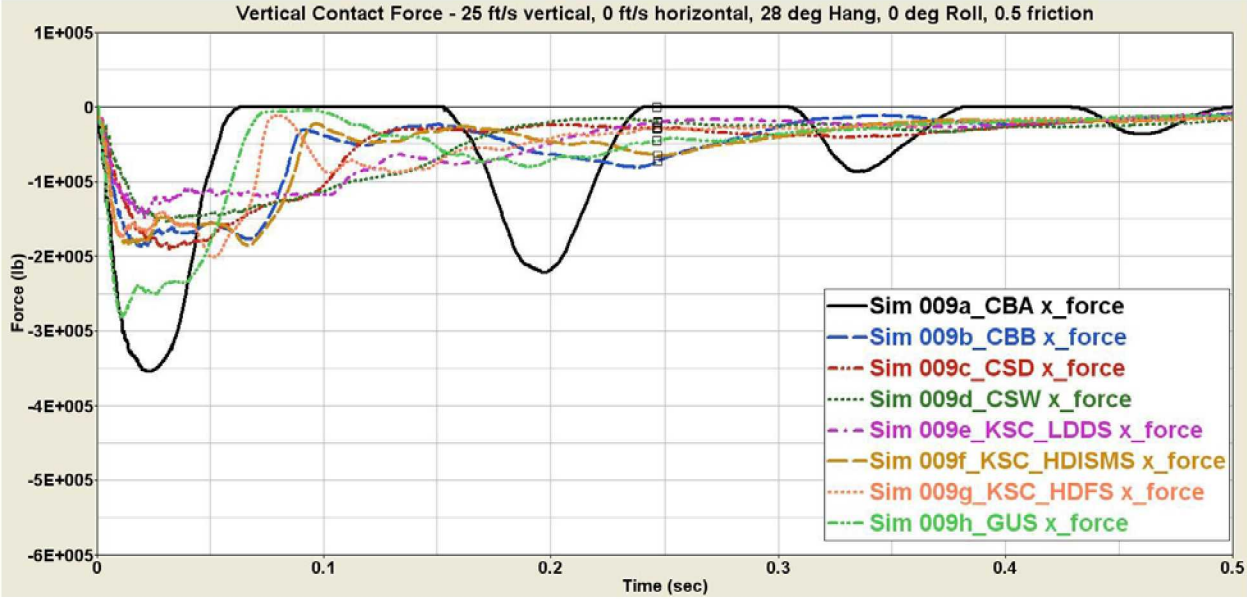

Figure 99. Vertical (global X-axis) Force for 0 ft/s Horizontal Velocity Case

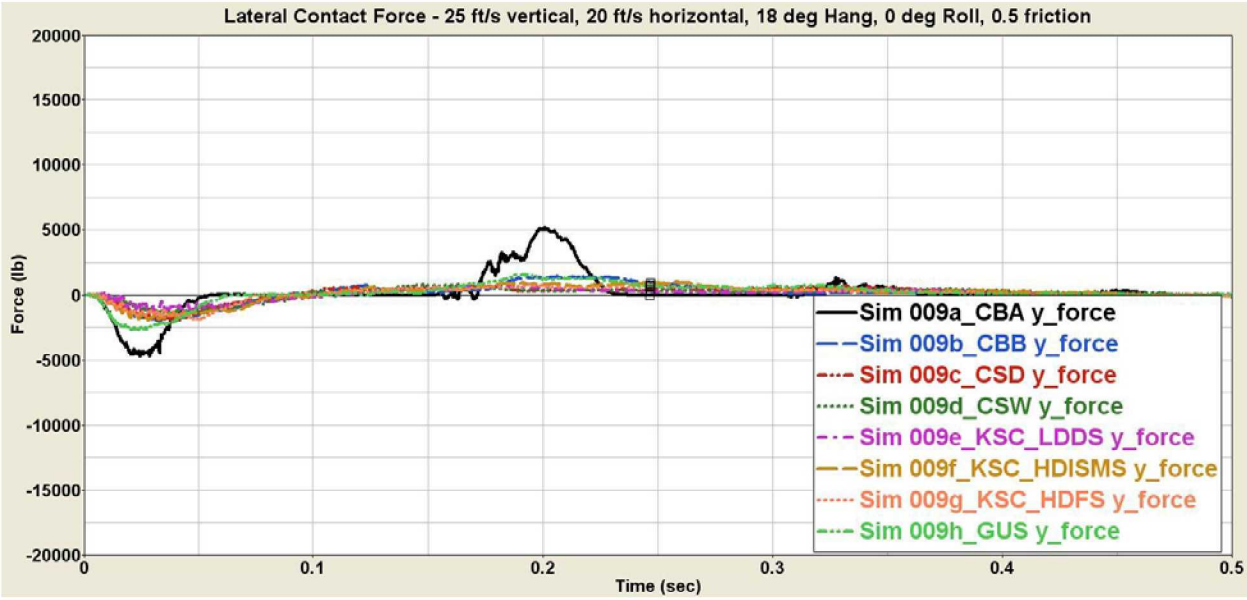

Figure 100. Lateral (global Y-axis) Force for 0 ft/s Horizontal Velocity Case

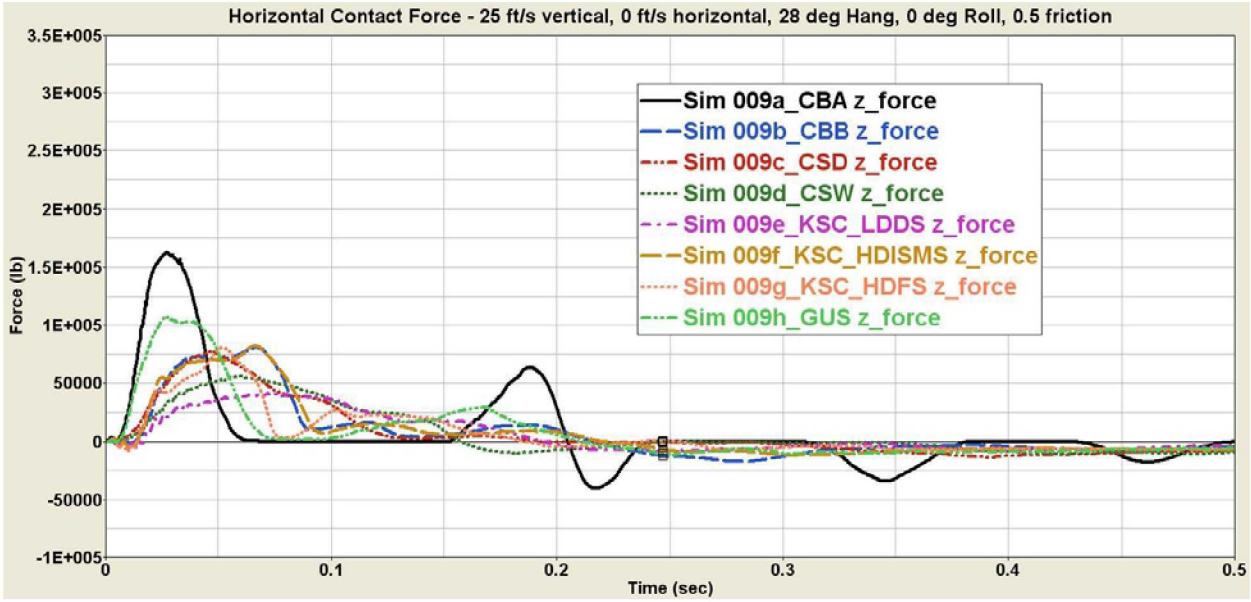

Figure 101. Longitudinal (global Z-axis) Force for 0 ft/s Horizontal Velocity Case

B.10 40 ft/s Horizontal Velocity Case

The vertical, lateral, and longitudinal contact forces for the 40 ft/s horizontal velocity case on the eight soil models are plotted in Figure 102, Figure 103, and Figure 104, respectively. For the 40 ft/s horizontal velocity case, the vertical contact forces are of the same magnitude as the baseline case, but the horizontal (longitudinal) contact forces are higher. Some numerical instability is visible in the longitudinal contact forces for Cuddeback B.

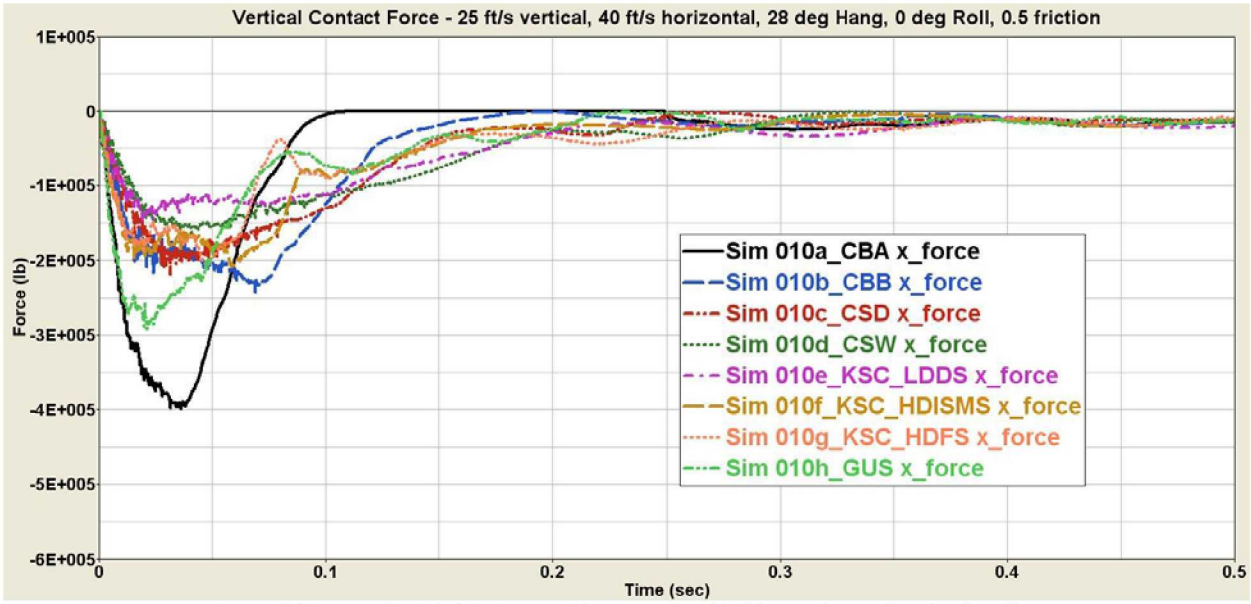

Figure 102. Vertical (global X-axis) Force for 40 ft/s Horizontal Velocity Case

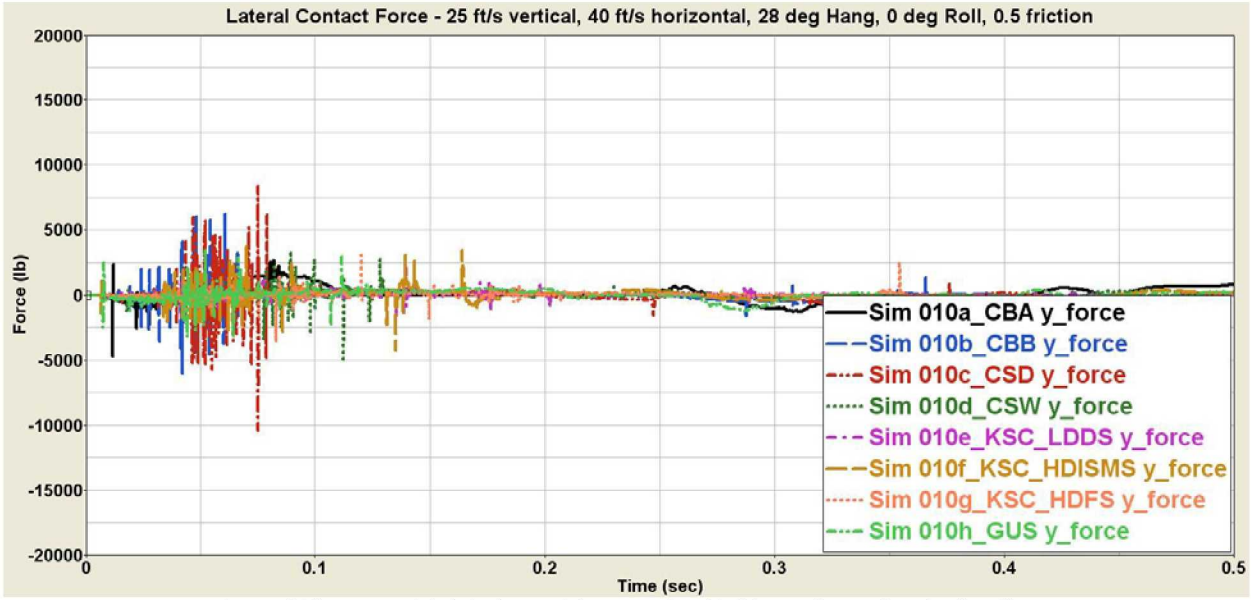

Figure 103. Lateral (global Y-axis) Force for 40 ft/s Horizontal Velocity Case

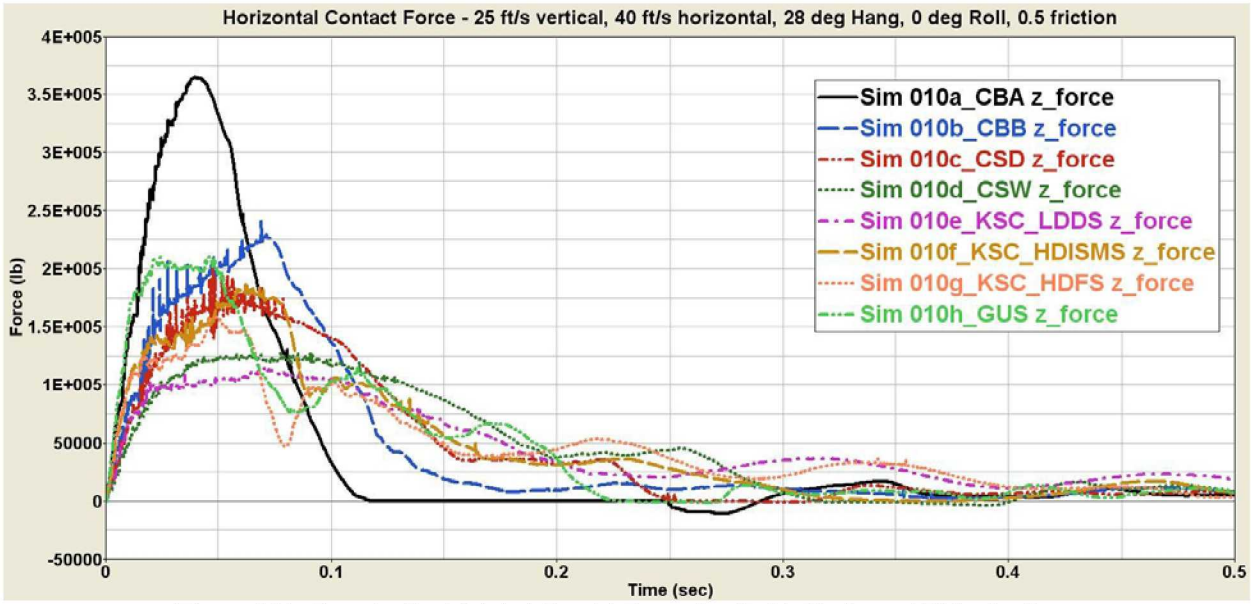

Figure 104. Longitudinal (global Z-axis) Force for 40 ft/s Horizontal Velocity Case

Appendix C: Additional CM Kinetic Energy Results

The following sections present the CM kinetic energy for all the simulation cases.

C.1 Baseline Case: 28° Hang Angle, 0° Roll Angle, 25 ft/s Vertical, 20 ft/s Horizontal

Figure 105 shows the CM kinetic energy versus time curves for the eight soil model cases.

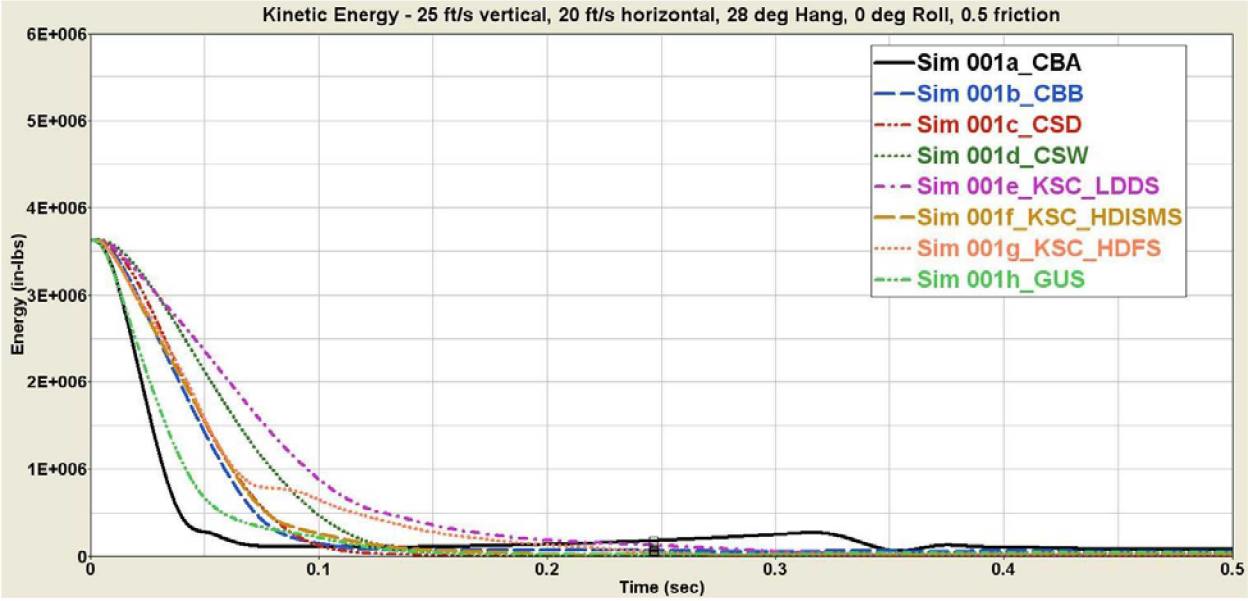

Figure 105. CM Kinetic Energy for Baseline Case

C.2 18° Hang Angle Case

The CM kinetic energy curves for the 18° hang angle case on the eight soil models are plotted in Figure 106. The CM kinetic energy dissipation follows different trends for different soils. The harder soils, such as Cuddeback A and the Gantry Unwashed Sand, impart larger forces on the CM, and thus reduce the CM kinetic energy at a higher rate. The Carson Sink Wet soil and the KSC Low Density Dry Sand have shallower rates of kinetic energy dissipation, with the other soils falling between these cases and the Cuddeback A soil and Gantry Unwashed Sand cases.

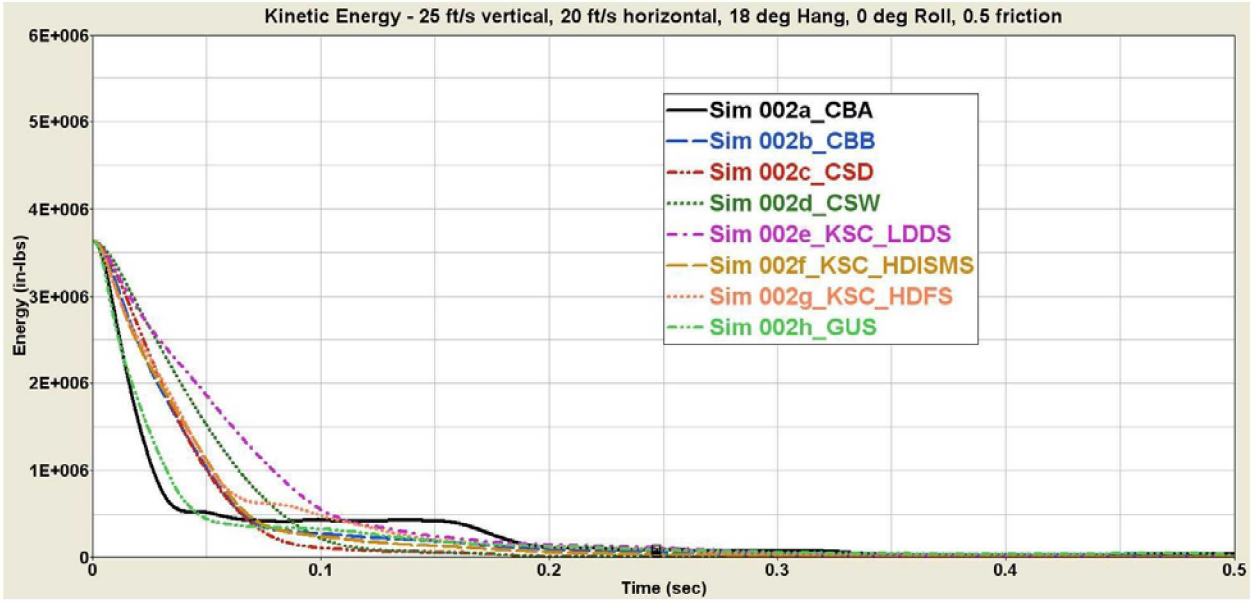

Figure 106. CM Kinetic Energy for 18° Hang Angle Case

C.3 38° Hang Angle Case

As shown in Figure 107, the 38° hang angle results the CM kinetic energy increasing again after 0.05 seconds when impacting the Cuddeback A soil. The CM gains additional kinetic energy as it rolls back onto the heat shield and the CG is lowered further in the gravity field; the CM trades potential energy for kinetic energy. The CM kinetic energy curve for the KSC High Density In-Situ Moisture Sand falls between the Cuddeback B and Carson Sink Dry soils.

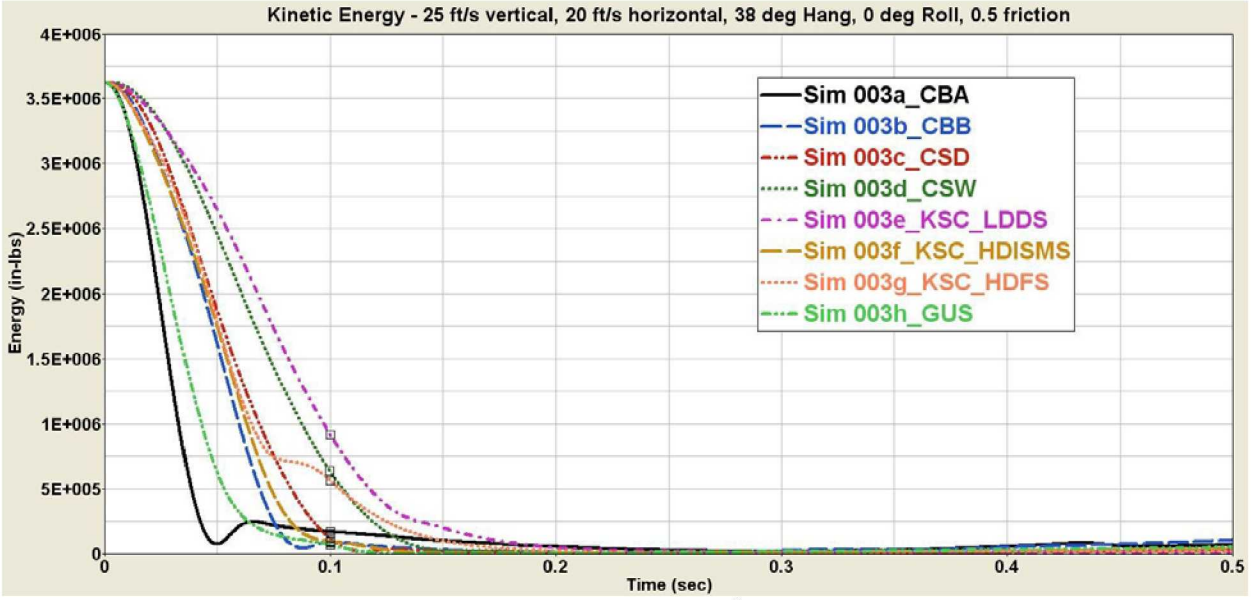

Figure 107. CM Kinetic Energy for 38° Hang Angle Case

C.4 45° Roll Angle Case

The CM kinetic energy curves for the 45° roll angle case on the eight soil models are plotted in Figure 108. The bouncing of the CM on the Cuddeback A soil results in the capsule kinetic energy rising up again after the initial impact before being reduced again at the second impact (at 0.25 seconds). Although initially as stiff as Cuddeback A, the Gantry Unwashed Sand does not maintain the same rate of kinetic energy reduction after 0.02 seconds, and the kinetic energy of the CM does not increase after the initial impact.

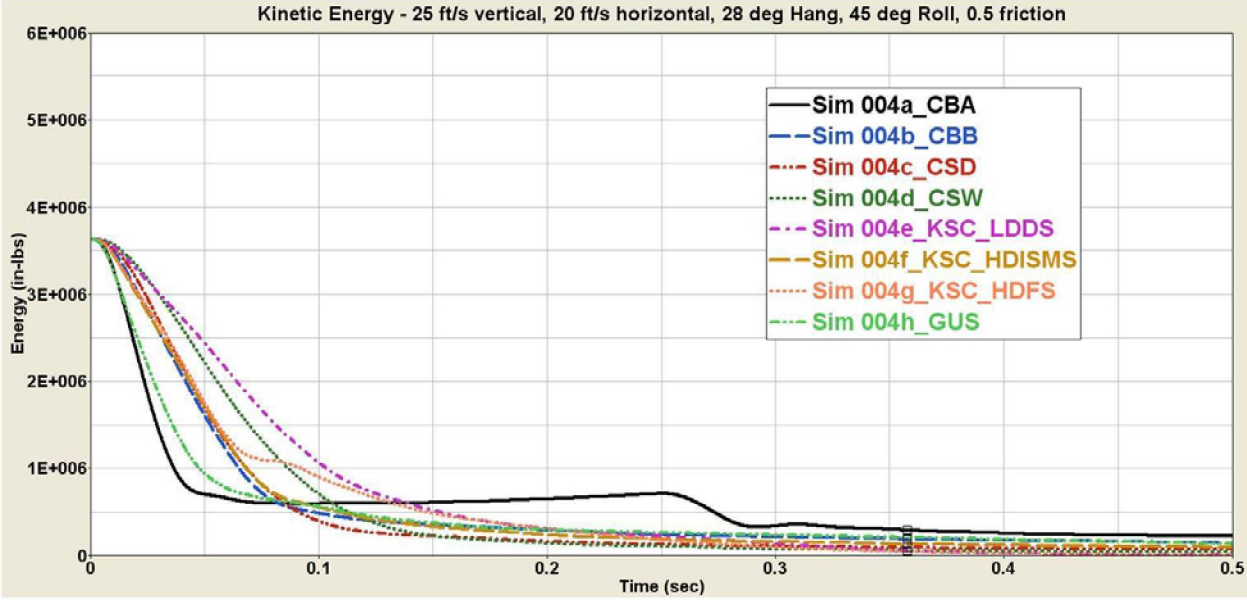

Figure 108. CM Kinetic Energy for 45° Roll Angle Case

C.5 90° Roll Angle Case

The CM kinetic energy curves for the 90° roll angle case on the eight soil models are plotted in Figure 109. The CM rolls and twists as it impacts for the 90° roll angle case, which on the hard Cuddeback A soil results in the capsule kinetic energy not being dissipated from 0.04-0.17 seconds. The CM kinetic energy responses on the Carson Sink Dry, Cuddeback B soil, and the KSC High Density In-Situ Moisture Sand are all essentially the same during the first 0.075 seconds.

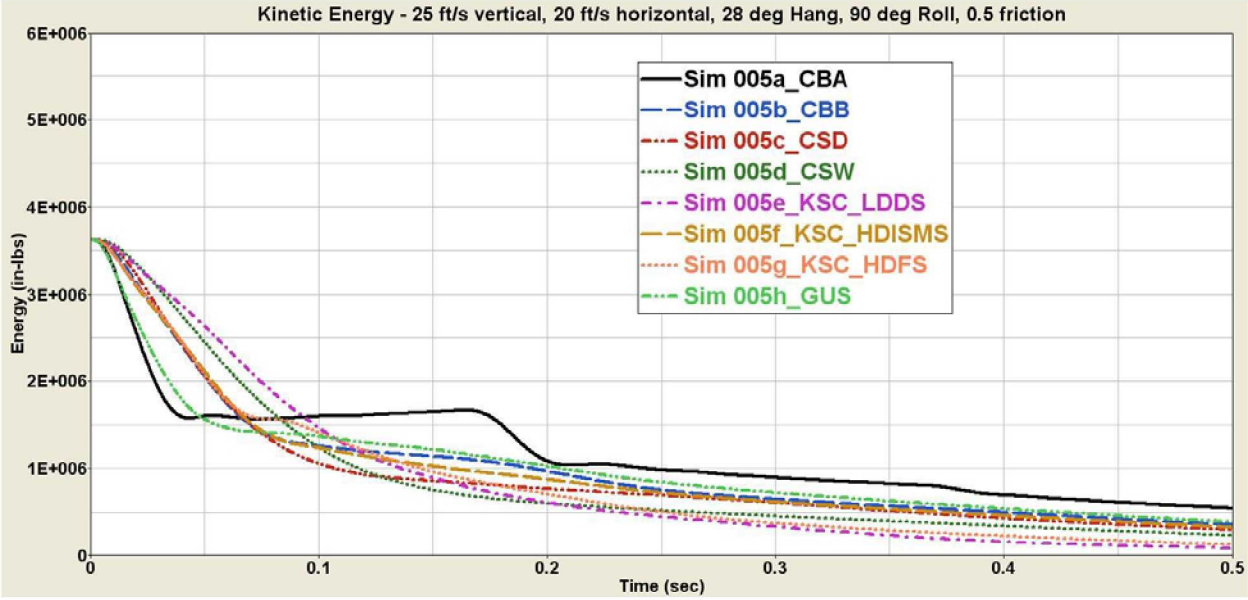

Figure 109. CM Kinetic Energy for 90° Roll Angle Case

C.6 180° Roll Angle Case

The CM kinetic energy curves for the 180° roll angle case on the eight soil models are plotted in Figure 110. Due to the orientation of the CM for this case (termed heel-in), the overall impact dynamics are different in that the vehicle pitches forward in the direction of the initial horizontal velocity. The CM is driven to pitch forward in this direction by both the vertical reaction force resulting from the ground contact and the longitudinal (Z-axis) force. The longitudinal force is a combination of the friction with the soil and the direct longitudinal reaction force against the soil when the CM digs into the soil. As a result, the kinetic energy does not diminish as much as the other landing condition cases upon initial ground contact, as the CM converts from pure translational velocity to a combination of translational and rotational velocity, and also exchanges potential and kinetic energy as the CG moves parallel to the gravity field. This is even more pronounced for the Cuddeback A soil and the Gantry Unwashed Sand, which show an extended time period between approximately 0.03 and 0.11 seconds where the kinetic energy does not decrease, and actually increases slightly for the Cuddeback A case (again also driven by the vertical height change of the CG).

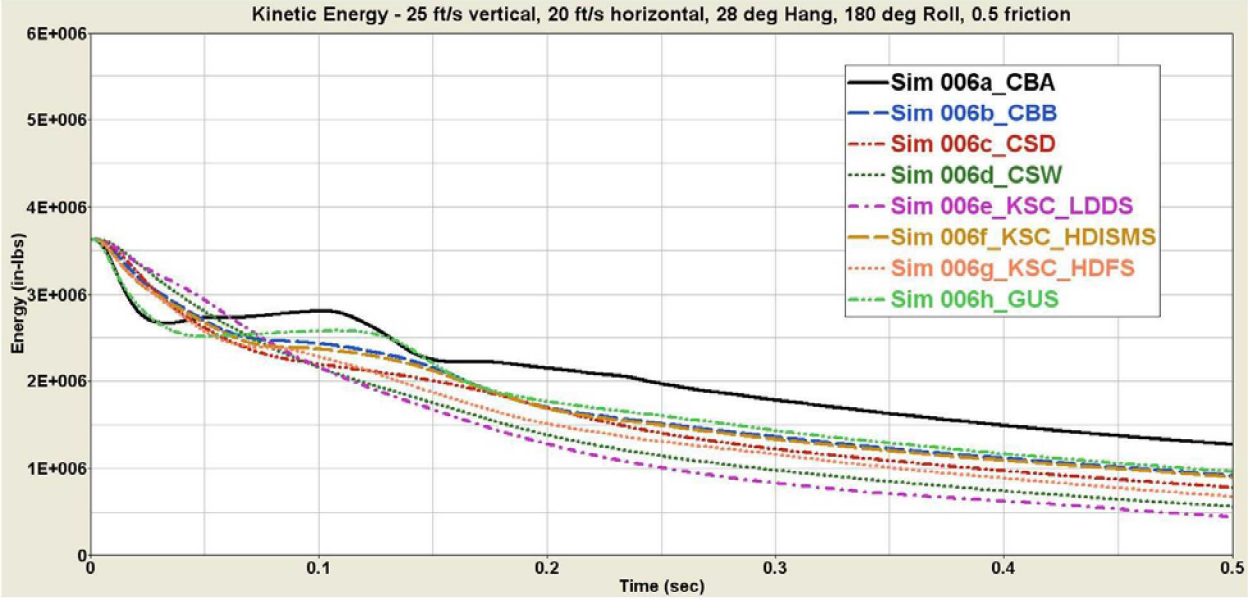

Figure 110. CM Kinetic Energy for 180° Roll Angle Case

C.7 15 ft/s Vertical Velocity Case

Figure 111 shows the CM kinetic energy curves for the 15 ft/s vertical velocity case on the eight soil models. The CM kinetic energy dissipates smoothly for all soils, except for the KSC High Density Flooded Sand, which shows a brief slippage between approximately 0.07 and 0.08 seconds, during which the CM kinetic energy remains approximately the same.

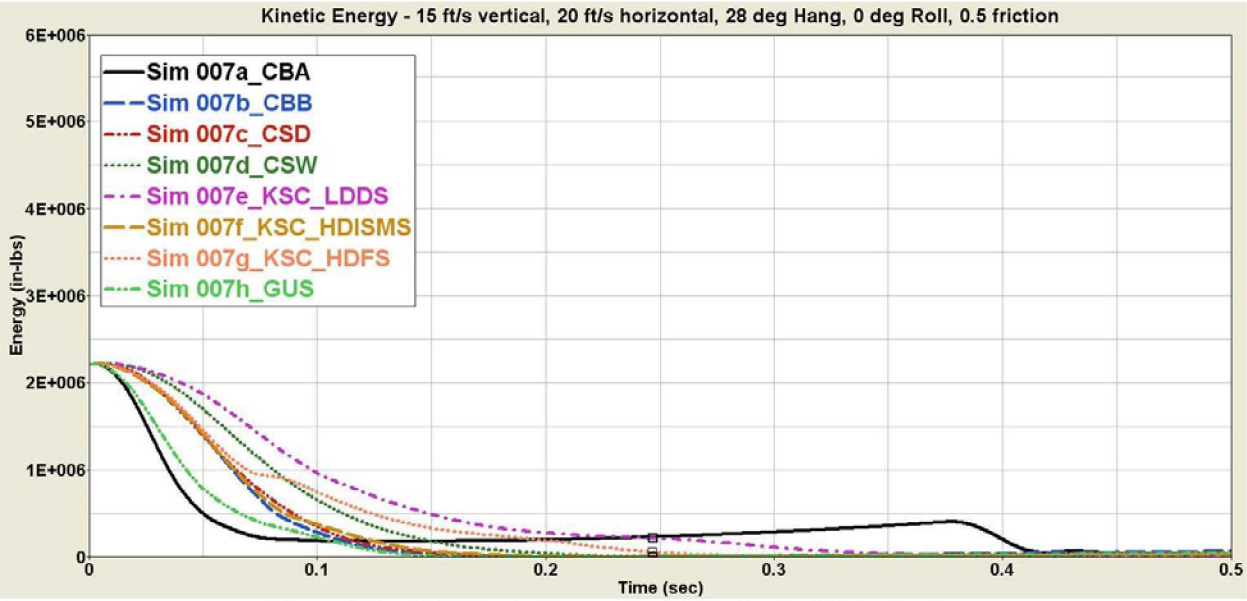

Figure 111. CM Kinetic Energy for 15 ft/s Vertical Velocity Case

C.8 35 ft/s Vertical Velocity Case

Figure 112 shows the CM kinetic energies for the 35 ft/s vertical velocity case on the eight soil models. The behavior of the soils is smooth, except for the KSC High Density Flooded Sand, which again exhibits a constant kinetic energy between approximately 0.07 and 0.08 seconds.

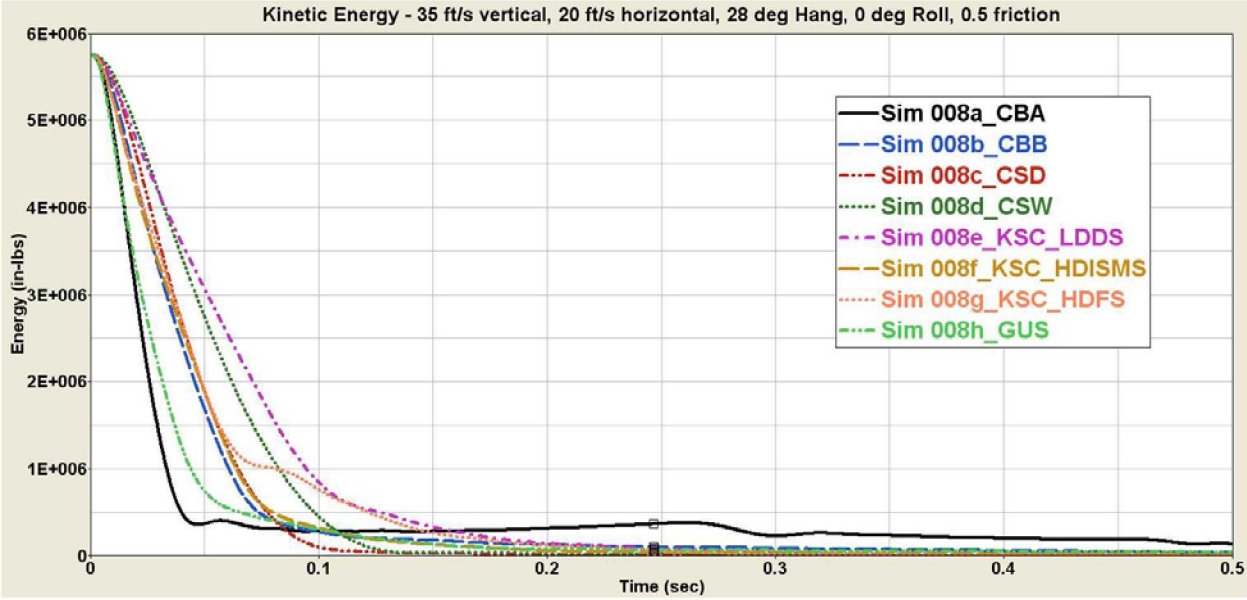

Figure 112. CM Kinetic Energy for 35 ft/s Vertical Velocity Case

C.9 0 ft/s Horizontal Velocity Case

Figure 113 shows the CM kinetic energy curves for the 0 ft/s horizontal velocity case on the eight soil models. Initial kinetic energy is lower for this case, due to the lack of horizontal velocity. The kinetic energy dissipation during the initial impact event is proportional to the soil stiffness. This pure vertical drop case removes the effects of digging into and pushing the soil, and thus better illustrates its vertical stiffness.

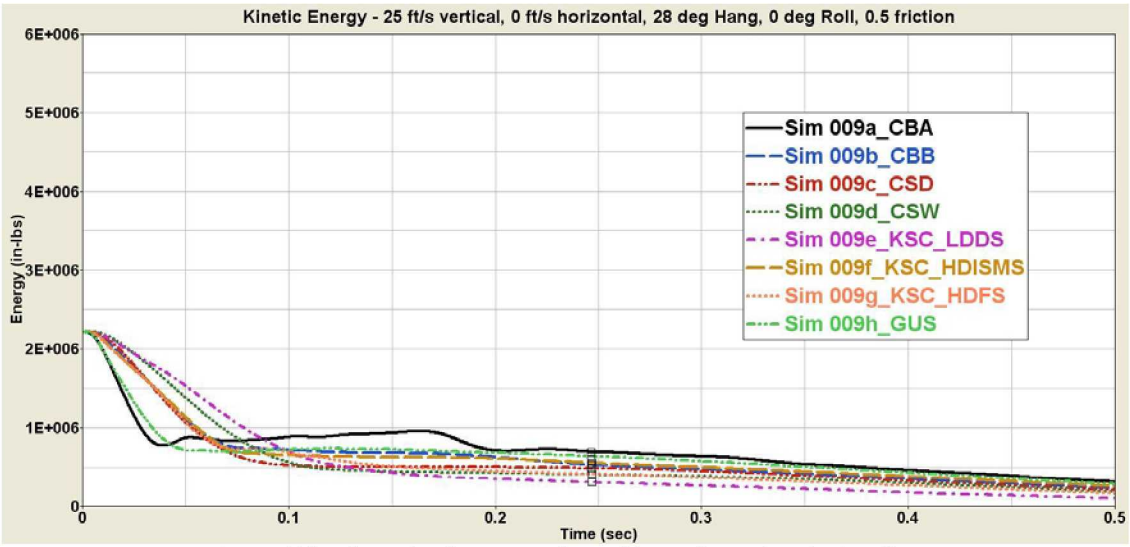

Figure 113. CM Kinetic Energy for 0 ft/s Horizontal Velocity Case

C.10 40 ft/s Horizontal Velocity Case

Figure 114 shows the CM kinetic energy curves for the 40 ft/s horizontal velocity case on the eight soil models. These landing conditions represent the highest initial CM kinetic energy case. The Cuddeback A soil case again has the sharpest drop-off in the kinetic energy, and the KSC Low Density Dry Sand case shows the slowest reduction, aside from the initially slightly slower level of the Carson Sink Wet soil case.

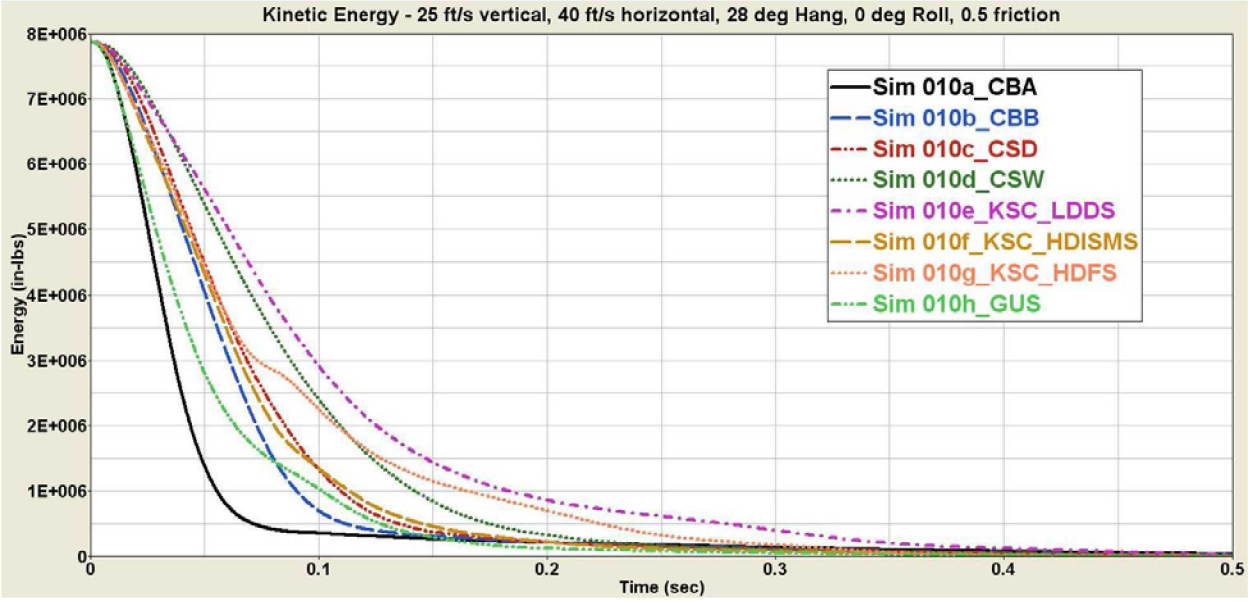

Figure 114. CM Kinetic Energy for 40 ft/s Horizontal Velocity Case

D. Summary of Soil Berm Height

During the impact event, sometimes the soil is either pushed up around the impact crater, or a berm builds up in front of the CM as it plows through the soil. Table 8 lists the vertical height change of the soil for all the simulations, and these results are plotted in Figure 115. For the KSC Low Density Dry Sand, High Density In-Situ Moisture Sand, and High Density Flooded Sand, and the Gantry Unwashed Sand, both the higher and lower hang angle cases have lower berm heights than the baseline. The KSC Low Density Dry Sand and High Density Flooded Sand exhibit the highest berm height sensitivity to the horizontal velocity and, correspondingly, the highest berm heights for the 40 ft/s horizontal velocity case. These two soils are very easily displaced, and also show the largest vertical displacement for the pure vertical drop landing condition (case 9). However, the berm heights of these same two soils are approximately the same for the baseline and 35 ft/s vertical velocity cases. The berm height for the KSC Low Density Dry Sand is not sensitive to the vertical velocity. Only the KSC Low Density Dry Sand and High Density Flooded Sand have a large berm after the impact event for the 38° hang angle, whereas the other soils have relatively deep craters without as much soil raised up.

Table 8. Height of Soil Berm (global X-axis – units are inches)

soil	case 1	case 2	case 3	case 4	case 5	case 6	case 7	case 8	case 9	case 10
	Base-line	18° hang	38° hang	45° roll	90° roll	180° roll	15 ft/s V	35 ft/s V	0 ft/s H	40 ft/s H
CBA	2.0	0.5	1.4	0.4	0.6	2.2	1.0	1.7	0.3	4.3
CBB	3.2	1.2	1.5	2.9	1.9	1.8	3.2	4.7	0.6	6.4
CSD	3.6	4.0	1.6	5.0	1.1	0.9	3.8	4.5	0.0	7.2
CSW	6.0	13.8	3.7	6.2	2.1	0.7	6.4	5.1	0.0	11.9
KSC_LDDS	16.3	9.0	12.6	14.9	7.4	7.2	17.0	15.9	1.5	30.0
KSC_HDISMS	7.2	5.4	3.7	7.6	2.8	2.2	5.2	10.6	0.4	11.6
KSC_HDFS	16.5	1.3	12.4	13.6	5.9	3.0	13.4	16.2	1.6	29.0
GUS	7.8	2.1	5	7.1	2.4	0.6	6.0	9.3	0.6	12.9

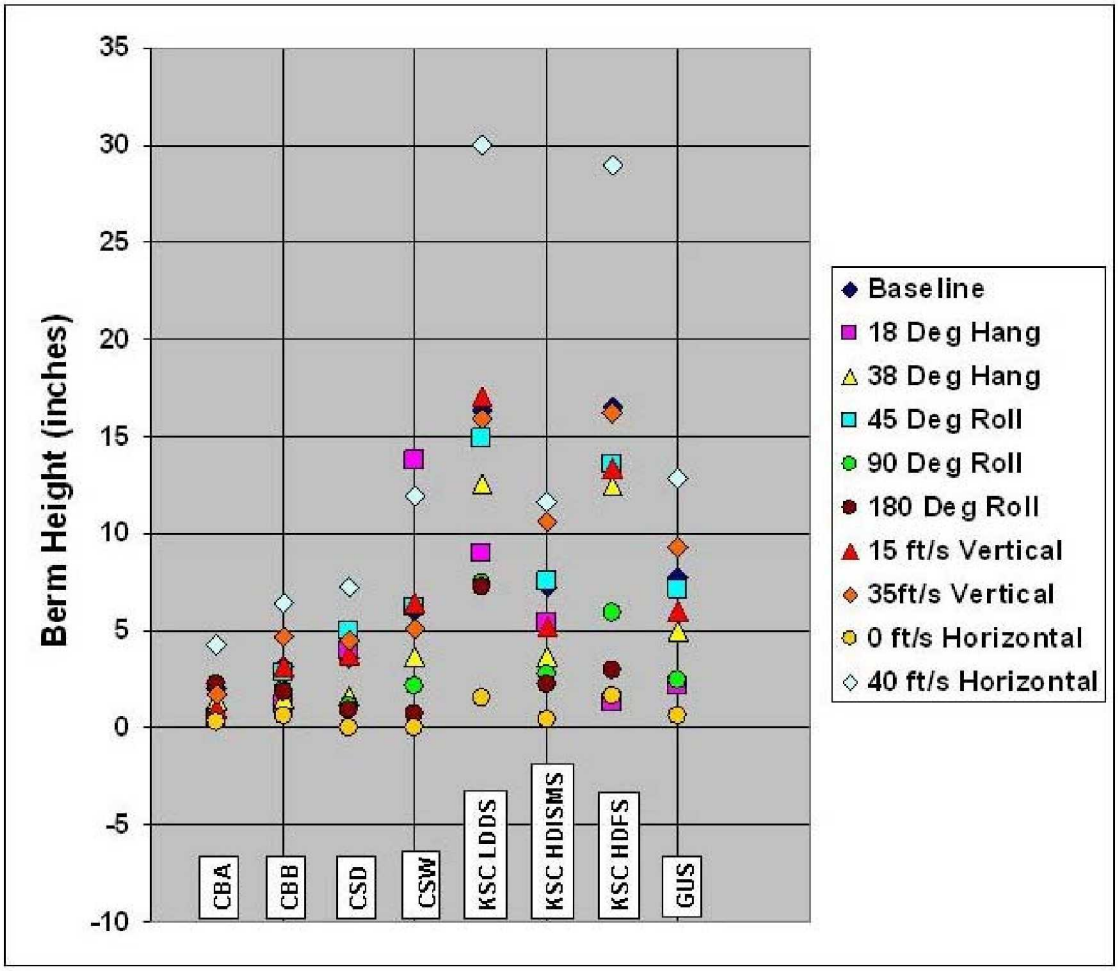

Figure 115. Plot of Height of Soil Berm (global X-axis)

REPORT DOCUMENTATION PAGE

Form Approved
OMB No. 0704-0188

1. REPORT DATE *(DD-MM-YYYY)*	2. REPORT TYPE	3. DATES COVERED *(From - To)*
01-06-2009	Contractor Report	

4. TITLE AND SUBTITLE
Orion Landing Simulation Eight Soil Model Comparison

5a. CONTRACT NUMBER
NNL07AA00B

5b. GRANT NUMBER

5c. PROGRAM ELEMENT NUMBER

6. AUTHOR(S)
Mark, Stephen D.

5d. PROJECT NUMBER

5e. TASK NUMBER

5f. WORK UNIT NUMBER
644423.06.31.03.14.04.01

7. PERFORMING ORGANIZATION NAME(S) AND ADDRESS(ES)
NASA Langley Research Center
Hampton, VA 23681-2199

8. PERFORMING ORGANIZATION REPORT NUMBER

9. SPONSORING/MONITORING AGENCY NAME(S) AND ADDRESS(ES)
National Aeronautics and Space Administration
Washington, DC 20546-0001

10. SPONSOR/MONITOR'S ACRONYM(S)
NASA

11. SPONSOR/MONITOR'S REPORT NUMBER(S)
NASA/CR-2009-215757

12. DISTRIBUTION/AVAILABILITY STATEMENT
Unclassified - Unlimited
Subject Category 39
Availability: NASA CASI (443) 757-5802

13. SUPPLEMENTARY NOTES
Langley Technical Monitor: Karen H. Lyle

14. ABSTRACT

LS-DYNA® finite element simulations of a rigid Orion Crew Module (CM) were used to investigate the CM impact behavior on eight different soil models. Ten different landing conditions, characterized by the combination of CM vertical and horizontal velocity, hang angle, and roll angle were simulated on the eight different soils. The CM center of gravity accelerations, pitch angle, kinetic energy, and soil contact forces were the outputs of interest. The simulation results are presented, with comparisons of the CM behavior on the different soils. The soils analyzed in this study can be roughly categorized as soft, medium, or hard, according to the CM accelerations that occur when landing on them. The soft group is comprised of the Carson Sink Wet soil and the Kennedy Space Center (KSC) Low Density Dry Sand. The medium group includes Carson Sink Dry, the KSC High Density In-Situ Moisture Sand and High Density Flooded Sand, and Cuddeback B. The hard soils are Cuddeback A and the Gantry Unwashed Sand. The softer soils were found to produce lower peak accelerations, have more stable pitch behavior, and to be less sensitive to the landing conditions. This investigation found that the Cuddeback A soil produced the highest peak accelerations and worst stability conditions, and that the best landing performance was achieved on the KSC Low Density Dry Sand.

15. SUBJECT TERMS
Constellation program; Contingency land landing; Crew module; Landing impact; Orion capsule; Soil modeling

16. SECURITY CLASSIFICATION OF:			17. LIMITATION OF ABSTRACT	18. NUMBER OF PAGES	19a. NAME OF RESPONSIBLE PERSON
a. REPORT	b. ABSTRACT	c. THIS PAGE			STI Help Desk (email: help@sti.nasa.gov)
					19b. TELEPHONE NUMBER *(Include area code)*
U	U	U	UU	88	(443) 757-5802